DOSIMETRIC CHARACTERISATION OF SILICA FIBRE THERMOLUMINESCENT SENSORS FOR MEDICAL AND NON-MEDICAL APPLICATIONS

FARHAD MORADI

FACULTY OF SCIENCE
UNIVERSITY OF MALAYA
KUALA LUMPUR

2018

DOSIMETRIC CHARACTERISATION OF SILICA FIBRE THERMOLUMINESCENT SENSORS FOR MEDICAL AND NON-MEDICAL APPLICATIONS

FARHAD MORADI

THESIS SUBMITTED IN FULFILMENT OF THE REQUIREMENTS FOR THE DEGREE OF DOCTOR OF PHILOSOPHY

DEPARTMENT OF PHYSICS
FACULTY OF SCIENCE
UNIVERSITY OF MALAYA
KUALA LUMPUR

2018

UNIVERSITY OF MALAYA

ORIGINAL LITERARY WORK DECLARATION

Name of Candidate: **FARHAD MORADI**

Matric No: **SHC140115**

Name of Degree: **DOCTOR OF PHILOSOPHY**

Title of Thesis: **DOSIMETRIC CHARACTERISATION OF SILICA FIBRE THERMOLUMINESCENT SENSORS FOR MEDICAL AND NON-MEDICAL APPLICATIONS**

Field of Study: **EXPERIMENTAL PHYSICS**

I do solemnly and sincerely declare that:

(1) I am the sole author/writer of this Work;
(2) This Work is original;
(3) Any use of any work in which copyright exists was done by way of fair dealing and for permitted purposes and any excerpt or extract from, or reference to or reproduction of any copyright work has been disclosed expressly and sufficiently and the title of the Work and its authorship have been acknowledged in this Work;
(4) I do not have any actual knowledge nor do I ought reasonably to know that the making of this work constitutes an infringement of any copyright work;
(5) I hereby assign all and every rights in the copyright to this Work to the University of Malaya ("UM"), who henceforth shall be owner of the copyright in this Work and that any reproduction or use in any form or by any means whatsoever is prohibited without the written consent of UM having been first had and obtained;
(6) I am fully aware that if in the course of making this Work I have infringed any copyright whether intentionally or otherwise, I may be subject to legal action or any other action as may be determined by UM.

Candidate's Signature Date:

Subscribed and solemnly declared before,

Witness's Signature Date:

Name:

Designation:

DOSIMETRIC CHARACTERISATION OF SILICA FIBRE THERMOLUMINESCENT SENSORS FOR MEDICAL AND NON-MEDICAL APPLICATIONS

ABSTRACT

Silica based optical fibres has been attracting researchers since 1980's due to various phenomenal observations via the exposure of ionizing radiation. Studies of such phenomena gradually eventuated the potentiality of silica fibres as radiation dosimeters. Focus was made mainly on thermoluminescence (TL) properties with various competitive advantages such as proper spatial resolution, non-hygroscopic nature, cost effectiveness, chemically inert and wide range dose response linearity etc. Available literatures concentrate on the increasing sensitivity of different composition silica fibres, some of their dosimetric characteristics and potential applications. However, there is a significant gap between the published works and practical needs before routine usage of such thermoluminescent dosimeters (TLDs). This study concentrates on properties of Ge-doped silica fibre TLDs, with the first and second phases of the study on characterisation of fibres for general and specific applications respectively. The applications included *in-vivo* dosimetry in intraoperative radiotherapy using low kV photon field, gamma irradiator dose mapping and high dose dosimetry. To maintain sensitivity and reproducibility of the dosimeter, stabilization process should be optimized. This was done as part of this study. The effect of accumulated dose on TL response and the role of heating on the sensitivity of fibres were investigated, and an optimized preparation procedure was obtained. It was shown that TL response would not be reproducible without applying a pre-dose and sufficiently high annealing temperature. Dependence of the fibre TL response on different beam parameters including beam angulation, beam energy and dose rate was also studied in parts of characterisation. Energy dependence is

expected from SiO_2 due to its high effective atomic number. It was proven that energy dependence correction factor for Ø=125 μm Ge-doped fibre with small sensitive part (8.5 μm core) at each keV energy can be approximated well by the ratio of mass energy absorption coefficient of the sensitive part of the fibre to that of medium. A considerable angular dependence was also observed from studied fibre TLD in free-in-air irradiations. This was decreased significantly in presence of phantom, where scattered radiation was involved. Respective coefficients at each situation were obtained. The results, in general, remark the importance of positioning and consideration of the angular dependence. Study was extended to introduce new applications benefiting small size, wide dose/response range and waterproof of silica fibres. Dosimetry for the INTRABEAM system, an electronic brachytherapy source, necessitated to characterize the fibres at different depth in water where dose rate and beam quality were simultaneously changed. In addition to experimental approach to achieve better insight into phenomenon, Monte Carlo simulations were also performed. Both the experimental and simulation approaches resulted in determination of calibration coefficients needed for patient dose assessment. In the last part, various silica fibres were tested in terms of their performance under high dose irradiation. Most fibre types showed saturation in doses below 50 kGy, with only borosilicate fibre showing linear dose response of up to 100 kGy. The results of this study generally help to promote the use of silica based fibres as practical TL dosimeters offering sufficient precision.

Keywords: Ge-doped silica fibre, Thermoluminescence, Dosimetry, Monte Carlo

PENCIRIAN DOSIMETRI SERAT SILIKA SENSOR TERMOLUMINESCENT UNTUK PERUBATAN BUKAN PERUBATAN APLIKASI

ABSTRAK

Serat optik berasaskan silika telah menarik perhatian para penyelidik sejak tahun 1980 kerana berlakunya pelbagai fenomena melalui pendedahan radiasi mengion. Kajian fenomena sedemikian secara beransur-ansur membolehkan serat silika digunakan sebagai dosimeteri sinaran. Fokus dibuat terutamanya pada sifat-sifat termoluminescence (TL) dengan pelbagai kelebihan daya saing seperti resolusi spatial yang betul, sifat non-hygroscopic, kos yang berpatutan , tidak lentur bahan kimia, garis lebar tindak balas dos dan lain-lain. Sastera yang ade lebih menumpukan pada kepekaan yang meningkat dari komposisi silika yang berbeza serat, beberapa ciri dosimetri dan aplikasi yang berpotensi. Walau bagaimanapun terdapat jurang yang ketara antara kerja-kerja yang diterbitkan dan keperluan praktikal sebelum penggunaan rutin TLD tersebut. Kajian ini menumpukan kepada sifat-sifat TLD gentian silika Ge-doped, dengan fasa pertama dan kedua kajian mengenai pencirian gentian untuk aplikasi am dan spesifik masing-masing. Aplikasi termasuk dosimetri dalam-vivo dalam radioterapi intraoperatif menggunakan medan foton kV yang rendah, pemetaan dos gamadi penyinaran dan dosimetri dos tinggi. Untuk mengekalkan kepekaan dan kebolehulangan dosimeter proses penstabilan perlu dioptimumkan. Perkara ini telah dilakukan sebagai sebahagian daripada kajian ini. Kesan dos terkumpul pada tindak balas TL dan peranan pemanasan pada sensitiviti gentian juga telah diselidiki, dan prosedur penyediaan optimum telah diperolehi. Keputusan menunjukkan bahawa tindakbalas TL tidak dapat dihasilkan tanpa manggunakan suhu pra-dos dan penyepuhlindapan yang cukup tinggi. Ketergantungan respon serat TL pada parameter balok yang berlainan, seperti angulation rasuk, tenaga rasuk dan kadar dos juga dikaji dalam bahagian pencirian. Ketergantungan tenaga dijangka daripda SiO_2 kerana

mengandungi bilangan atom yang tinggi. Hal ini telah membuktikan bahawa faktor pembetulan kebergantungan tenaga untuk Ø = 125 μm Serat ge-doped dengan bahagian sensitif kecil (8.5 μm teras) pada setiap keV tenaga boleh dianggarkan dengan baik oleh nisbah penyerapan tenaga jisim bahagian sensitif serat. Satu pergantungan sudut yang besar juga diperhatikan dari kajian TLD serat dalam penyinaran bebas udara. Perkara ini menurun dengan ketara dengan phantom, di mana radiasi bertaburan terlibat sama. Koefisien pada setiap keadaan telah diperolehi. Keputusan, secara umum, menyatakan pentingnya kedudukan dan pertimbangan kebergantungan sudut. Kajian diperluaskan untuk memperkenalkan aplikasi baru yang memberi manfaat kepada saiz kecil, pelbagai dos / tindanan pelbagai dan kalis air gentian silika. Dosimetri untuk sistem INTRABEAM, sumber brachytherapy elektronik, yang diperlukan untuk mencirikan gentian pada kedalaman yang berbeza di dalam air di mana kadar dos dan kualiti rasuk juga berubah secara serentak. Di samping pendekatan eksperimen untuk mencapai keputusan yang lebih baik terhadap fenomena, simulasi Monte Carlo juga dilakukan. Kedua-dua pendekatan eksperimen dan simulasi menghasilkan penentuan koefisien penentukuran yang diperlukan untuk penilaian dos pesakit. Pada bahagian terakhir, pelbagai serat silika diuji dari segi prestasi mereka di bawah penyinaran dos yang tinggi. Kebanyakan jenis serat menunjukkan tepu dalam dos di bawah 50 kGy, dengan hanya serat borosilikat yang menunjukkan tindak balas dos linear sehingga 100 kGy. Hasil kajian ini secara umumnya membantu mempromosikan penggunaan gentian berasaskan silika sebagai dosimeters TL praktikal yang menawarkan ketepatan yang mencukupi.

Kata Kunci: Ge-doped silica fibre, Thermoluminescence, Dosimetry, Monte Carlo

ACKNOWLEDGEMENTS

Dedicated to my best friend, my love, my wife, for all her patience, kindness and endless support during completion of my PhD

I would like to express my deepest gratitude for the immense conduction and support that I received from my supervisors Associate Professor Dr. Mayeen Uddin Khandaker, Dr. Ung Ngie Min and Dr. Ghafour Amouzad Mahdiraji, without them, completion of this project could not be fulfilled. I will never forget their endless backing and goodness during my PhD carrier.

I also would like to appreciate Professor David Andrew Bradley for his valuable guidance whenever I needed during this work.

I would also like to thank Dr. See Mee Hoong and department of surgery for the financial support provided under the University of Malaya Research Grant (UMRG) number RPO46-15HTM.

And finally, the kind cooperation of the personnel of Medical Physics Unit in the University of Malaya Medical Centre (UMMC) and staff in charge for high dose facilities in Malaysian Nuclear Agency during the completion of this study, is highly appreciated.

TABLE OF CONTENTS

LIST OF FIGURES

LIST OF TABLES

LIST OF ABBREVIATIONS

CPE	:	Charged particle equilibrium
CSDA	:	Continuous slowing down approximation
CVD	:	Chemical vapor deposition
EDX	:	Energy dispersive X-ray
EDXRS	:	Energy dispersive X-ray spectrometry
EXAFS	:	X-ray absorption fine structure
FBG	:	Fibre Bragg Grating
FESEM	:	Field emission scanning electron microscope
FF	:	Flat fibre
FWHM	:	Full width at half maximum
GC-220	:	Gammacell 220
GDSF	:	Ge-doped silica fibre
HDR	:	High dose rate
IC	:	Ionization chamber
ICRP	:	International Commission on Radiological Protection
ILRG	:	Integrated Lightwave Research Group
IMRT	:	Intensity modulated radiation therapy
IORT	:	Intraoperative radiation therapy
IRM	:	Internal radiation monitor
IMTS	:	Interactive multiple trap system
LINAC	:	Linear accelerator
MC	:	Monte Carlo
MCNP	:	Monte Carlo N Particle
MCVD	:	Modified chemical vapor deposition

MOSFET	:	Metal oxide semiconductor field effect transistor
NIST	:	National Institute of Standard and Technology
OSL	:	Optically stimulated luminescence
PCF	:	Photonic crystal fibre
PMMA	:	Poly-methyl-meth-acrylate
PMT	:	Photomultiplier tube
RC	:	Recombination centre
RIA	:	Radiation induced absorption
RIL	:	Radiation induced luminescence
RL	:	Radioluminescence
RS	:	Relative sensitivity
SD	:	Standard deviation
SDD	:	Source to detector distance
SEM	:	Scanning electron microscopy
SMF	:	Single mode fibre
TC	:	Trapping centre
TDT	:	Thermally disconnected trap
TL	:	Thermoluminescence
TLD	:	Thermoluminescence dosimeter
TSC	:	Thermally stimulated conductivity
TSEE	:	Thermally stimulated exoelectronic emission
TTP	:	Time temperature profile
UH NA	:	Ultra-high numerical aperture
UMMC	:	University of Malaya Medical Centre
XRS	:	X-ray source

CHAPTER 1: GENERAL INTRODUCTION

1.1 Overview

1.1.1 Radiation dosimetry

There is an essential need to measure the amount of energy deposited in the matter known as "dose" from ionizing radiation, since changes or damages in matter are directly proportional to radiation dose. Media subjected to radiation in which the dose should be measured can be instruments such as facilities around a nuclear reactor, spacecraft electronic circuits, radiation shielding around a radioactive source etc. or a biological sample like human tissue. Whatever the media, dosimeter must have some general characteristics allow determination of dose within an acceptable uncertainty. The main dosimeter characteristic is to show a growing response with absorbed dose. This growth may follow linear or non-linear function, the linear one generally provides higher degree of accuracy for dose determination. Another important specification is the reproducibility of the dosimeter response i.e. repeatable response when irradiated to identical dose. Several dependences may role as artifacts by affecting the dosimeter response, i.e. causing response to be not only proportional to absorbed dose. Energy dependence, angular dependence and dose rate dependence are the most common of such artifacts.

Various dosimeter types have been developed that function based on different phenomenon caused by ionizing radiation in different detector materials. As examples, ionization chamber (IC) measures charges created in a gas filled small size cavity, or radiochromic film can measure dose by changes in color as a result of chemical reactions caused by radiation. Luminescent dosimeters release visible light after being exposed to radiation. In all cases a measurable change in detector material is observed which is proportional to radiation dose, thus allow for dose assessment. Thermoluminescent

dosimeters (TLDs) that are the subject of this study are described in the following Sections.

1.1.2 Conventional thermoluminescence (TL) dosimeters

The thermoluminescence (TL) characteristics of irradiated solids, insulating or semiconducting materials, were first enunciated in 1946 via a model of electron traps in crystalline media (Garlick & Gibson, 1948; Herman & Meyer, 1946), the release of light by such media occurs when subjected to high temperatures. The efficiency of release depends on the distribution of trap depths, the emission spectrum related to the conversion of deposited/trapped energy into light via the release of electrons from these defects. Subsequent application of TL phenomena in radiation dosimetry, first referred to in the 1950's, was direct recognition of the utility of the accumulation of this trapped energy (Daniels et al., 1953). Since then and now for more than a half century thermoluminescence dosimeters (TLDs) been utilized as convenient, cheap and reliable dose measuring tools. Most of the traditional TLDs are formed from familiar phosphors such as CaF_2, Al_2O_3, LiF, incorporating impurities that include Mg, C, Mn, Cu etc. The commercial forms of these go by names such as: TLD-100, TLD-200, TLD-300 and so on. These commercial TLDs have a range of desirable characteristics, primarily linear response with respect to absorbed dose, appropriate sensitivity (offering a TL yield that suits the needs of particular applications), reproducibility and stability (against appreciable fading). A brief list of widely used conventional TLDs with their TL properties has been documented in Table 1.1 (Chen & McKeever, 1997).

Table 1.1: A list of popular commercial TLDs from (Chen & McKeever, 1997)

Phosphor	Commercial names	Main TL peak (°C)	Main emission (nm)	Z_{eff}	Max sensitivity	Linear dose range (Gy)	Saturation dose (Gy)	Energy response (30 keV/^{60}Co)
LiF:Mg,Ti	TLD-100	~235	415	8.2	1	5×10^{-6}-1	$\sim10^{5}$	1.3
LiF:Mg,Cu,P	GR-200	~210	410	8.2	~35	3×10^{-6}-10	~10	Anomalous
CaF_2:Mn	TLD-400	~310	495	16.3	~7	10^{-5}-10	$\sim2\times10^{2}$	~13
CaF_2:Dy	TLD-200	~185	480.575	16.3	~30	10^{-5}-10	$\sim5\times10^{2}$	~13
CaF_2:Tm	TLD-300	~170	360.450	16.3	~3	1-10	~10	~13
Al_2O_3:C	TLD-500	~210	420	10.2	~30	10^{-6}-10^{2}	~50	~2.8
Al_2O_3:Mg,Y	D-2/D-3	~280	320	10.2	~1	10^{-3}-10^{4}	$\sim10^{4}$	~2.8
$CaSO_4$:Dy	TLD-900	~225	480.575	15.5	~50	10^{-6}-10	$\sim10^{5}$	10-12
$Li_2B_4O_7$:Mn	TLD-800	~190	600	7.4	~0.4	10^{-4}-3	$\sim10^{4}$	~0.9

In spite of many successful applications of conventional TLDs, there are a number of imperfections in terms of particular therapy and non-therapy applications, a situation which highlights the need for dosimeters that offer improved performance. Among the drawbacks of conventional dosimeters are permeability, low sensitivity at limited dose, saturation of response at very high doses, and spatial resolution of the order of millimeters, each providing limitation in use for particular therapy modalities, as in brachytherapy and small field radiotherapy applications. Consequently, efforts have been made to produce and optimize novel forms of TL dosimeter.

1.1.3 Silica based fibres as TL materials

Various types of material, in different physical and chemical forms have been investigated as TL materials. Silica-based fibres are one of the more recently developed group of materials. They are water-resistant, cost effective and with spatial resolution down to about 100 μm, thus provide the possibility of precision measurement of dose in tissues. The first apparent study reporting the potential of commercial optical fibres as TL materials was that of Friebele in the 1980s (Friebele, 1979). The idea was conceived following the observation of a reduction in the performance of telecommunication optical

fibres when placed in radiation environments (Friebele, 1979; Gilbert, 1982). It was observed that the light absorbing properties of fibre optics change as a function of quality (type and energy) and quantity (intensity) of radiation, such that the absorbed dose from radiation can be estimated in comparing the light absorbed in the optical fibre before and after exposure. However because of prompt post-irradiation fading of the effect, its use did not result in a reliable form of dosimeter. A more favourable alternative for dosimetry is the occurrence of luminescence, an effect that has been shown to be proportional with radiation dose (Marrone, 1983). Optical fibre properties for radiation monitoring are summarized in Table 1.2. One further alternative has the optical fibre connected to a signal carrier that provides for transmission purpose only, the assembly being referred to as an extrinsic sensor (as opposed to intrinsic sensors in which the main traceable phenomenon occurs within the fibre) (Sporea et al., 2012). Various other effects of radiation in optical fibres have been studied, including changes in mechanical, optical and radiative properties, as discussed in brief by Lyons (1986). However, the most well studied characteristics of fibre optics as radiation dosimeters concerns their stable trapping of ionizing radiation in use for thermoluminescence dosimetry.

Table 1.2: Optical fibre properties used in radiation sensing according to functional basis

Sensor type	Observed phenomena	Measured parameter
Intrinsic sensors (the essential interaction for sensing occurs inside the optical fibre)	Optical radiation scattering and signal loss in optical fibre under irradiation	Radiation induced absorption (RIA)
	Radioluminescence in optical fibre during and post irradiation	Radiation induced luminescence (RIL)
	Generation of Cerenkov radiation under charged particle flux in both silica and plastic optical fibres	Cerenkov radiation
	Phase shift variation of a coherent radiation inside an optical fibre under irradiation	Refractive index change
	Shift of the peak wavelength in Fibre Bragg Grating (FBG) under irradiation	Grating peak wavelength shift
	Luminescence at high temperatures after irradiation	Thermoluminescence yield

1.2 Motivation and scope of this research

Silica based TLDs have been focused of numerous research groups in recent years. Although their potential in various dosimetric applications has been proved, there is still a significant gap between the reported works and the practical use of such TLDs in routine dosimetry. Germanium doped fibres have been shown as the most sensitive material among silica fibres [Bradley et al, 2012; Yusoff et al, 2005]. Following the recent report works on silica based TLDs, one of the most sensitive Ge-doped silica fibres with 125 μm diameter is selected for this study. The main objective of this study is to perform general characterisation of Ge-doped silica fibre based dosimeter that can be used in routine dosimetry followed by detail analysis of specific applications. In specific, the objectives of this study can be listed as following:

- To characterize TL response of Ge-doped silica fibre in the entire dose range of use
- To develop a recipe that can be used for preparing the dosimeter for routine dosimetry
- To study different parameters affecting dosimeter response including angular dependence, energy dependence and dose rate dependence
- To access feasibility of the use of dosimeter for routine measurement of dose distribution inside a gamma-ray irradiator
- To characterize and suggest suitability of the fibre dosimeter for INTRABEAM radiotherapy system
- To characterize and compare dosimetric performance of different silica fibres and recommend a suitable fibre dosimeter that can be used for high-dose applications

1.3 Thesis structure

This thesis is written based on the article style method in which each chapter follows the pattern of an independent article. Chapters 1 and 2 present general introduction and literature review, respectively. Chapter 1 (general introduction) includes a general introduction to radiation dosimetry and in specific, thermoluminescence dosimetry and finally about TL dosimetry using silica based fibres. In Chapter 2, more details about the structure of silica fibres and the role of dopants on their luminescence process are presented. Theory of thermoluminescence is also explained in brief in this Chapter. This Chapter is completed with a comprehensive literature review of previous dosimetric characterisation performed on silica fibres which basically is supposed to be extended in this research.

The main body of the thesis is presented in Chapters 3 to 8 including Chapters 3, 4, 5 on general characterisation of Ge-doped silica fibres and Chapters 6, 7 and 8 on characterisation of fibres for specific applications or feasibility studies. General characterisation is including dose history effect, annealing and reproducibility presented in Chapter 3, energy dependence in Chapter 4 and angular dependence in Chapter 5. Chapter 6 describes the use of fibres for dose mapping inside the Gammacell 220 gamma irradiator in comparison with Monte Carlo dosimetry. Chapter 7 includes characterisation of silica fibres for the purpose of *in vivo* dosimetry during intraoperative radiation therapy of breast cancer using the low keV photon field of INTRABEAM system. Detailed characterisation is performed to verify the effect of changes in beam quality and dose rate caused by changing the depth of measurement. The extensive Monte Carlo simulations are also presented to recognize the INTRABEAM radiation field and distinguishing the effects of dose rate and beam quality. Chapter 8 focuses on the use of silica fibres for application in ultra-high dose dosimetry with examining TL response of various fibre types at high dose level from both industrial electron and photon sources. Then more

detailed dosimetric performance of the sample with highest saturation level is evaluated. And finally Chapter 9 presents the conclusion of this research and some idea for further work.

CHAPTER 2: BACKGROUND AND LITERATURE REVIEW

2.1 Silicon dioxide structure and defects

Since the thermoluminescence properties of the silica fibre arise from defects in the amorphous structure of the material, a concise description on the defects generation processes is significant. The repeat unit, albeit forming an amorphous assembly, is formed of one silicon atom at the centre and four oxygen atoms at each apex of a tetrahedron, the molecule thus constituting SiO_4, the basic structural unit of silicate glass and optical fibres. Silica does not produce single molecules (O=Si=O) since double bonds are not created. Si atom with four electron vacancies in outer layer joining to four O atoms each with two electrons ready to share to other atoms, resulted to having O atoms seeking to another Si atom and connecting to another tetrahedron. Eventually, this process produces the net chemical formula: SiO_2 (Figure 2.1).

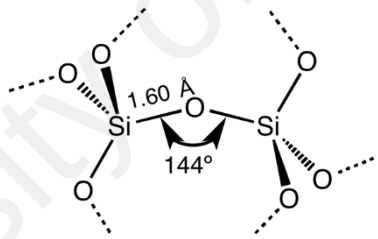

Figure 2.1: Basic structure of α-quartz (the most common kind of crystalline form of silica SiO_2 in normal condition), changes in lengths and bond angles causes the variations in silica structures (picture taken from Wikipedia)

Then depending on the linking procedure of tetrahedrons together, different types of Silica structure may be formed (Salh, 2011). Vacancy of a Si or O atom or presence of any unpaired electrons could results in creation of structural defects in silica structure (Yusoff et al., 2005). More than 10 types of intrinsic defects linked to Si or O atoms have been ever known. Those are usually created in fabrication process and dictated by drawing condition such as temperature, pressure and mechanical tension (Chen & McKeever, 1997; Fitting et al., 2004; Salh, 2011; Trukhin et al., 1998). Various types of spectroscopic methods have been utilized to identify the inherent characteristics of defects

in SiO_2 structure and have yielded valuable vision by finding a large number of defect types, but still have not been able to give a clear model for all of them in silica network. A detailed description about the nature of some known defects can be found in (Salh, 2011, Pacchioni et al., 2000). Existing and created defects in silica structure generally alters all kinds of material properties including TL characteristics. TL generator centers are significantly modified by introduction of impurities in optical fibre structure that are usually added as doping.

2.1.1 Role of dopants

Dopants are basically added to optical fibre core to change the refractive index of the core for transmission purpose, for example germanium (Ge) to increase and boron (B) to decrease the refractive index. It has been proved that presence of impurities is one of the vital factors for the creation of new defects or converting existing defects to other defects, and alter the traps concentration. More than 100 types of defects have been recognized involving the presence of impurity (extrinsic defects) in silica (Salh, 2011). From the viewpoint of signal loss, pure silica is a less vulnerable fibre under irradiation (Griscom, 1985) and it does not show a considerable sensitivity to radiation (Hashim et al., 2010), however, a recent study reported an increasing sensitivity by designing new forms of pure silica fibres like flat fibre (FF) or photonic crystal fibre (PCF) (Bradley et al., 2015) that was referred to the creation of intrinsic structural defects in SiO_2. Even it has been shown (Girard et al., 2006) that the further amount of radiation induced attenuation was occurred under transient exposures (against continuous irradiations) in pure silica glass compared to the Ge-doped fibre. Sensitivity of the TL material to radiation can be greatly improved by addition of dopants, and the amount of improvement depends on the type, concentration and distribution of the dopants. Substitution of the dopant atoms in Silicon sites at tetragonal geometry of silica has been shown using extended X-ray absorption fine structure (EXAFS) method (Yusoff et al., 2005). Addition of dopants can also change

the absorption property of silica fibre, but shows only a small variation when compared with the mass energy absorption coefficient of different doped fibres. Herein, using the elemental data extracted from (Hubbell, 1969) and the $^{\mu_{en}}/_{\rho}$ coefficients obtained via the mixture law (Equation 2.1), a comparison was made between SiO_2 samples doped with identical 5 % doping weight of different elements. The results are shown in Figure 2.2. Only Germanium with considerable higher atomic number indicates a small amount of higher dose absorption in keV energy range. The significant increment of TL yield by addition of dopants is the result of defect generation not the alteration in dose absorption properties. The mass energy absorption coefficient of a compound can be calculated by using Equation 2.1 where w_i represents weight fraction for element i.

$$(^{\mu_{en}}/_{\rho})_{mixture} = \sum_i (^{\mu_{en}}/_{\rho})_i w_i \tag{2.1}$$

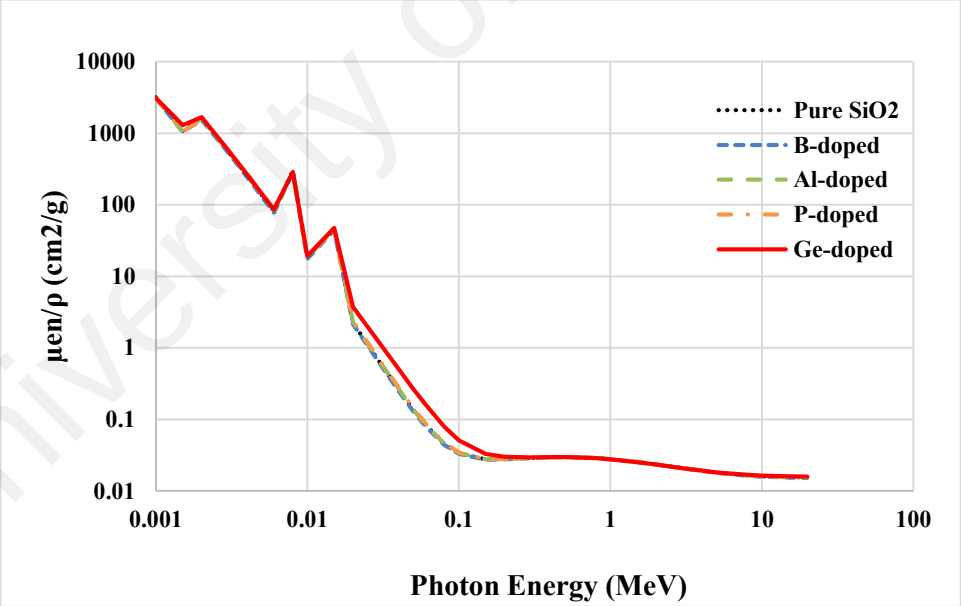

Figure 2.2: Comparison of mass energy absorption coefficient of different doped fibres

2.1.2 Types and concentration of dopants

The effect of doping using different elements including Cu, Ge, Mn, Sn, Zn and Er (Yusoff et al., 2005), Al (Hashim et al., 2009; Yusoff et al., 2005), Nd, Yb and Yb-Tb (Sahini et al., 2014), Tm (Alawiah et al., 2015) and B (Abdul Sani et al., 2017; Mahdiraji et al., 2015) etc. on TL response of SiO_2 has been studied under photon and electron irradiations. Yusoff et al., (2005) showed that doping of silica with some elements (Ge and Zn) does not change α-cristabolite tetrahedral structure of silica while some other dopants such as Cu (I), Cu (II) and Er alter the structure from α-cristabolite to cristabolite cubic structure, albeit with unequal effects. Best results in terms of TL yield has been obtained using Ge and Al-doped fibres, and Ge-doped optical fibres have been confirmed as the most sensitive one in recent years. Thus, most of the recent studies on TL properties of doped glass have focused on Ge-doped fibres. Type and amount of impurity atoms strongly changes the concentration of the traps. Increasing dopant concentration results in TL yield growth up to an optimum amount. After this optimum point (which is different for each type of dopant), the excess increment in dopant concentration leads to decrease the distance between traps (recombination centers) resulting to instability of traps and self-absorption phenomenon. Yusoff et al., (2005) have also presented the optimum concentration of Ge and Al dopants as 0.25 mol% and 4 mol% respectively to obtain highest TL yield by sol-gel method. Variations in TL yield of a specific fibre optic could be the result of non-uniformities in dopant distribution (Hashim et al., 2013). Parameters that affect the dopant distribution in the fibre are fibre drawing condition such as temperature during the fabrication process and shape of the fibre (Lyytikäinen et al., 2004). As for instance, Abdul Sani et al., (2014) have compared concentration of Ge dopants in cylindrical and flat shaped fibres and obtained a very thin Ge-doped region in the flat fibre center which results in a poor TL response, while Begum et al., (2013) studied the effect of increasing core size (doped area in center of the fibre) from 20 μm

in 120 μm fibre to 100 μm in 604 μm fibre and obtained higher response for the larger core size.

2.2 Radiation interaction and energy deposition

Entrance of ionizing radiation into the lattice structure of material (here silicon dioxide) results in various types of interactions in atomic or nuclear scale depending on the type and energy of the radiation. The result of these phenomena is dose deposition in the media. In case of optical fibre, dose deposition causes creation of defects in amorphous structure of the glass and electron-hole transitions between valence band, conduction band and interstitial energy states (preexisting defects). New defects generated by radiation are not stable and will be annihilated in the form of luminescence if the fibre has enough time between irradiations to recover. There is a permanent competition between defect generation and defect annihilation in a lattice under irradiation. Three distinguished processes may occur that results in reducing the number of defects, including thermal annealing, radiation annealing and photo bleaching (Griscom, 1985). Above a saturation dose of the order of kGy (for example 3 kGy is reported in case of P-doped silica fibre (Henschel et al., 1992) permanent defects has been observed to be created in glass lattice. Many earlier studies on optical fibres behaviour under irradiations have surveyed this kind of defect, where it was called radiation damage, because telecommunication properties of fibre were affected by ionizing radiation (Chen & McKeever, 1997; Griscom, 1985; Lyons, 1986). Parameters affecting radiation induced attenuation in fibre optics are including fibre fabrication, fibre composition and dimension, history of thermal and radiation treatments, and elapsed time between exposure and measurement (Soares, 1994).

Fast charged particles may have elastic or non-elastic collisions with atoms in the matter, and initially the amount of energy loss by collisions is very small and increases when particles' energy is decreased. Minimum energy of 25 eV has been estimated to be needed to separate an atom from its place in crystal lattice (Seitz & Turnbull, 1958). This vacancy can be a defect and energy of the separated atom might be sufficient to detach other atoms from the lattice. Energy loss of charged particles in the matter can be as the results of various phenomenon including Coulomb interactions, bremsstrahlung radiation, nuclear interactions and emission of Cerenkov radiation (Tsoulfanidis, 1995). The contribution of each interaction type in energy loss of a particle depends on the type and energy of the particle and the atomic number of the material. Since the basic substance of the glass and fibre optics is SiO_2, the probability of bremsstrahlung production is minimized even for light charged particles like electrons. For alpha and electron beams less than 20 and 10 MeV respectively, one can also assume the negligible portion of energy loss by entering to a nuclear interaction. Cerenkov light signal have been observed in optical fibres under electron irradiation (Lyons, 1986) and luminescence observed at very high dose-rates ($> 10^4$ Gy/s) is that of Cerenkov radiation (Soares, 1994), but its contribution in losing beam energy at usual dose rates may not be significant. The dominant portion of the energy loss is due to the result of Coulomb interactions with atomic electrons that results to excitation and ionization. It is also possible that atoms may be displaced because of the direct momentum transfer from electrons.

The molecular binding energies of SiO_2 (several eV) are negligible against kilo voltage or higher energy photon beams. Outer electrons in an atom (with binding energy less than 0.1 keV for both O and Si atoms) can be considered as free electrons, and they interact with photons via Compton scattering. Innermost electrons which are not involved in molecular interactions of atom, absorb full energy of a photon and are separated via Photoelectric effect. Photons with energy more than of 0.5 keV and 2 keV can detach

innermost electron from O and Si atom (Bearden & Burr, 1967; Cardona & Ley, 1978). Therefore gamma radiation produces ionization and causes a lot of radiation phenomena, i.e. emission of characteristic X-rays. Pair production is the dominant reason for energy loss of the photons in MeV energy range and again results in electrons generating. Secondary electrons produced by photon interactions deposit energy in the matter during Coulomb interaction, thus photons also might be the cause of atom displacements.

Energy of neutrons in the matter is lost by a large number of elastic collisions with nucleus which leads to the creation of displaced atoms. Such wanderer atoms have usually high energy enough to generate other displaced atoms. Existence of hydrogen impurities (OH content in silica fibres) may also contribute in production of recoil protons which have the strong capability of creating displaced atoms. After slowing down, defect generation by neutrons can be more efficient if material includes neutron absorbing elements like lithium and boron (B-doped fibres). Neutrons then be captured by atoms and result in atomic transmutations. Thermoluminescence performance of Ge-doped optical fibres under gamma, neutron and proton irradiations have been studied by Benabdesselam et al. (2013). They have found the same pattern in all TL curves despite the different types of radiation with modest particles' fluence, which indicates that the origin of defects generation in the fibers is dominated by ionization and not by displacement damage.

2.3 Theory of thermoluminescence

Emission of light from specific materials with crystalline structures, after absorption of energy from ionizing radiation is called thermoluminescence, if stimulation of luminescence be caused by heat. The similar phenomenon if caused by ionizing radiation itself or light as the source of energy, are called radioluminescence (RL) and optically stimulated luminescence (OSL), respectively. The current understanding of TL

phenomenon is generally based on energy band theory of solids which tries to explain luminescence observed from different materials (McKeever, 1983). In ideal insulator and semiconductor crystals, only localized energy levels inside valence band and conduction band are allowed for electrons while a forbidden band gap between these two bands cannot be occupied by electrons. Presence of intrinsic defects or extrinsic ones i.e. impurities in the crystalline lattice (usually called activator) cause creation of new energy levels within the band gap, because of production of imperfections in the material structure and eventually allow possession of those energy levels by electrons. Interaction of ionizing radiation with such material excites it with creation of pairs of free electrons and holes (site of electron when it is detached). A portion of charge carriers (electron and holes) may be trapped in metastable energy levels of the band gap during irradiation. Heating of the material then will elevate the energy level of those charge carriers to conduction band where they tend to fall back to valence band or a recombination centre above the valence band again. Eventually a light photon can be produced with an energy equal to energy level difference of trapping and recombination centre. Intensity of emitted light is proportional to the total absorbed dose by the material. A device called photomultiplier tube (PMT) can be used to collect optical photons. A glow curve is usually the result of light collection, counting and its conversion to electric charges. On the material glow curve, temperature in which luminescence is produced, is indicator of trap depth. A simple schematic diagram of TL phenomenon is shown in Figure 2.3 where (A) and (B) demonstrate irradiation and heating stages, respectively. Electron trapping centre, hole trapping centre and recombination centre are abbreviated as ETC, HTC and RC while E and H shows electron and hole created after absorption of energy from ionizing radiation. It should be noted that HTC acts also as RC in this case. During irradiation stage, concentration of charge carriers in trapping centres is increased while it is decreased during the heating stage.

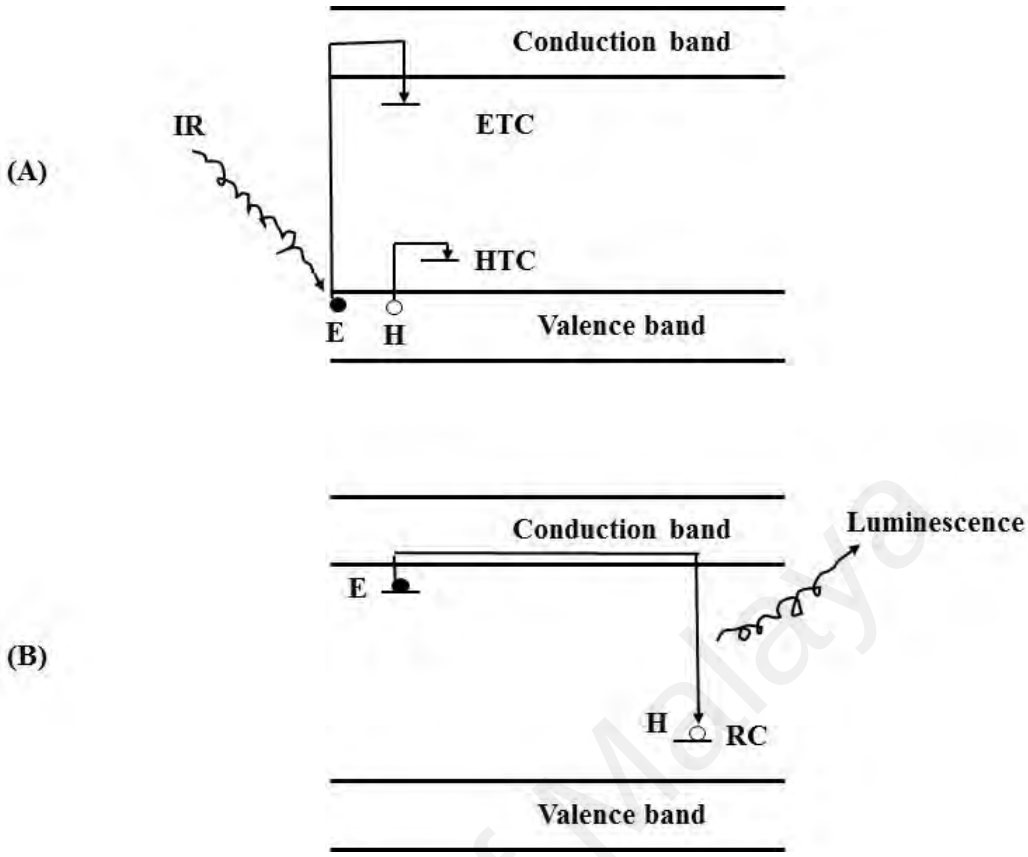

Figure 2.3: Schematic diagram of simple two-level model of TL A) irradiation stage of the TL material B) heating stage of TL material

2.4 Complex TL models

In addition to process shown in Figure 2.3, recombination may take place in electron centre or even valence band. Not all of possible recombination events are radiative and results in photon emission. The model described in Section 2.3 with two energy level is the simplest model that can be used to explain thermoluminescence and obviously is not sufficient to describe thermoluminescence from a real TL material at least because it cannot predict presence of several TL peak in a material glow curve as it is seen in the most popular TLD, LiF, with four glow peaks. Experimental observations have suggested the existence of a range of trapping and recombination centres (Cooke & Rhodes, 1981; Fairhild et al., 1978) as can be seen schematically in Figure 2.4. Presence of several traps with one recombination centre provide possibility of several TL peaks at different temperatures (because of different trap depth), while existence of several recombination

centres (RC) for one trapping centre (TC) allow emission of different energy photons from a TL material (McKeever, 1983).

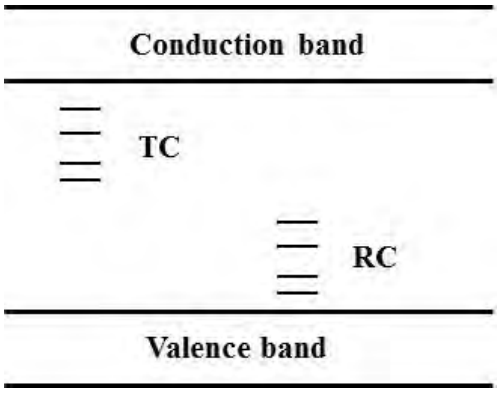

Figure 2.4: Schematic diagram of TL model with multi-level trapping and recombination centres

Broad glow curves observed from polycrystalline or amorphous samples like SiO_2 that do not show distinct TL peaks, are in agreement with expectations from such multi-trap and recombination centres model. However another consequence of this model associated with the release of electrons from trap to conduction band during heating stage and before occurring a recombination event, is observation of a thermally stimulated conductivity (TSC) and therefore increase in conductivity of the material during heating stage. But more detailed examinations showed that TSC and TL curve are not well matched in case of quartz (Medlin, 1968) unlike LiF (Bohm & Scharmann, 1971). Dussel & Bube, (1967) had suggested a band gap model including a thermally disconnected trap (TDT) much deeper than normal traps that can be filled during irradiation stage but not releasing electrons during heating stage like normal (shallow) traps. Incorporation of TDT helps along justification of wide glow peaks of amorphous silica and other experimental observations from such materials. In general, theoretical studies have been made and are still in process introducing more complex models to explain characteristics observed from various TL materials.

2.5 Characteristics of Ge-doped silica fibre (GDSF) TLDs

In spite of many studies conducted on the suitability of silica optical fibres as a radiation dosimeter, the contribution of various parameters and the lack of a proper pre-defined framework for experiments including sample preparation, irradiation set up, read out system and environmental conditions during these stages, a comprehensive integration of the results and predicting the behavior of a particular sample under irradiation is not possible. This can also be due to the limitations of facilities used by different research groups. Thus, the studied characteristics available in the literature are summarized here in a systematic manner. Many studies have been reported the performance of the silica based optical fibres under photon and electron irradiations, but less about other ionizing radiation (alpha, proton, heavy ions and neutrons) was found in the literature.

2.5.1 Sensitivity

Thermoluminescence yield is affected by parameters related to the absorbent media and radiation. Media-related parameters are atomic number and density which affect the absorbed dose and abundance and depth of traps which determine TL response. Type and energy of radiation also determine the deposited energy and TL yield. To compare the TL yield obtained from given samples, a simple quantitative criterion is better to be defined. The common definition of the sensitivity of a particular TLD material is the amount of TL signal per unit absorbed dose and normalized to the unit mass (Chen & McKeever, 1997), which can be expressed by nC/mg.Gy unit and be plotted as a function of absorbed dose in order to show dose response of a given TL material. One may represent the sensitivity of a TL material in terms of the sensitivity of TLD-100 by defining relative sensitivity (RS) (Equation 2.2).

$$RS(D) = {S(D)_m}/{S(D)_{TLD100}} \quad (2.2)$$

Where, S(D) is the TL signal at dose D. Furthermore, heating rate and general TLD readout regime also affect the sensitivity. Espinosa et al., (2006) demonstrated the better sensitivity (1.3 fold) of SiO_2 optical fibres relative to TLD-100. As for examples, relative sensitivity of some recently examined optical fibres, all irradiated at the same condition to identical dose and read out at the same TTP are shown in Table 2.1 (Bradley et al., 2015; Hashim et al., 2015; Mahdiraji et al., 2015b).

Table 2.1: Recent results on the relative sensitivity of some silica fibres

TLD type	Relative sensitivity
Ge-doped capillary fibre	0.10
Pure silica Flat fibre	0.16
Ge-doped fibre (SMF-2)	0.18
Ge-doped flat fibre	0.59
Ge-doped fibre (SMF-1)	3.18

As explained in Section 2.1.2, Ge doping has been approved to create most sensitive silica fibres and a survey in literature showed that Ge-doped single mode fibre (SMF-1) with average 4.9 % Ge weight at the fibre core (Mahdiraji et al., 2015b) has shown the most sensitivity observed from Ge-doped fibres. Therefore this fibre was selected as the main TL material being investigated in this study.

2.5.2 Dose response linearity

A desirable TLD should have a linear response over a favorable range of dose, so wider range of response linearity may promise a potential option for novel applications. TL response of various types of silica fibres with different structures, core sizes, dopant

concentrations etc. have been reported in the literature (see for instance, Hashim et al., 2009; Issa et al., 2011; Ong et al., 2009), but most have been investigated only in the limited clinically used dose range of up to several Gy. For other applications where measurement of high radiation doses is necessary, novel dosimeters that can keep sensitivity and do not be affected by accumulated dose due to radiation damage are still required. Espinosa et al. (2006) reported monotonic increase in response of a 150 μm core SiO_2 fibre up to 10 kGy. Abdul Rahman et al. (2010) reported the linear growth in TL yield with dose range of 1 Gy to 2 kGy for Ge-doped silica fibre and measured 30% loss in TL yield following saturation in 5 kGy dose of synchrotron microbeam radiation with 107 keV mean energy, thus range of linear response and saturation dose of Ge-doped optical fibres might be considered up to 2 kGy (Bradley et al., 2012). However some samples like single mode fibre (SMF-1) reported in (Mahdiraji et al., 2015b) may show a dose dependent behavior and supra-linearity (higher sensitivity at higher doses) even in clinical dose range. Therefore in practical use, pre-determination of the dose dependence is essential for the specific TL material. Also some different doped fibres have been observed that do not show sensitivity in low dose of radiation but become sensitive with linear response at higher dose levels. These types of fibres can be characterized to be used in high dose measurements (See in Chapter 8).

2.5.3 Effective atomic number (Z_{eff})

Interaction probabilities for photons within a medium is determined by the atomic number (Z) of that medium, and for a compound material, a single value of effective atomic number (Z_{eff}) is introduced. It is an important characteristic of a material for dosimetry applications especially for medical uses and indicates its tissue equivalency. The energy-dependence behaviour of a dosimeter is revealed from the deviation in the Z_{eff} of the dosimeter material than that of the tissue (or water), because tissue (or water)

do not show that difference in energy absorption from different energy radiation. Z_{eff} can be estimated by Mayneord equation (2.3) (Khan, 2003).

$$Z_{eff} = \sqrt[2.94]{(a_1 Z_1^{2.94}) + (a_2 Z_2^{2.94}) + \cdots + (a_n Z_n^{2.94})} \quad (2.3)$$

Where, $a_1 \ldots a_n$ coefficients represent the fractional contributions of each element to the total number of electrons in the compound. Some other theoretical and experimental methods have been presented to determine effective atomic number of a complex material (El-Kateb & Abdul-Hamid, 1991; Jackson & Hawkes, 1981; Perumallu et al., 1984), however for the present purpose this equation can provide a good approximation. By using elemental fractions of the samples obtained by SEM (scanning electron microscopy) and EDXRS (energy dispersive X ray spectrometry) analyses, Z_{eff} for various silica fibres has been calculated in several reports (Hashim et al., 2014; Hashim et al., 2013; Ramli et al., 2009) and the obtained values are listed in Table 2.2. Since Z_{eff} of silica fibres is larger than that of tissue (7.4), its energy dependence behaviour should be investigated.

Table 2.2: Calculated Z_{eff} for different silica fibre samples

Sample information			**Z_{eff}**
Fibre type	**Core diameter**	**Dopant concentration**	
Ge-doped fibre	125 µm	0.15 – 0.19 mol % Ge	11.4
Ge-doped fibre	49.3 µm	0.19 – 0.38 mol % Ge	11.93 – 13.41
Photonic crystal fibre	---	Without dopant	10.3 - 11.3
Flat fibre	---	Without dopant	11.3 – 11.8
Ge-doped fibre	20-100 µm	3.23 – 3.85 mol % Ge	13.25 – 13.69

2.5.4 Energy dependence

As it was shown in Figure 2.2, mass-energy absorption coefficient of SiO_2 increases significantly in kilovoltage energy range and especially at energies lower than 100 keV. This is due to the change in interaction probabilities i.e. predominance of photoelectric absorption compared to Compton scattering at low keV energy range. This will subsequently enhance the TL yield from the sample at low keV photon energy range, as instance several fold higher response of fibres to 80 kVp X rays compared to 6 MeV photons has been reported by (Mahdiraji et al., 2015a). However in megavoltage energy range, energy dependence has been reported to be insignificant (Bradley et al., 2015; Mahdiraji et al., 2015b; Ong et al., 2009). In general where a range of ionizing radiation with various energies are to be measured, correction factor for energy dependence at each radiation energy should be measured and applied.

2.5.5 Dose rate dependence

Depart from accumulated dose, the rate of energy deposition into dosimeter has also been reported to affect its response in case of some TL materials (Kvasnicka, 1983). Also theoretical possibility of both increment and reduction of thermoluminescence response with increasing dose rate has been proved (Chen & Leung, 2000). However, Ong et al., (2009) and Noor et al., (2014) have reported independent TL response of silica fibres to dose rate in the range of 179-335 cGy/min and 100-600 cGy/min respectively, which are the usual ranges of dose rate in routine radiotherapy. Abdul Rahman et al., (2011) found 3.4-3.9 % dependence for electron dose rate of 100-1000 cGy/min and 2.4-2.9 % for photon dose rate of 100-600 cGy/min and the trend in both cases of photon and electron beams was yielding higher responses at lower dose rates. Mady et al. (2013) in a more general study showed that dose rate effects may be observed in different fibres depending on the dose range and dopant concentration with the latter one determining the trap

occupation. Therefore, for a specific fibre in a specific application (dose rate range), such effects should be verified.

2.5.6 Angular dependence

Silica optical fibre dosimeters with cylindrical shape are expected to be almost angular independent, if they are positioned perpendicular to the beam direction (Noor et al., 2014) which is due to the symmetry of their both geometry and crystalline structure. However, angular dependence of TL response of fibres in non-perpendicular condition as well as for non-cylindrical shape fibres like flat fibres has not been reported yet.

2.5.7 Minimum detectable dose

The favorable amount of lower limit of dose detection is as low as possible to be appropriate for environmental monitoring (background radiation). This threshold is a sensitivity-related parameter which is also limited by the read out system and regime, and can be estimated as three fold of standard deviation (SD) respective to the background signal of the unexposed TLD. Furetta et al. (2001) suggested the following equation to calculate the detection limit.

$$D_0 = (B + 2\sigma_B) \times F \tag{2.4}$$

Where, D_0 and B are threshold dose and mean TL background signal of annealed but unexposed sample, and σ_B and F are the SD of B and TL system calibration factor (in terms of Gy/TL), respectively. F can be derived from dose response curve of the given material. D_0 calculated by this expression varies by changing in TLD reader system. Hashim et al. (2015) reported the threshold detectable dose of 90 μGy for TLD-100 and 8.22 mGy for pure silica flat fibre. Experimental estimation of these values for TLD-100 and Ge-doped fibre was reported before as 4 and 30 μGy (Hashim et al., 2009).

2.5.8 Glow curve characteristics

Glow curve is a plot of propagated light (luminescence) intensity in terms of applied temperature for releasing trapped energy from TL material. The area, position (T_m) and height of the glow peak depend on intrinsic parameters such as activation energy (trap depth (E)), frequency factor (s) and concentration of traps, all of these are strongly impressible by fabrication process, and extrinsic ones such as heating rate (β) and absorbed dose (Chen et al., 1981). Mentioned trap parameters can be derived from the respective glow curves. For instance, Nicholas & Woods, (1964) presented methods of calculation of activation energies from a TL glow curve, while (Chen & Haber, 1968) expressed that only "initial rise" method is expected to be useful for all possible orders of the process. Each maximum glow peak comes out from a trapping level and each activation energy could be indicative of a defect type. Temperature increment results in exponential rising of the curve because of releasing more trapped charged carriers. This increment in TL intensity continues until the point in which the number of trapped electrons in the metastable state is sufficiently depleted and then the TL intensity falls down. A narrow TL peak obtained from a crystal is related to point defects, but in case of silica fibres, flattened TL glow peaks indicate the extension of traps due to the amorphous structure of the fibre (Benabdesselam et al, 2013a). For Ge-doped fibre, position of the main peak is reported at around 327 °C (Ong et al., 2009) constant for doses from 0.2 to 12 Gy whether from electrons or photons, 257 °C (Benabdesselam et al., 2013a) and 277 °C (Benabdesselam et al., 2013b), with the latter one reported no change in T_{max} with radiation type (γ, neutrons and proton). For the single mode Ge-doped silica fibre studied in this work (SMF-1) the peak has also been reported to be around 277 °C (Mahdiraji et al., 2015b). Variation in heating rate during TL readout process can be the cause of such discrepancies among reports of different groups (Benabdesselam et al., 2014; Furetta, 2010). It is to be mentioned here that in addition to glow curve structure, it is possible to

acquire information about the type of defects in the material by analysis of TL emission spectra of the sample, by the use of a TLD reader equipped with spectrometer to distinguish various emission wavelength.

2.5.9 Signal fading and optical bleaching

Fading is defined as reduction of TL response as a function of time after irradiation process. Presence of low temperature peaks in a particular TL material glow curve indicates shallower trapping levels which results in loss of accumulated energy and faster signal fading. Fading regime of a TLD is fully dependent on structure and defects. Also preserving condition and specifically storage temperature affect the signal fading. Signal fading for Ge-doped silica fibres has been reported 2.5 % in 6 h, 7 % in 30 days (Abdulla et al., 2001) and 20 % after 6 months (Abdulla, 2003). Another study reported fading about 0.4 % per day within the first week and 1.2 % per day in the second week after irradiation for Ge-doped fibre (Bradley et al., 2012). Noor et al., (2012) in a complementary investigation obtained an exponential decay fit that can be used to correct fading effect, the results of signal loss after 133 days was 11 % and 8 % for 9 μm and 50 μm core Ge-doped fibres respectively, that do not seriously differ from that of TLD-100 (5 % in 133 days).

Silica fibres like other TL materials are sensitive to light. 85 % and 96 % signal fading of Ge-doped silica fibre after 1 and 6 hours exposed to sunlight is reported by (Abdulla, 2003), where less degree of bleaching has been observed under fluorescent light. So opaque containers should be utilized for fibre preservation between irradiation and reading stages to minimize TL fading by de-trapping and bleaching (Hashim et al., 2014; Hashim et al., 2015).

2.5.10 Reproducibility

Showing a repeatable sensitivity and the same TL response of a TLD after several irradiation and annealing cycles is usually called reproducibility. It also may refer to repeatability of the response for different samples fabricated from the same preform through the same process to be an indicator of samples uniformity. Several studies measured the reproducibility of Ge-doped fibres TL response over a batch of fibres or after several cycles of usage and reported different values from ±1.5 % (Abdul Rahman et al., 2011) to ±3 % (Bradley et al., 2012), ±5 % (Noor et al., 2014) and 13 % (Mahdiraji et al., 2015b) where the reasons behind these variations remained unclear.

2.5.11 Annealing procedure

Annealing process is one of the most important stages in thermoluminescence dosimetry, since it can alter basic TL properties of the material. There was not found any report in the literature to investigate the proper annealing regime for silica fibre TLDs except the report by Abdulla, (2003) which has explored the effect of annealing temperatures from 100 to 500 °C and annealing times from 10 to 90 minutes and proposed 400 °C for 1 hour as the optimum regime that provides the highest TL response with lowest variation. This procedure has been followed by all researchers so far.

CHAPTER 3: DOSE HISTORY EFFECT, ANNEALING AND REPRODUCIBILITY

3.1 Introduction

Among all events that happen in silica fibres during interaction with ionizing radiation, excitation of electrons from the valence band to metastable states is the principal phenomenon, and they stacked in the trapping centres which results in saving the energy from ionizing radiation that used for radiation dosimetry. This energy can be released in the form of luminescence, immediately (RL) or with a time delay, if stimulated later by light (OSL) or heat (TL). If the intensity of TL increases with respect to absorbed dose, material can be used as a TL dosimeter, as long as the increment of the TL intensity with dose is predictable. However, nature of silica based fibres has been observed to be sensitive to radiation, meaning that structural defects in fibres can be affected by radiation. Lyons (1986) suggested that structure of trapping states in silica fibres may change by creation of radiation induced defects. This phenomenon which is usually called radiation damage (Griscom 1985) can change the sensitivity (amount of luminescence for dose unit) of fibres. Therefore, the reproducibility of the dosimeter response may be challenged by such variable sensitivity. Many investigations can be found in the literature concerning the effect of accumulated dose on sensitivity of different types of dosimeters. Some observations on luminescent dosimeters can be mentioned here for example. Al-Senan & Hatab (2011) reported the sensitivity of OSL dosimeters to show a decrease after every irradiation cycle, resulting in a high uncertainty of 42 % in dose prediction after a high accumulated dose. In case of LiF-TL dosimeters, gradual decrease in response for accumulated dose of 1 to 100 Gy was observed by Janovsky & Ross (1993), and reported 12 % lower response for a 100 Gy dose history. Even a permanent damage in LiF TLDs after accumulated dose of 87 Gy had been reported earlier (Marrone & Attix, 1964).

TL theory has always been utilized to explain different experimental observations on various TL materials, and TL models have been developed to justify sensitization (increasing sensitivity) and desensitization (decreasing sensitivity) of materials subjected to ionizing radiation. Quartz (SiO_2) and alumina (Al_2O_3) have been attracted in most of the experimental as well as theoretical works, due to their interesting properties at different situations. Probably, the first observation on changing the TL sensitivity of quartz by radiation and heat have been reported by Fleming & Thompson (1970) together with the proposal of a dating method based on so called "pre-dose" method. This sensitization was then justified by suggesting reservoir centres acting as deep traps that capture the holes during stimulation caused by radiation, and release them when a high temperature applied in the post-readout annealing stage (Zimmerman, 1971). Zimmerman model was modified by Chen (1979) because another trap was needed in the model to explain the linearity of low temperature peak with the "test dose". Increase in TL response of silica fibres as a result of pre-irradiation is also reported by Ellis et al. (1989). They also conducted spectral analysis and found that a green emission band is responsible for increase in TL response of silica fibre (both RL and TL signals) which also shows linear growth with dose history, finally suggesting a re-readable dosimeter that is useful for high dose applications. Sensitization model was again modified by Chen et al. (1994) by emphasis on the competing trapping states and elimination of the hole reservoirs. In general, models with higher degree of complication were created gradually to explain new experimental observations in different TL materials. For example in a simulation study by Mady et al. (2006), it has been considered a competition between recombination events and re-trapping at deep (disconnected) traps with highlighting the role of thermally stimulated exoelectronic emission (TSEE).

Since silica fibres have been the focus of frequent and numerous investigations (Yusoff et al., 2005; O'Keeffe et al., 2008; Bradley et al., 2012), and in particular, recent works on Ge-doped fibres (Benabdesselam et al., 2013b; Begum et al., 2015; Mahdiraji et al., 2015b) suggested them as advantageous potential radiation sensors, the effect of pre-irradiation or dose history on the TL sensitivity and reproducibility of these dosimeters (which was not found in the current literature) should be studied.

On the other hand, stabilization process of TL response usually necessitates applying special annealing or pre-dose regimes. As for instance, LiF TLDs are exposed by 10^3 Gy dose in order to increase their sensitivity and stabilize their response, and two steps of short and long time annealing procedures are usually suggested (Chen & McKeever, 1997). A relatively comprehensive list of different established annealing procedures for various TL materials can be found in (Furetta, 2010). However, in case of silica fibres, there was not found any comprehensive study on their standard annealing regime. A usual annealing procedure followed by several research groups in the field (Noor et al., 2014; Bradley et al., 2015; Mahdiraji, et al., 2015b) is annealing temperature of 400 °C for 1h, which is probably suggested initially by Abdulla (2003), where he tested temperatures of 100 to 500 °C and found 400 °C to give maximum sensitivity with minimum standard deviation of TL response.

This Chapter is supposed to investigate the effect of accumulated dose in Ge-doped silica fibres (GDSF) for the extended dose range of 1 to 1000 Gy as well as the reproducibility of fibres for successive irradiations at radiotherapy doses. Furthermore, the effect of different thermal treatments on the response of GDSF will be investigated. Expectation is to find an optimum stabilization process that provides maximum sensitivity along with preserving of dosimetric performance of fibres such as linearity and repeatability of the response after successive irradiations.

3.2 Materials and methods

3.2.1 Preparation of silica fibre samples

Different composition/types of silica fibres were used in this study, some were manufactured in-house at Integrated Lightwave Research Group (ILRG-University of Malaya) and some others were commercially available. In general, most of the characterisation part presented in this Chapter is focused on the properties of a very high sensitive Ge-doped fibre with 4.9 % average Germanium concentration at the fibre core. This fibre, a commercially available standard single mode fibre, called here as SMF-1 has a cladding diameter of 125 μm and core diameter of about 8.5 μm. Another single mode fibre (so-called SMF-2) was also used in parts of this study to certify about the generalization of the results. SMF-2 has the same core and cladding diameters as SMF-1. Elemental analysis of SMF-2 using energy dispersive X-ray (EDX) showed the average concentration of 4.3 % Ge at the fibre core. A detailed physical and principal dosimetric characterisation of both fibres has been reported by Mahdiraji et al. (2015b). Si and O are the other compositions of the fibre core with respective average weight concentration of 31.7 % and 63.4 % for SMF-1 and 34.7 % and 60.9 % for SMF-2.

Commercial silica optical fibres have a polymer coating layer to protect inferior parts and also giving flexibility to the lengthy fibres. This jacket was removed using its chemical solvent, chloroform. A cotton tissue was then used to ensure about removal of all polymer material from fibre surface. To form the fibres as dosimeters, a commercial optical fibre cleaver (FC-6M, SUMITOMO ELECTRIC Japan) was used to cut the samples into 5 mm length pieces. Cleaver was modified and adjusted to produce fixed 5 mm samples, because unequal sample length (mass) will result in variation of TL response among samples. Fibre cleaver with 5 mm sliced samples are shown in Figure 3.1.

Figure 3.1: Optical fibre cleaver

The next stage after sample preparation was annealing of fibre samples which was performed using a programmable annealing furnace (CMTS model MB3, Malaysia) shown in Figure 3.2. Samples were annealed at different temperatures and time based on the experimental needs which will be explained in case of each experiment.

Figure 3.2: Annealing furnace

3.2.2 Samples irradiation using Gammacell 220

Gammacell 220 is an industrial gamma irradiator that produces a high dose rate of ^{60}Co gamma rays in its cavity which is used as sample chamber. This machine has various applications in the fields of medicine, biology, agriculture etc. The gamma ray irradiator that used in this study is located at the Physics Department of University of Malaya (See in Figure 3.3). This machine had a dose rate of 2.39 Gy/min at the centre of its sample chamber at the time of this study.

Prior to irradiation, fibre samples were annealed at 400 °C temperature for 1 hour. This is the usual annealing regime for fibres as explained. Samples were then left to cool down to ambient temperature gradually. This was to avoid temperature shock which may affect the TL sensitivity of fibres. Fibres in the groups of 10 pieces, were irradiated to allow averaging TL response over 10 samples. Fibres were attached on small (1.2×1.9 cm^2) paper labels and positioned at the centre of the Gammacell sample chamber to ensure about uniform doses received by all samples. Experimental set up for irradiation is schematically shown in Figure 3.3. All these were performed in order to get more accurate results. Groups of samples were irradiated from 25 s to 7 h to receive doses ranged from 1 to 1000 Gy. A 24 hours relaxation time was considered between irradiation and reading process of all samples in this study to ensure about same signal fading.

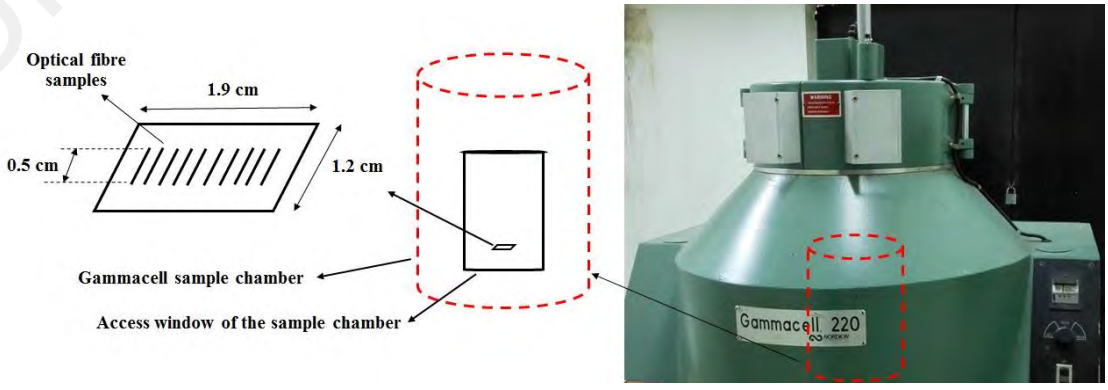

Figure 3.3: Gammacell 220 irradiator and setup for fibre irradiation

3.2.3 TL measurement of the fibre samples

Harshaw 3500 TLD reader (Thermo Fisher Scientific, USA) was used for reading all samples mentioned in this work. This TLD reader is able to heat sample up to 600 °C linearly with heating rates ranged from 1 to 30 °C/s. WinREMS software installed on the computer system enables user to observe glow curve of samples, save and analyze the results of reading. Figure 3.4 shows Harshaw 3500 reader with the screen showing a common glow curve related to a GDSF sample. This reader has a planchet (size of 7×7 mm^2) that allows the positioning of 5 mm fibre samples conveniently. The only encountered problem during the reading of GDSF samples with this reader was the inherent luminescence of the metallic planchet at above 350 °C which also increases with temperature. By the way, TL glow curve of Ge-doped fibre shows a peak around 290 °C which is extended to temperatures beyond 400 °C. Subsequently, it will have an overlap with the background of the TLD reader and since the amount of the reader background quite prevails the TL yield of GDSF and even its variation is comparable with the fibre TL yield, thus it is not possible to distinguish these two signals at temperatures above 400 °C. Therefore, 400 °C was selected as the maximum temperature to read TL yield of all samples in this study. To select the proper heating rate for reading of fibre samples, SMF-1 samples were irradiated for the same dose and read with heating rates of 1 to 30 °C/s. It was observed (Figure 3.5) that increasing heating rate from 1 to 10 °C/s moved the peak temperature (T_{max}) in forward direction, however beyond 10 °C/s to 30 °C/s, there is just a slight increase in peak intensity not T_{max} position. Since heating rates lower than 1 °C/s are not applicable for frequent practical dosimetry (like clinical condition), they were not being tested in this work. Instead a relatively higher heating rate of 25 °C/s was used to preserve the experimental time. Pre-heat temperature was considered 50 °C to allow removal of lower temperature trapped carriers. Therefore total acquisition time of 20 s was needed for reading of each sample.

Figure 3.4: Harshaw 3500 TLD reader connected to WinREMS software

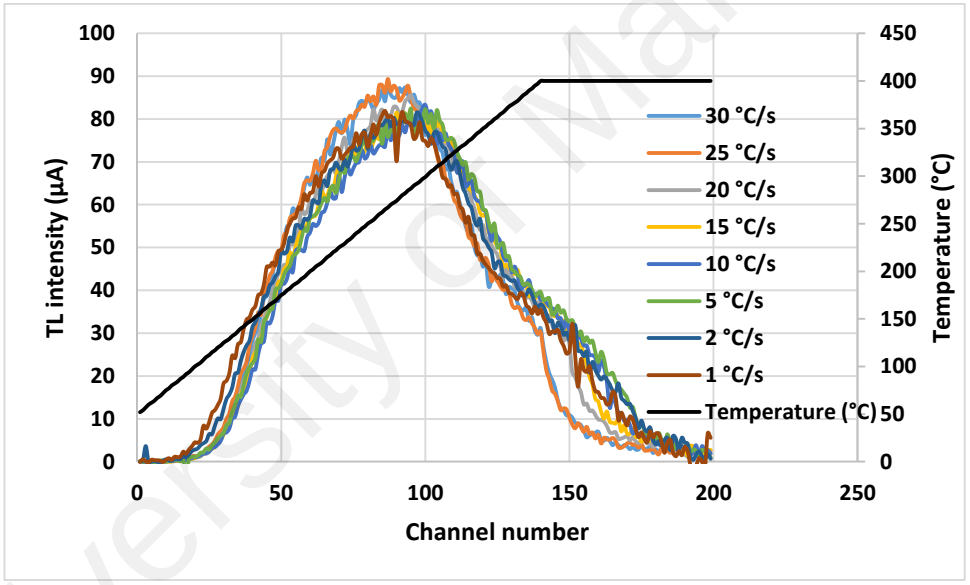

Figure 3.5: Glow curve of SMF-1 for 1 Gy dose obtained at maximum temperature 400 °C with various heating rates

3.3 Results and discussion

3.3.1 Linearity of TL response with dose

TL response of samples in terms of dose for both SMF-1 and SMF-2 fibres in dose range of 2 to 1000 Gy are shown in Figure 3.6. As explained before, 10 samples have been irradiated and read for each point on the plots, then error bars have been used to indicate the variation around the average value of 10 samples.

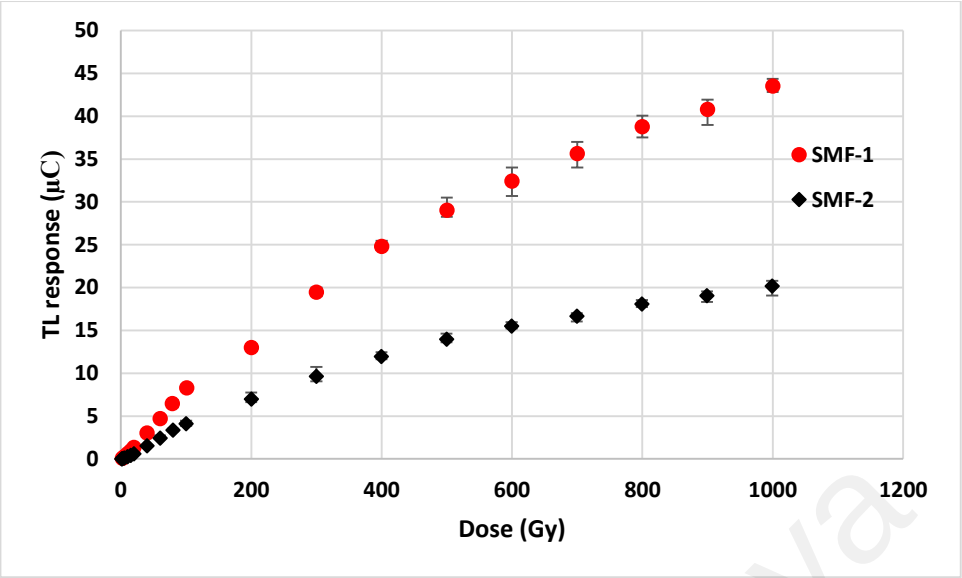

Figure 3.6: TL response of Ge-doped silica fibres for dose range of 2 to 10^3 Gy

Figure 3.7 shows the linearity of the TL response of both fibres with dose at different dose ranges. Therefore, these fibres can be used in a wide range of dose with considering different linearity slopes in their calibration stage. In fact, lower slope at higher doses demonstrate decreasing in sensitivity, apparently starting from 100 Gy for both fibres, however not still resulting in saturation until 1000 Gy.

Samples groups irradiated to doses ranged from 1 to 1000 Gy were then annealed again at 400 °C for 1 h and all were exposed to the same dose of 1 Gy from ^{60}Co gamma rays. Figure 3.8 and Figure 3.9 show the TL response to the second irradiation cycle of SMF-1 and SMF-2 samples, respectively. An increase of TL response with accumulated dose is observed up to 100 Gy for SMF-1 and 20 Gy for SMF-2. TL response of SMF-2 seems to be constant from 100 to 400 Gy and then fluctuates at higher dose histories. Since all samples have been passed an annealing process after their first irradiation cycle, this dependence of the second cycle TL response to previous accumulated dose needs clarification. This may be due to the remaining effect of pre-irradiation on fibres which has not been completely removed during annealing process and material is not returned

to the ground state. A hypothesis is that charge carriers remained in trapping centres have been stimulated during annealing and second irradiation cycle and released from very deep traps to a deep or shallower trap and finally involve in a recombination process in second cycle reading stage.

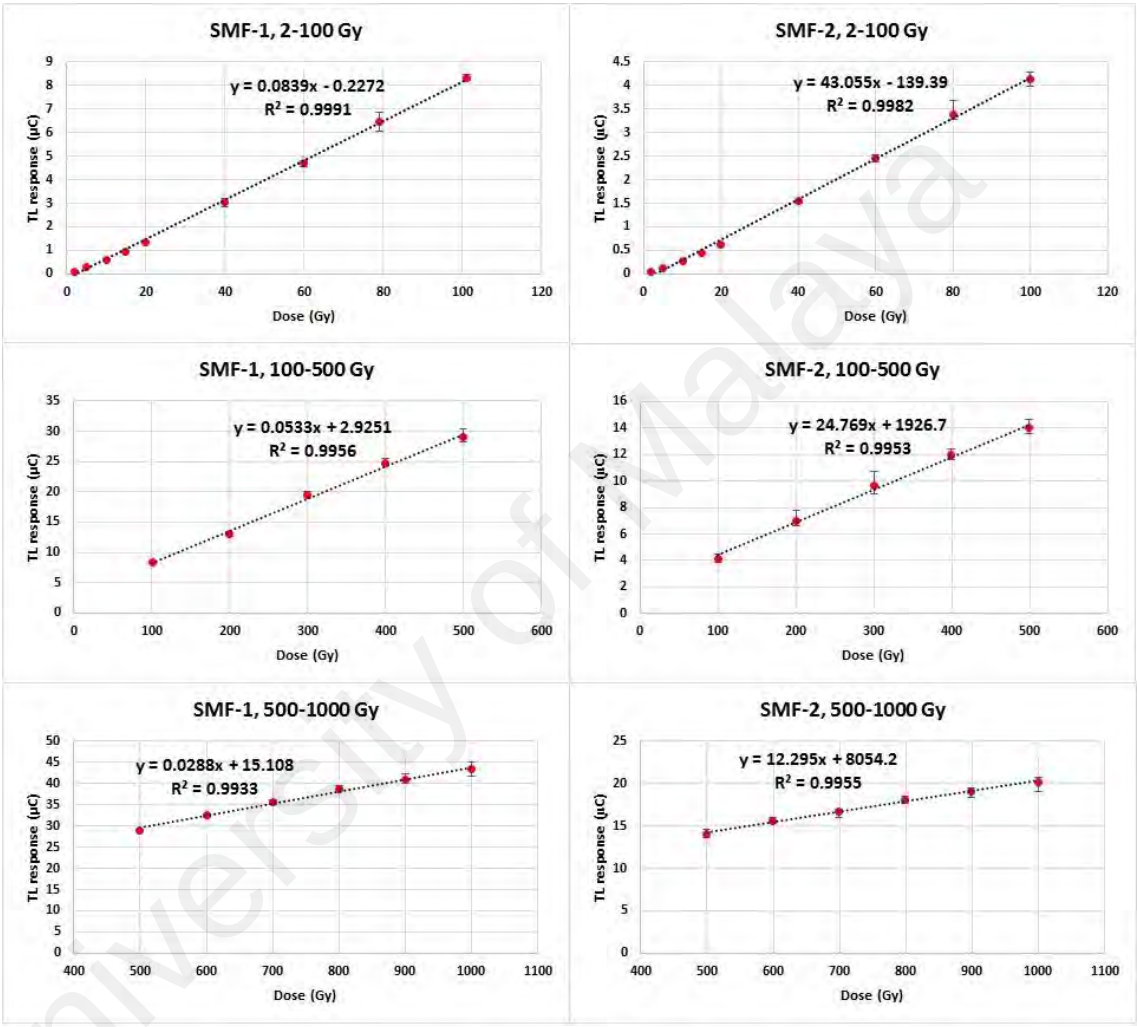

Figure 3.7: Linearity regions in the TL response of SMF-1 and SMF-2

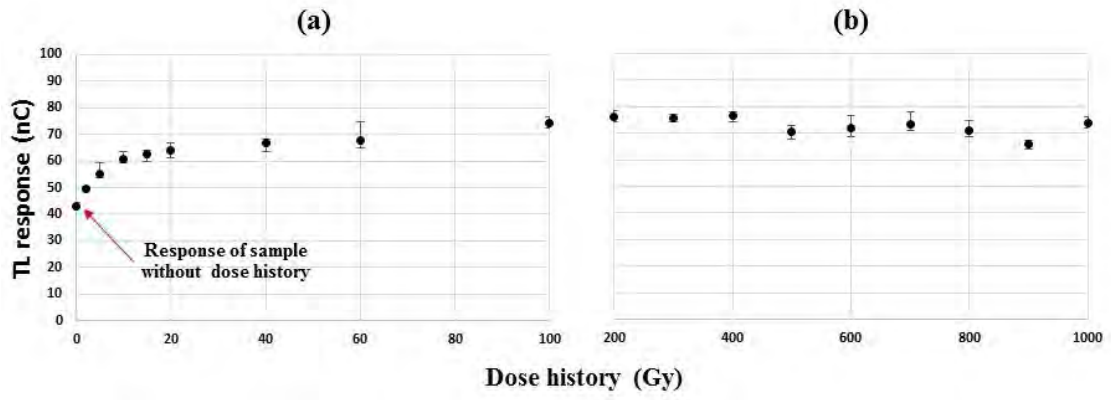

Figure 3.8: Effect of different dose histories a) 0-100 Gy and b) 200-1000 Gy on TL response of SMF-1

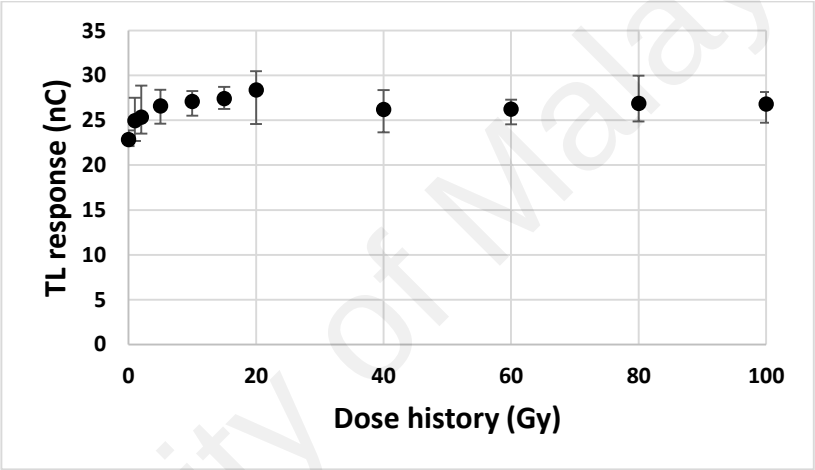

Figure 3.9: Dose history effect for SMF-2 (0–100 Gy)

Another possibility which is apparently more consistent with the TL theory necessitates the presence of deep traps and their contribution in re-trapping process. Chen et al. (1991) developed the TL model to explain sensitization of quartz. Unreleased charged carriers trapped in deep trapping centres are suggested to be responsible for this increment of response. The same trend on the effect of pre-dose has been predicted in a simulation study by Chen & Leung (1991). In more recent simulations of TL phenomenon, such as those conducted by Mady et al. (2006) and Pagonis & Kitis (2012), an interactive multiple trap system (IMTS) is used to explain and predict material behaviour via trapping, re-trapping and recombination events. Stopped increasing

response of SMF-2 at 20 Gy dose history compared to 100 Gy for SMF-1 can suggest less efficiency of deep traps in SMF-2 for re-trapping and contributing in decrease of recombination rate and TL response. In the next Section, TL glow curve of samples in first and second irradiation cycles are investigated for better understanding of the pre-dose effect.

3.3.2 Glow curve analysis

Glow curves of SMF-1 fibres after absorbing radiation dose of 2 to 80 Gy and 100 to 1000 Gy, are indicated in Figure 3.10 and Figure 3.11, respectively. Figure 3.12 and Figure 3.13 also show the glow curves related to SMF-2 for the same dose ranges. The same trend is observed in the shift of the peak position (T_{max}) of both samples. Figure 3.14 particularly indicates this shift respect to dose. T_{max} is going forward to higher temperatures till 10 Gy (309 °C for SMF-2) and 40 Gy (296 °C for SMF-1) and then moving backward to lower temperatures at higher doses till 300 Gy. The peak position then experienced an increment up to dose levels of 400 Gy (SMF-2) and 500 Gy (SMF-1) and the gradual fall to reach to 263 °C (SMF-1) and 278 °C (SMF-2) at 10^3 Gy. Alawiah et al. (2016) have also reported the same behaviour of moving T_{max} backward for Ge-doped flat fibre subjected to ultra-high dose of electron radiation but at dose ranges above kGy. It is interesting that, the trend of shifting the T_{max} position of both fibres follow a similar pattern and increase and decrease at similar dose levels.

Results of numerical modeling, reported by Pagonis & Kitis (2012), showed that changes of the peak position strongly depends on the competition process during TL reading. First increase of T_{max} with dose can be due to the increasing probability of re-trapping events which compete with recombination events. As long as re-trapping is considerable compared to recombination, T_{max} moves toward higher temperatures, because some of the released charge carriers at a given temperature are involved in

another trapping event which eventually might be released at higher temperatures. But at a higher dose level (40 and 10 Gy for SMF-1 and SMF-2, respectively), probability of re-trapping decreases perhaps due to the filling of some deep traps which acted as re-trapping centres, and afterward higher doses will only increase the population of carriers in trapping states and therefore more carriers will be released at any certain temperature, resulting in higher recombination rate and TL intensity.

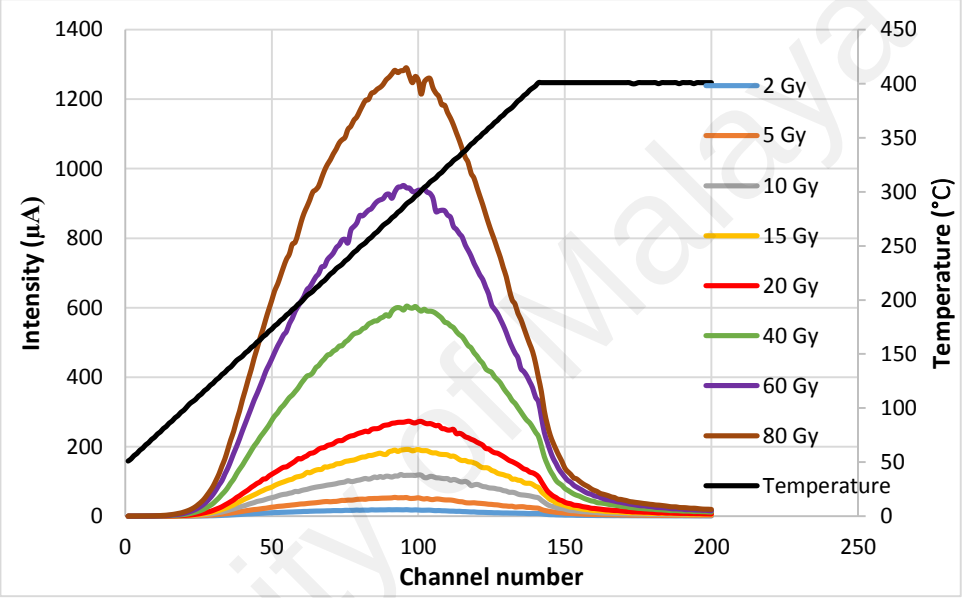

Figure 3.10: Glow curves of the SMF-1 samples for doses ranges from 2-80 Gy

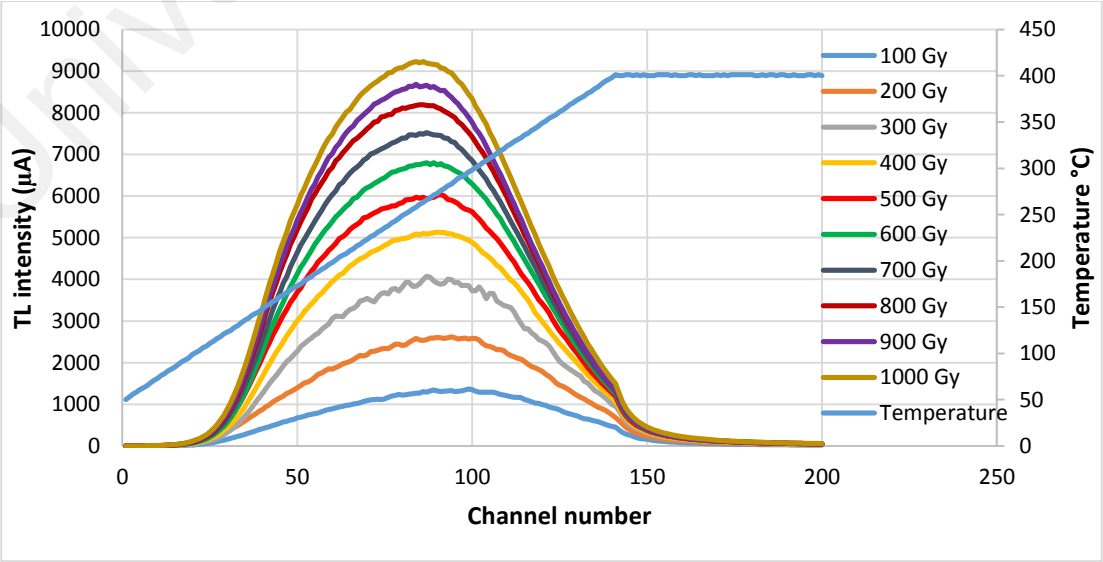

Figure 3.11: Glow curves of the SMF-1 samples for doses ranges from 100-1000 Gy

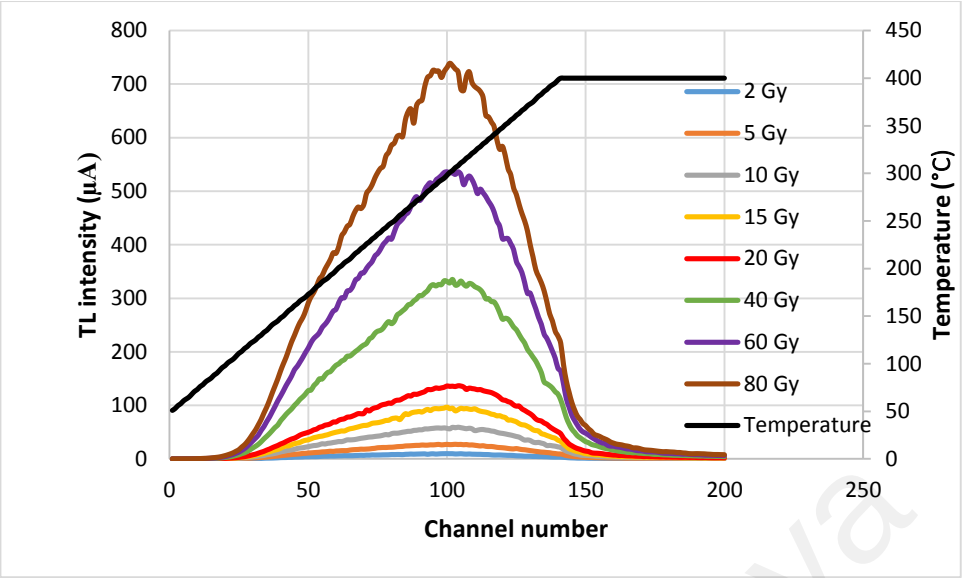

Figure 3.12: Glow curves of the SMF-2 samples for doses ranges from 2-80 Gy

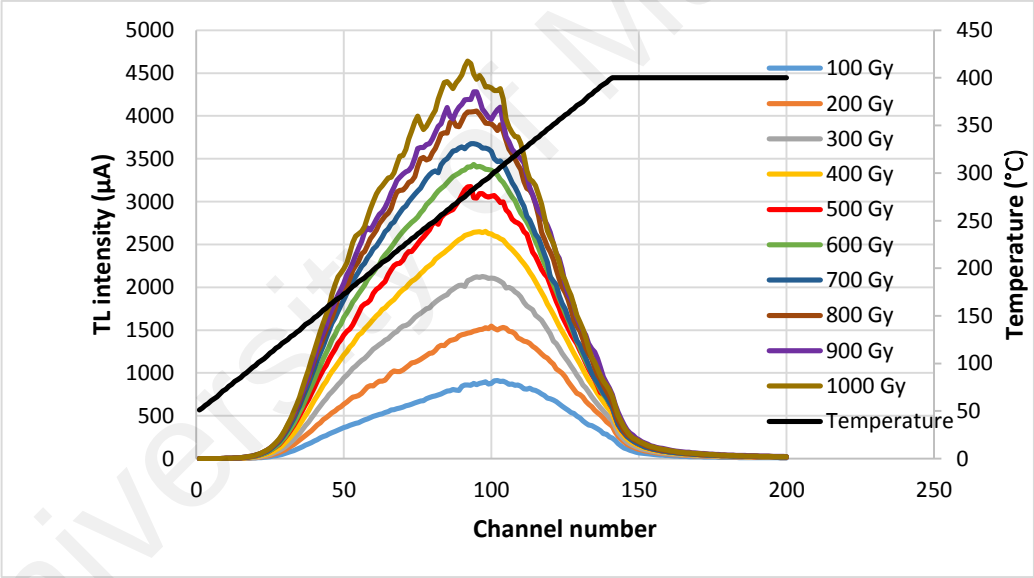

Figure 3.13: Glow curves of the SMF-2 samples for doses ranges from 100-1000 Gy

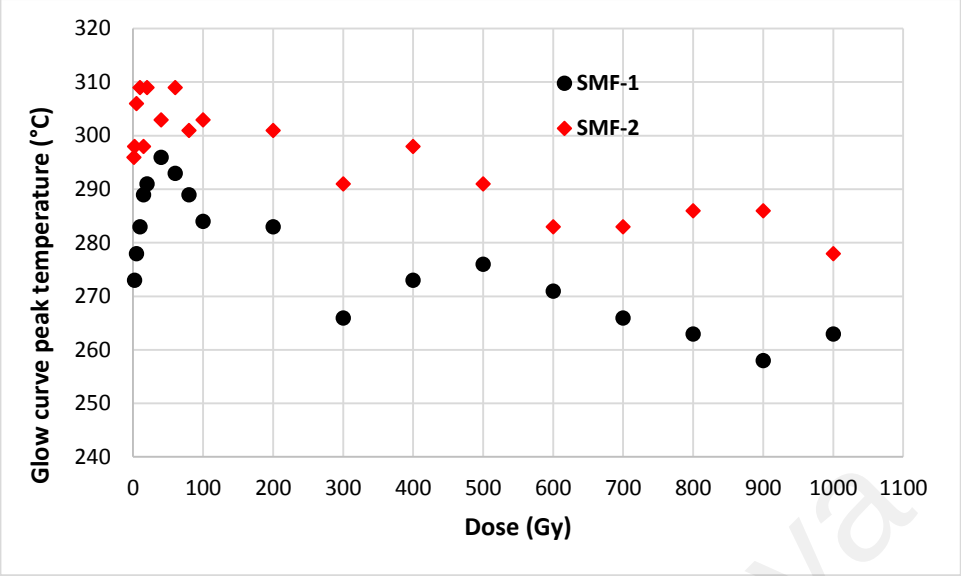

Figure 3.14: Changes in peak position of glow curve in terms of absorbed dose

Glow curves of SMF-1 samples irradiated in the second cycle, all to the same dose of 1 Gy, but with different dose histories (pre-dose) ranged from 2 to 10^3 Gy are shown in Figure 3.15 (0 to 200 Gy) and Figure 3.16 (0 to 10^3 Gy). Glow curves are demonstrated to be compared with the glow curve of un-irradiated sample (zero dose history). Broad TL peaks are usually assumed to be due to the low rate of recombination between electrons and holes, which results in dispersing of recombination events in a wider temperature range. Therefore trapped carriers will be released at higher temperature and TL peak becomes wider. This situation occurs when recombination probability becomes less than re-trapping on active traps. As it can be seen in Figure 3.15, increasing dose history, increases width of SMF-1 glow curve and also propel the T_{max} position. This may be due to deep (thermally disconnected) traps occupation after absorption of a high dose which decrease their potential ability for re-trapping and therefore recombination rate on active trap is increased, resulting in an increase in TL intensity and moving T_{max} forward. Such behaviour of thermally disconnected traps and effect of absorbed dose has been well predicted by numerical modeling (Mady et al., 2006).

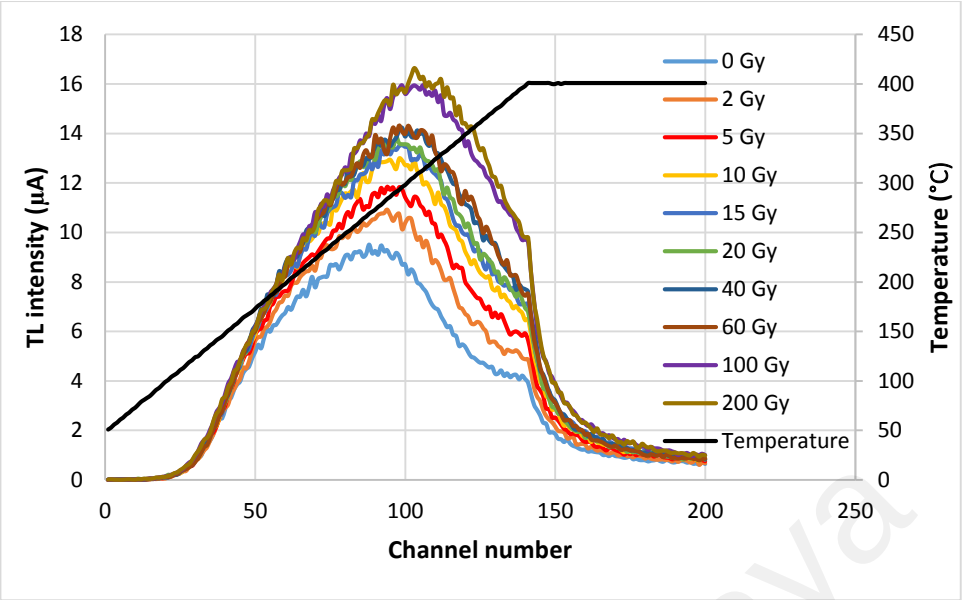

Figure 3.15: Comparison of the glow curves for the SMF-1 samples irradiated for 1 Gy but with different dose histories from 2 to 200 Gy

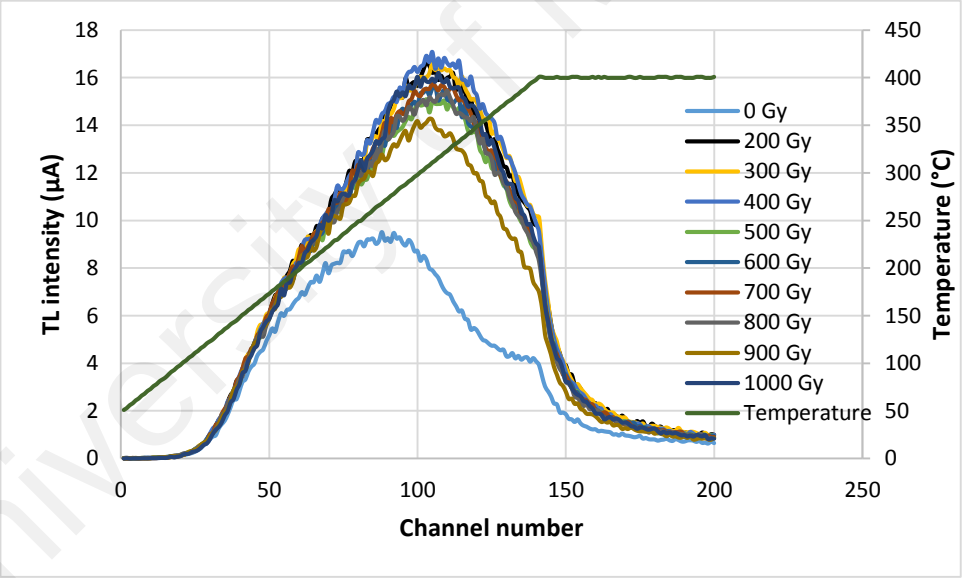

Figure 3.16: Comparison of the glow curves for the SMF-1 samples irradiated for 1 Gy but with different dose histories from 200 to 1000 Gy

As Figure 3.16 implies, increasing peak intensity of the TL glow curve has stopped at 100 Gy dose history and after that just changed at random. Therefore 100 Gy may be considered as the pre-dose level resulting in maximum recombination and minimum re-trapping rate in this material.

Generally, described observations in the glow curves of fibres reflect the effect of deep traps on the TL response in next irradiation cycles. Since these trapping states has not been emptied during the annealing process, therefore annealing procedure of this material needs to be studied.

3.3.3 Effect of annealing

Several groups of fibre samples each including 10 number of samples were prepared and pre-annealed with three annealing temperatures 400, 500 and 600 °C for a constant annealing time of 60 min to check whether the effect of pre-dose can be removed. The same irradiation cycles explained in previous Sections for 400 °C annealing, were repeated for 500 and 600 °C, i.e. in first cycle samples were exposed to different doses ranges from 2 to 100 Gy and after annealing at intended temperature, in second cycle, all samples were exposed to the same dose of 1 Gy. Results of samples reading are presented in Figure 3.17. The annealing temperatures of 500 and 600 °C seem to be more efficient in stopping increment of TL response with accumulated dose. The standard deviation of TL yield among the fibres with various dose history was 1.68 and 1.99 for 500 and 600 °C respectively that suggests 500 °C as a better annealing temperature for removing the effect of dose history in fibre samples. Another significant observation is that even after 500 and 600 °C annealings, TL response of the samples with and without pre-dose is still different and none of the annealing temperatures used here could make the TL response of exposed fibres as similar as a pristine fibre TLD sample.

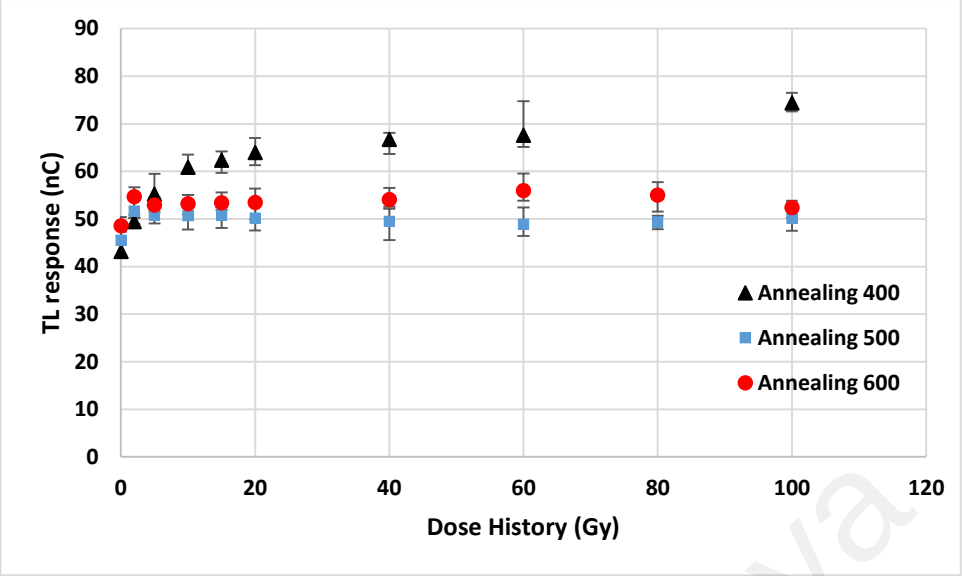

Figure 3.17: Comparison of the response of fibres (SMF-1) with different dose histories annealed at different temperatures (1 Gy test dose)

The effect of fast and gradual cooling procedures combined with different annealing temperatures were also examined, which results are shown in Figure 3.18. To provide for fast cooling, samples were taken out from the furnace immediately after 60 min annealing, while for gradual cooling they were left for 2 h in the furnace with the furnace door keeping open to a small amount to allow for gradual decrease to ambient temperature. To ensure about the results veracity, cooling down tests were repeated twice showing the same TL responses. TL yields of the samples in the first cycle show a slight increment with annealing temperature of 500 and 600 °C compared to 400 °C. Fast and gradual cooling down processes give the same TL response for 400 and 500 °C annealing, however for 600°C, fast cooling results in 8 % higher response. 400 °C is demonstrated to give the minimum amount of variation among 10 samples for both cooling down procedures. Fast cooling increased the variations in case of 500 °C and more significantly in 600 °C.

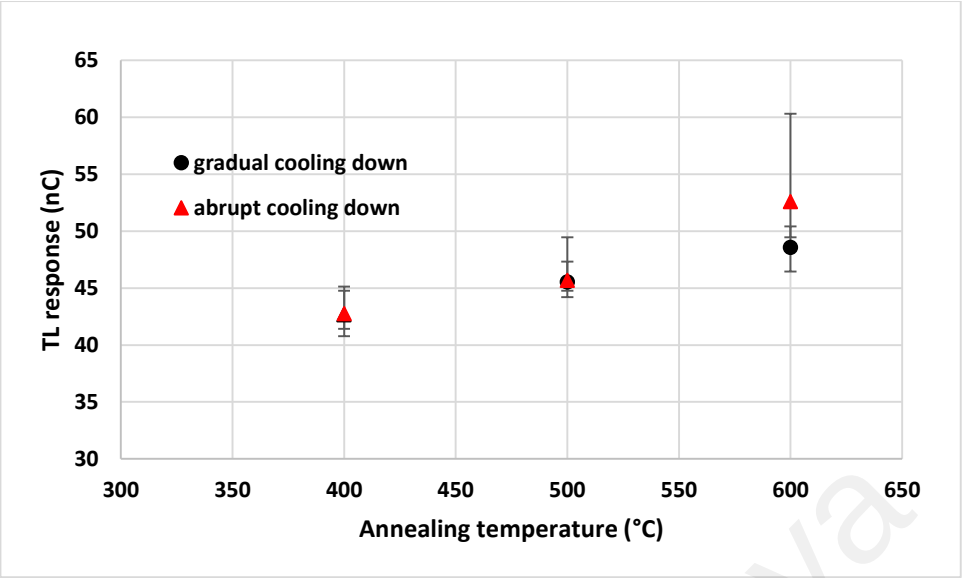

Figure 3.18: Comparison of cooling down procedures at different annealing temperatures on TL response of SMF-1 in first irradiation cycle (1 Gy test dose)

Glow curves of samples annealed at three different temperatures are shown in Figure 3.19. The maximum temperature of TLD reading has been set to 500 °C in this experiment to allow observation of the whole glow curve. To solve the problem of high background of the TLD reader (luminescence from reader planchet itself) in temperatures above 400 °C, the pure background signal was subtracted from the fibres glow curve. However this method is useful for observation purpose in this case, but cannot be implemented for routine sample reading due to the large variation of the TLD reader background at temperatures higher than 400 °C (especially higher than 450 °C), as it can also be seen at the end of the TL glow curve in Figure 3.19. The increase of annealing temperature from 400 °C to 500 °C does not change the shape of the glow curve, however it is seen that 600 °C has added another peak in TL glow curve of this fibre. It should also be mentioned that no sensible difference was found between the forms of the glow curves related to samples cooled down with different procedures. Since 600 °C annealing temperature has changed the shape of the glow curve, the linearity of the response with dose also needs to be checked which will be investigated in Section 3.3.5. Groups of samples were annealed

at 600 °C for different annealing durations of 10, 20, 30, 40, 50 and 60 min to check the time dependence of the creation of the second peak. Figure 3.20 shows that the second peak has been composed even after 10 min annealing time at 600 °C temperature.

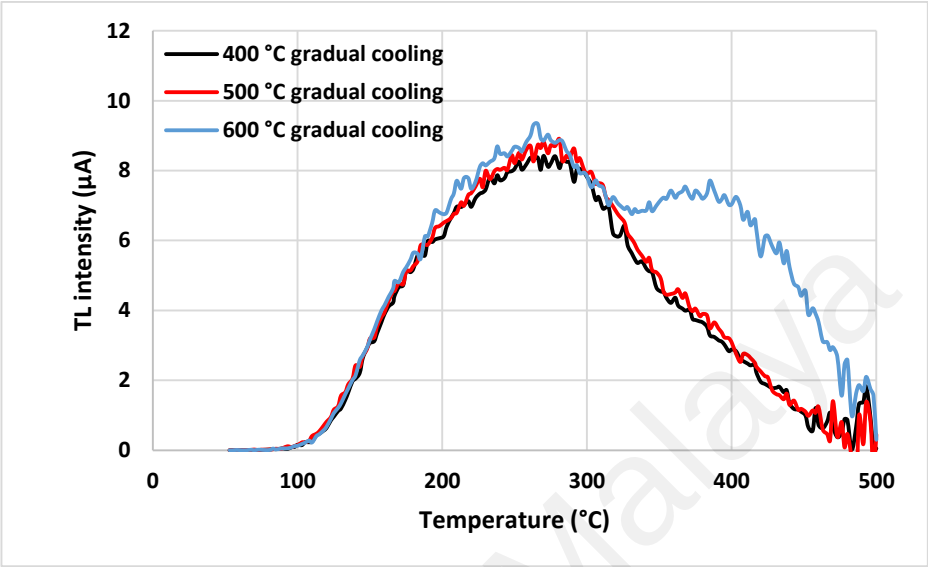

Figure 3.19: Comparison of the glow curves for the SMF-1 samples annealed at different temperatures and irradiated for 1 Gy

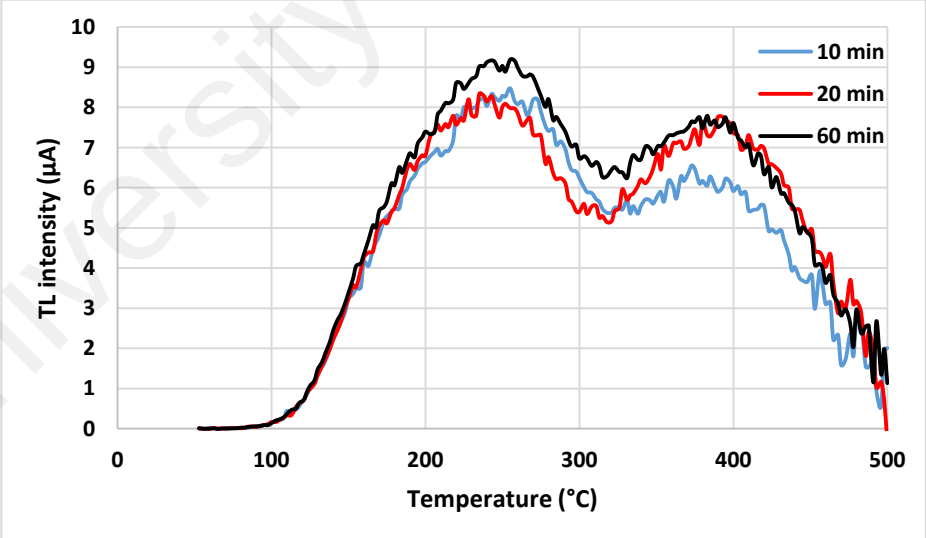

Figure 3.20: Creation of second peak in SMF-1 glow curve due to 600 °C annealing temperature (1 Gy test dose)

3.3.4 Reproducibility

Observations on the pre-dose effect necessitate the study of the reproducibility of fibre response, since practical dosimetry needs a repeatable response of the detector in

successive cycles of annealing, irradiation and read out. A total of 10 pieces of Ge-doped fibre samples (both types) were exposed to 1 Gy dose from the ^{60}Co source. After the usual reading procedure, samples were annealed at 400 °C for 1 hour and these stages were repeated for 10 successive cycles for both fibre types. The results of samples reading are presented in Figure 3.21.

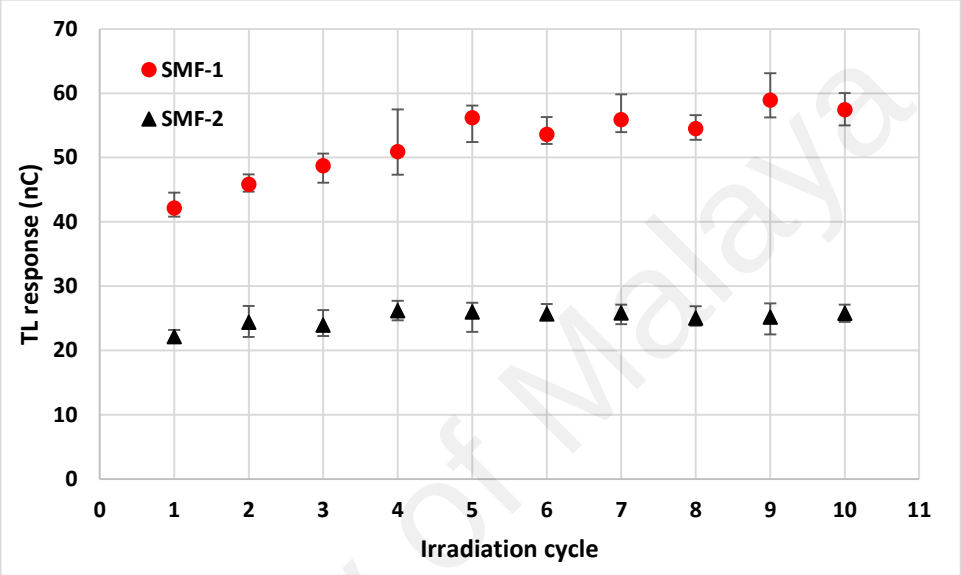

Figure 3.21: Reproducibility test for 10 cycles (before each read out, samples were annealed at 400 °C and exposed to 1 Gy dose)

SMF-1 shows the increase in response in the first 5 irradiation cycles, but SMF-2 just have a negligible growth from first to fourth cycles and then its response become practically constant, while SMF-1 response still fluctuates. This increment in response in first cycles, again reflects the inefficiency of annealing process and can be clarified using the performance of deep traps. Since re-trapping in deep traps is responsible for variations in response, it may be possible to obtain a constant TL response in successive cycles by filling these deep traps (up to their saturation level) via applying a high pre-dose in preparation stage. Therefore 100 Gy and 1000 Gy doses were applied to groups of samples, and then they were examined in the reproducibility test as explained before. The results compared to previous one (without pre-dose) are demonstrated in Figure 3.22.

Samples with pre-dose show the same trend as reported by Chen et al. (1994) related to synthetic quartz. They have also qualitatively justified this behaviour using the competing trapping states with TL model. When the deep traps are empty, they highly contribute to re-trap charged carriers and this will decrease recombination rate and TL response. Each irradiation cycle fills a portion of deep traps and therefore decrease their re-trapping ability, eventually causing an increase in recombination rate and TL yield after any cycle. After a few irradiation cycles where the deep traps saturate, recombination will considerably dominate while re-trapping becomes less effective. Figure 3.22 shows a converse trend in case of samples with 100 and 1000 Gy pre-dose. Since the deep traps are already saturated by initial radiation thereby, the highest recombination rate is observed at the beginning of the reproducibility test. But then, recombination rate is decreased after any cycle, perhaps because of the annealing that has partially release the trapped carriers from deep traps. This initial drop in response in the first five cycles is followed by an almost constant response in the next irradiation cycles. Decrease in TL response of samples with pre-dose would be mainly because of insufficient annealing temperature that cannot completely vacant the deeper traps.

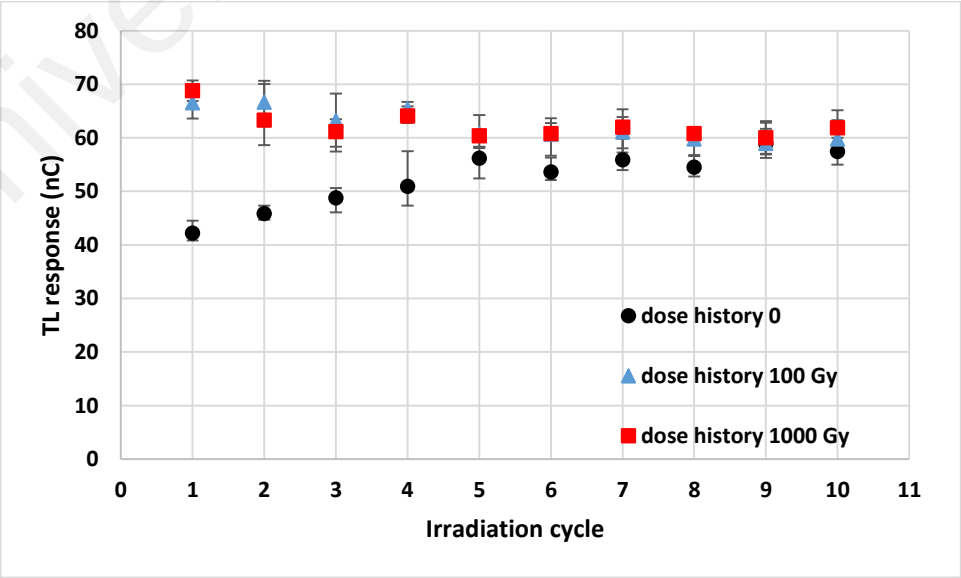

Figure 3.22: TL response of the SMF-1 samples with different dose history in successive irradiation cycles (test dose in all cycles is 1 Gy)

It is also seen that response of samples with pre-dose even after a few cycles and reaching to the stable level is still higher compared to the samples without pre-dose. Chen et al. (1994) have also reported the same pattern in the sensitization behaviour of quartz. But the numerical simulations reported in that work showed that the TL response of quartz with pre-dose and without pre-dose reach to each other after few irradiation cycles. Current results (Figure 3.17) also approved that the fibre with pre-dose, even after annealing at higher temperatures (500 and 600 °C) still showed higher response compared to the fibres without pre-dose. Thus said, this additional response would be due to the radiation damage or creation of radiation induced defects caused by gamma irradiation that change the structural properties of the fibre (McKeever, 1983).

With this description another procedure was tested to achieve a reproducible response from the first irradiation cycle. 10 fibre samples annealed at 400 °C, were exposed to 100 Gy dose and again annealed at 400 °C and further irradiated again to a dose of 10 Gy. The second irradiation was done to decrease the response to the stability level. Samples were annealed for the third time and examined in reproducibility test for 12 cycles with 1 Gy dose in every cycle. The results in Figure 3.23 show a fixed response of these samples at least until 5th cycle with ± 6.27 % variation in response over 12 cycles.

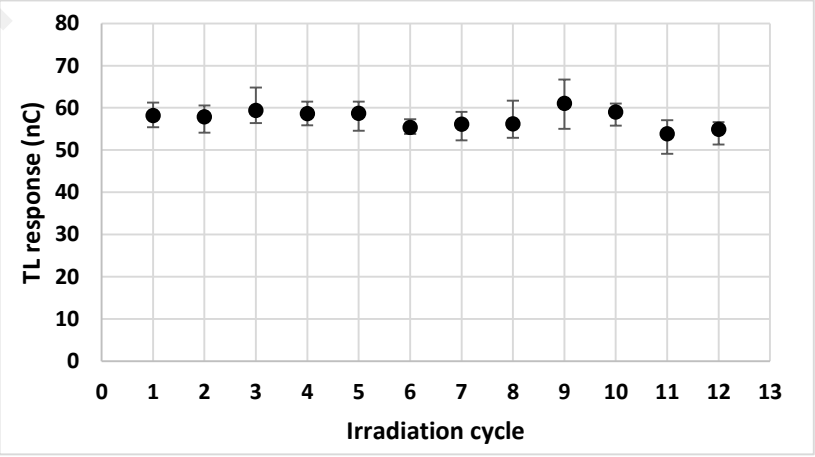

Figure 3.23: Reproducibility test for the SMF-1 samples with dose history of 100+10 Gy and annealing temperature of 400 °C (1 Gy test dose)

Reproducibility test was also performed for samples annealed at different temperatures of 500 and 600 °C. Results displayed in Figure 3.24 suggest that 500 °C temperature is more efficient to keep the TL sensitivity uniform but still does not provide fully repeatable response as slight growth can be seen in the first four cycles. This is probably due to the changes induced by successive cycles of irradiation and annealing, which still cause a low increase in TL response.

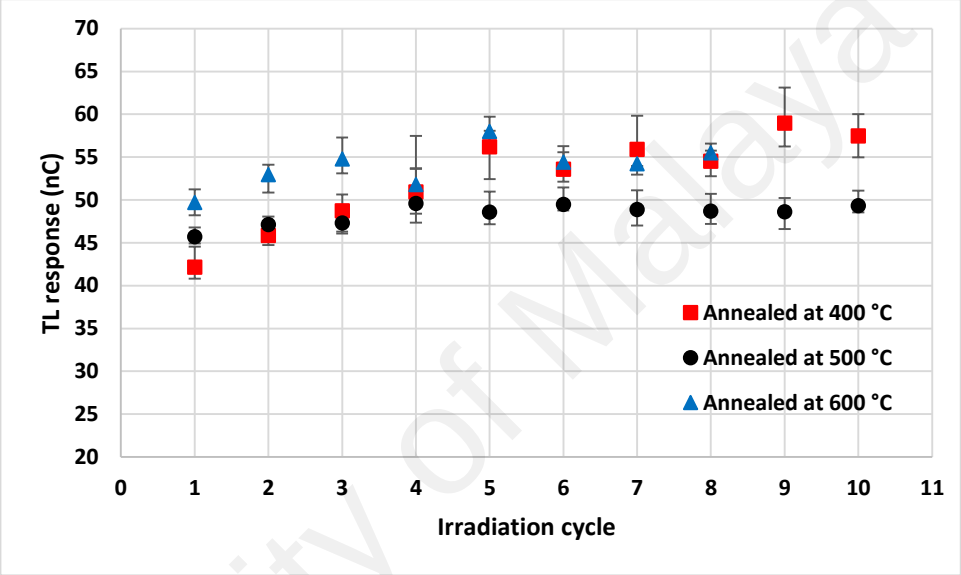

Figure 3.24: Comparison of the reproducibility behaviour of the SMF-1 samples annealed at different temperatures (1 Gy test dose)

Since it was observed that higher temperature can decrease the effect of pre-dose in fibres, thus to control sensitization of fibres and get a reproducible response the same reproducibility experiment were performed using the samples annealed at 500 °C and with different dose histories of 0, 100 and 110 (100+10) Gy. Samples have been annealed at 500 °C in every cycle. The results are shown in Figure 3.25. The variation calculated for the points on Figure 3.25 are ± 4.03 %, ± 2.35 %, and 2.76 % for the 0, 100, and 110 Gy pre-dose, respectively. Therefore, a 100 Gy pre-dose combined with 500 °C annealing resulted the best reproducibility obtained in this work.

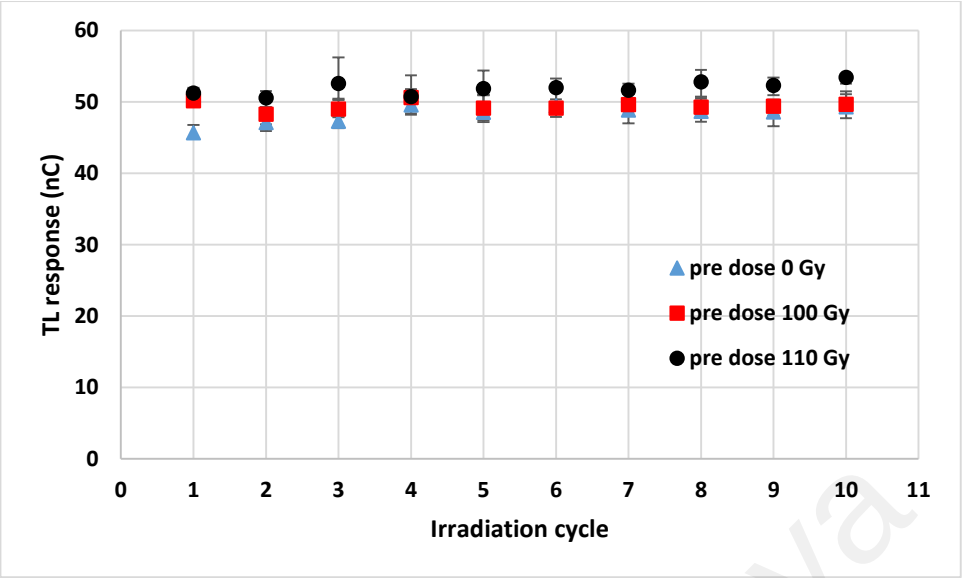

Figure 3.25: Comparison of the reproducibility of TL response related to the SMF-1 samples annealed at 500 °C with different dose history (1 Gy test dose)

3.3.5 Linearity test after pre-dose and annealing treatments

Since stabilization process of TL response of fibres involved in relatively higher annealing temperature as well as a pre-dose treatment, the linearity of the fibre response with dose after such treatments needs to be evaluated. Therefore linearity test was conducted using the samples with different accumulated dose (0 and 100 Gy) and samples annealed at different temperatures (400, 500 and 600 °C). TL response of samples exposed to doses of 2 to 20 Gy are presented in Figure 3.26 and Figure 3.27. The results show that linearity is unchanged and even better correlation is obtained with pre-irradiated samples and also at higher temperatures.

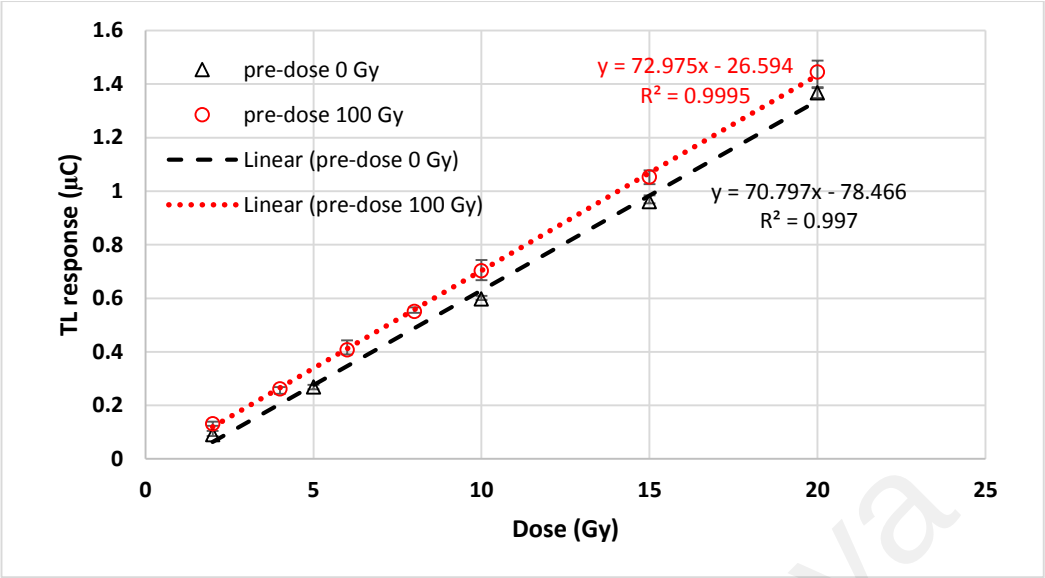

Figure 3.26: Comparison of dose-response linearity between the SMF-1 samples with 0 and 100 Gy dose history

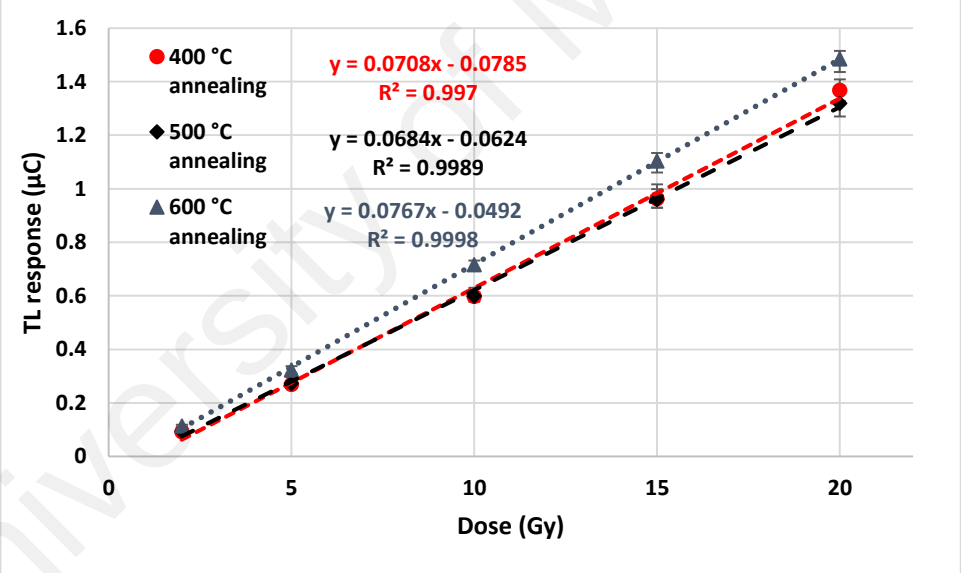

Figure 3.27: Comparison of dose-response linearity among the SMF-1 samples annealed at different temperatures

3.4 Conclusion

Two different aspects of using GDSFs as thermoluminescent dosimeters were studied here. These are including the effect of pre-dose or pre-irradiation and effect of annealing regime on the fibre TL response. In this context, reproducibility of the fibre response during successive cycles of irradiation, reading and annealing was the main

characteristics to be checked, and optimum treatment for stabilizing the TL response to minimize the TL yield variations was the main goal to be achieved. The first experiments showed that accumulated dose (pre-dose) will affect the fibre response in next cycles. Response of the fibres with pre-dose was higher than the pristine samples when they both annealed at 400 °C and this additional response increased with the amount of pre-dose until 100 Gy pre-dose which increased the response to 1.72 fold of the pristine fibre. With variations observed here, not very stable TL response over multiple irradiation cycles obtained. In other words, the response was not reproducible. Glow curves observations revealed that increment in fibre response with dose history is mainly due to the decrease in re-trapping rate by deeper traps when they proceed toward saturation.

An outcome from the comparison of SMF-1 and SMF-2 was that more sensitive fibres to ionizing radiation show higher considerable growth in TL response after receiving a pre-dose. As it was observed, SMF-1 reached to its relatively stable TL response after 100 Gy pre-dose, while SMF-2 with slightly lower sensitivity, just after 20 Gy dose history. Study was extended to find the optimum treatment to mitigate the variations and stabilize TL response.

Considering annealing treatment alone, without applying pre-dose, three annealing temperatures of 400, 500, and 600 °C were applied for one hour duration in which 500 °C was shown to be the most optimum treatment. However, some variations were still observed and the stabilization in TL response was achieved after 5 cycles of 1 Gy irradiation dose. Also gradual and fast cooling methods in annealing were checked and was shown to be not distinct for 400 and 500 °C but considerable in case of 600 °C. Reproducibility test with samples passed to stage pre-dose (100+10 Gy) with 400 °C annealing resulted in ± 6.27 % variation over 12 cycles. Finally a good reproducibility with only ± 2.35 % variation in response was achieved using 500 °C annealing

temperature in combination with a pre-dose of 100 Gy. This optimized procedure for the Ge-doped fibre is not necessarily the optimum regime for other fibre types but, as it was shown for SMF-2, in case of less sensitive fibres variations are expected to be insignificant.

CHAPTER 4: ENERGY DEPENDENCE

4.1 Introduction

Ability of using a new TL material as a dosimeter involves many considerations. One of the most important parameters is the response of sensor to different energy values that is called energy dependence of the response or energy-response. Energy dependence is due to the variant absorption properties of different materials from different radiation energies. The emphasis on the tissue equivalence of a dosimeter is to produce minimum perturbation effect by introducing the dosimeter into the measurement medium but more importantly because of energy dependent response of non-tissue equivalent materials. Mass energy absorption coefficient (μ_{en}/ρ) curve shows significantly higher absorption from photon beams in the energy range below 100 keV (as was shown in Figure 2.2), because of the predominance of photoelectric effect in this region which is more considerable for elements with higher atomic number (Z). Kilovoltage energy range is the energy range mostly used in diagnostic applications and utilization of TL dosimeters in diagnostic applications have been usually an interesting issue (Chappie et al., 1990; "IAEA HUMAN HEALTH SERIES No. 24 ", 2013).

Since the effective atomic number of SiO_2 (11.5-13.4) (Hashim et al., 2013) is approximately 1.5 to 1.8 fold larger than tissue equivalent materials with approximate Z_{eff} of 7.5 (Khan, 2003), it is expected to have different absorption relative to soft tissue, water or air from the same energy spectrum with the large difference in keV energy range. The response of silica fibre TLDs have been proposed in keV energies (Mahdiraji et al., 2015a) and higher response relative to MeV range with a sensitivity even higher than traditional TLDs in several order of magnitude has been reported.

The purpose of work in this chapter is to evaluate energy response of available GDSF at different keV photon energies relative to the reference energy of ^{60}Co gamma rays 1.25 MeV (average of two main gamma lines 1.1732 and 1.3325 MeV). Since dosimeters are usually calibrated at the reference photon energy, correction factors obtained for different keV energies can then be used for energy dependence correction.

4.2 Theoretical predictions

Cavity theories have been proposed to relate the absorbed dose in the cavity to the absorbed dose in the medium by using Equation 4.1.

$$D_m = f_{m,c} D_c \tag{4.1}$$

Where, D_c is the absorbed dose in the cavity and D_m is the absorbed dose in medium material with the same size of the cavity. $f_{m,c}$ is the conversion coefficient which generally varies with photon energy, cavity dimensions and material composition of the cavity and measuring medium. Herein for irradiations in air of silica fibres, air and SiO_2 are considered medium and cavity materials respectively. Based on Burlin's general cavity theory (Burlin, 1966) for cavities small enough compared to the range of electrons (secondary electrons produced by photon interactions) inside the medium, i.e. cavity size many times smaller than the range of electrons, ratio of absorbed dose in cavity to absorbed dose in medium is equal to the ratio of average mass stopping powers (Equation 4.2).

$$\frac{1}{f_{m,c}} = \frac{D_c}{D_m} = \frac{SP_c}{SP_m} \tag{4.2}$$

This ratio is converted to the mass absorption coefficient of the cavity to that of medium, in case of large cavities (cavity size much more than the electron's ranges) (Equation 4.3).

$$\frac{D_c}{D_m} = \frac{(\mu_{en}/\rho)_c}{(\mu_{en}/\rho)_m} \tag{4.3}$$

For intermediate cavities with dimensions comparable with the ranges of electrons, the electrons spectrum inside the cavity cannot be determined by the cavity or medium material individually, rather it should be calculated (Burlin, 1966; Mobit et al., 1996) (Equation 4.4).

$$\frac{D_c}{D_m} = d\left(\frac{SP_c}{SP_m}\right) + (1-d)\frac{(\mu_{en}/\rho)_c}{(\mu_{en}/\rho)_m} \tag{4.4}$$

Where SP_c and SP_m present stopping power of cavity and medium material and d is a weighting factor dependent on cavity size and photon energy. The value of $\frac{D_c}{D_m}$ in Equation 4.4 for very small cavities ($d \rightarrow 1$) approaches to Equation 4.2 and for very large cavities ($d \rightarrow 0$), approaches to Equation 4.3.

The values of stopping powers and mass attenuation coefficients of different compounds at different photon energies was extracted from NIST (National Institute of Standard and Technology) ESTAR (Berger et al., 2017) and NIST XCOM (Berger et al., 2010) databases, respectively. Considering SiO_2 as the cavity material for irradiation being made in air as the medium material, the ratio of stopping powers and mass attenuation coefficients at photon energies ranged from 1 keV to 10^5 MeV was calculated as the results are shown in Figure 4.1. The Figure also shows ratios for Ge-doped SiO_2. The values of stopping power and attenuation coefficients for Silicon dioxide doped with 4.9 % Ge concentration were derived from the same databases, however it could also be easily calculated using mixture law. This is the specification of core of the SMF-1 fibre, which is assumed to produce the main TL response from sample as proved by Mahdiraji et al. (2017).

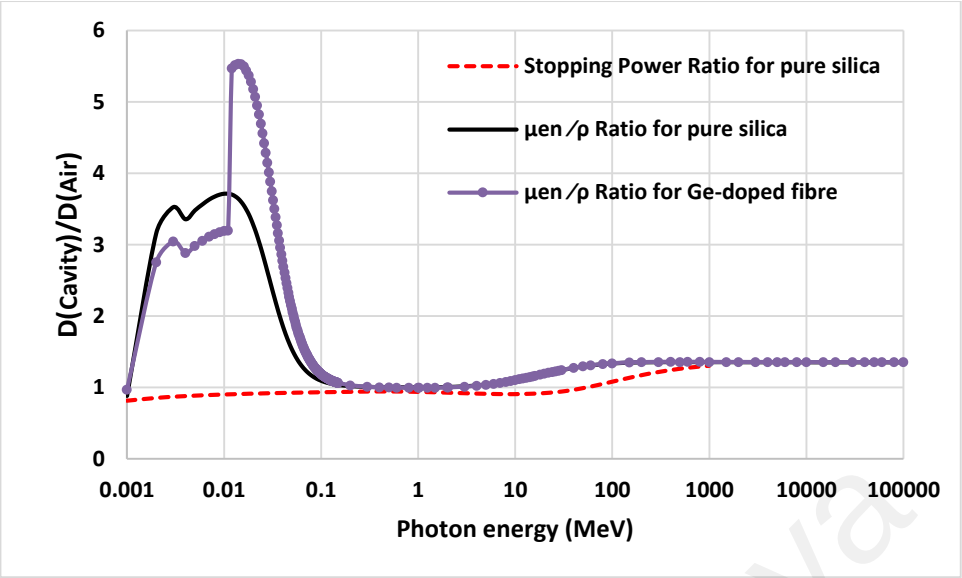

Figure 4.1: Ratio of SP and μ_{en}/ρ of SiO_2 relative to air

Sudden increment in ratio of μ_{en}/ρ for Ge-doped fibre to air at 11 keV photon energy is due to the location of K edge of the Germanium atom at this energy as shown in Figure 4.2. The experimental approach to obtain energy response of Ge-doped fibres at different keV energies relative to reference energy will be explained in the following Section.

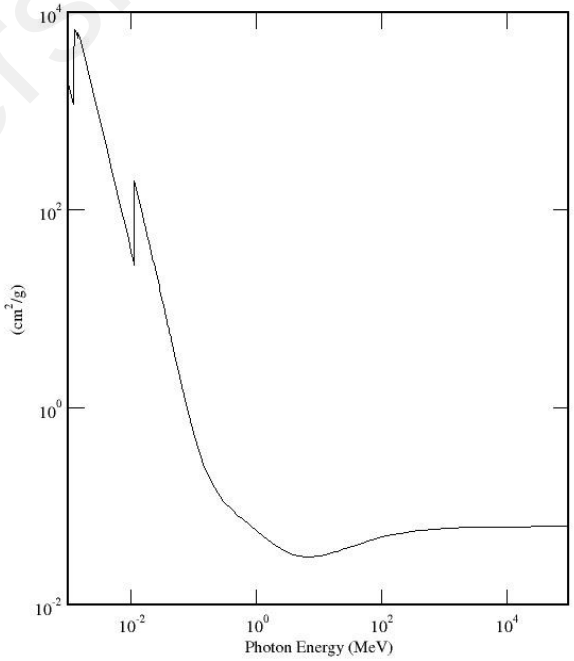

Figure 4.2: Total mass attenuation coefficient of Ge (log scale)

4.3 Materials and methods

4.3.1 X-ray tube

In parts of the study which keV photons were needed for fibre irradiation, ERESCO X-ray generator (model 200 MF4-R, General Electric, Germany) located at Physics Department of University of Malaya was used. This machine can generate X-ray photon energies ranged from 10 kVp up to 200 kVp with the current up to 10 mAs. Photons are created in this tube by accelerating electrons and hitting to the Tungsten target with 20° anode angle. Photons are then filtered by 0.8 mm inherent Be filter plus 2 mm additional Al filter (to remove photons with energies lower than 10-12 keV) before the exit window. X-ray tube with its optical pointer used to determine geometrical centre of radiation field are shown in Figure 4.3.

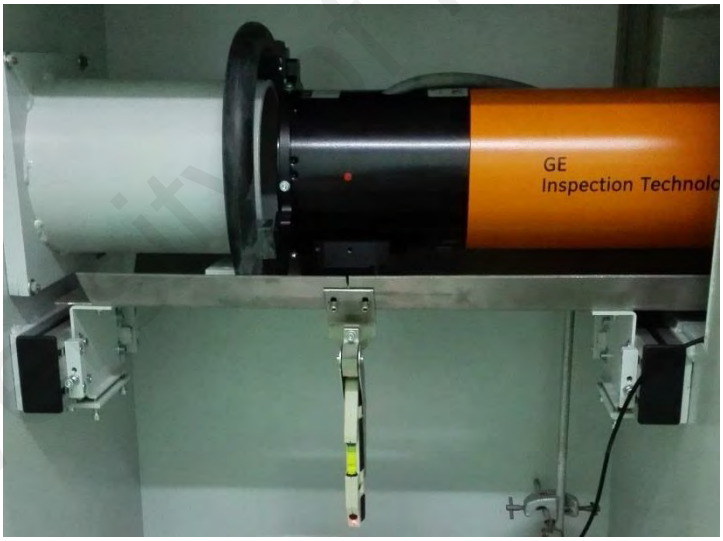

Figure 4.3. ERESCO X-ray tube

4.3.2 Unfors Xi R/F ionization chamber

This detector is a low keV dosimeter manufactured by Unfors RaySafe AB (Billdal, Sweden) that can measure the dose in the range of 10^{-8} to 10^{4} Gy with uncertainty of less than 5% in the energy range of 40 to 150 kVp. Unfors Xi base unit and chamber positioned under the X-ray tube for irradiation are displayed in Figure 4.4 A and B, respectively.

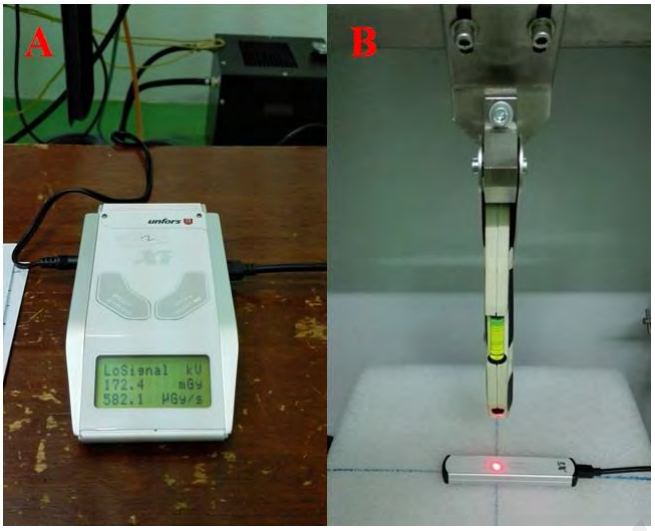

Figure 4.4. (A) Unfors Xi base unit and (B) detector under X-ray tube window

Due to the large variations in the output dose rate from X-ray tube at different distance from exit window (dose rate fall off with distance) and probable effects of such variations on the TL response of the current fibre material which are unclear, dose rates in air produced with different mA and kVp combinations at various distance from X-ray tube exit window were measured using Unfors dosimeter and specific distances and currents that can produce the similar dose rates using different kVp ranged from 40 to 150 kVp were determined. This was done to avoid any additional variation in response caused by dose rate effects and to allow more accurate assessment of energy dependence effect.

4.3.3 SpekCalc program

To provide a general estimation about the output photon spectrum from the X-ray generator, SpekCalc program (Poludniowski et al., 2009) was used. This software allows fast approximation (in a few seconds) of photon spectra from X-ray tubes with Tungsten target considering both Bremsstrahlung and characteristic X-rays. Mean and effective energy of the calculated spectra are presented as well. The calculation by the program covers a wide range of kVp and anode angles ranged from 40 to 300 kVp and 6 to 30°,

makes it proper to be used in this work. Figure 4.5 shows a sample of input parameters in the program for available source and calculated spectrum.

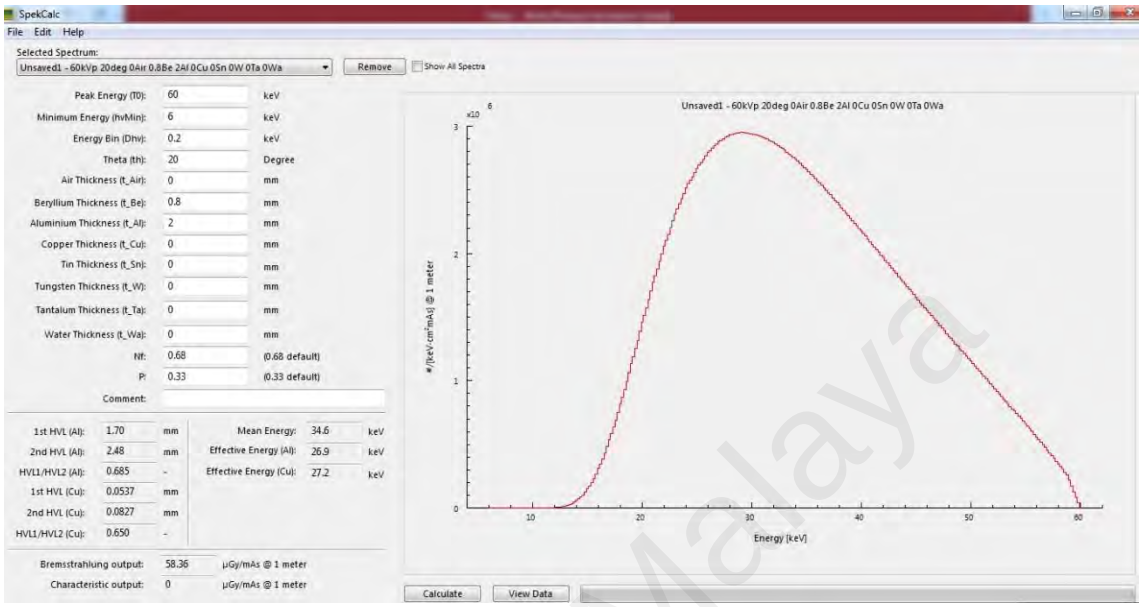

Figure 4.5: Demonstration of the SpekCalc software calculation window

4.4 Results

Calculated spectrums by SpekCalc program for different selected kVp from ERESCO X-ray generator used in energy dependence evaluation including 40, 50, 60, 80, 100, 120 and 150 kVp are shown in Figure 4.6 while Table 4.1 presents the values for mean and effective energies of the spectrums. Mean energy values calculated by program show similarity with beam qualities presented by International Electrotechnical Commission (2005).

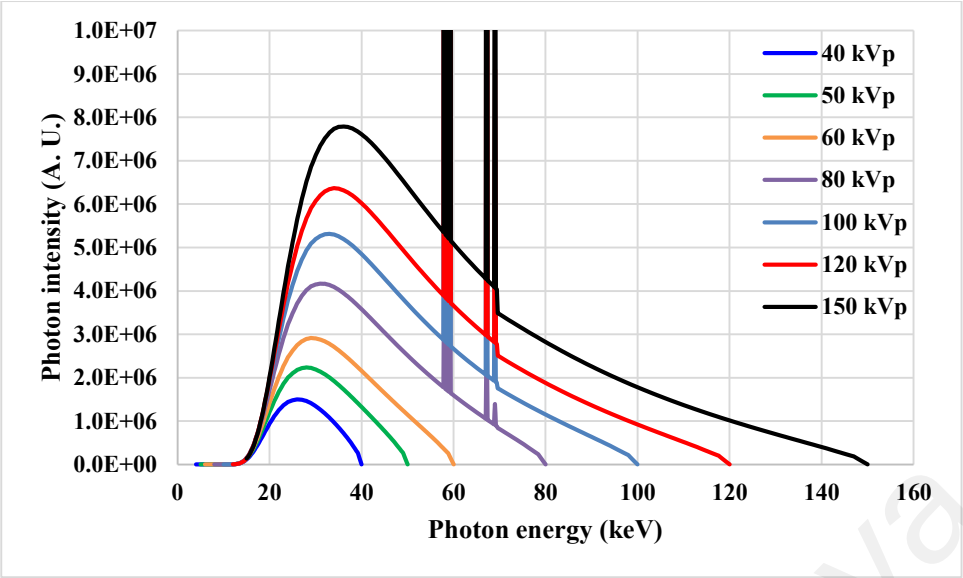

Figure 4.6: X-ray spectrums of various kVp calculated by SpekCalc software

Table 4.1: Mean and effective photon energies calculated for different kVp from the X-ray tube

kVp	Mean energy (keV)	Effective energy (keV)
40	27.3	23.6
50	31.2	25.5
60	34.7	26.9
80	41.2	29.5
100	47.2	32.1
120	52.2	34.7
150	58.8	38.8

Dose rates measured in air at two different distances from Al filter of the X-ray tube are presented in Table 4.2. Different mA values are resulted from inherent limitation of the X-ray tube that decreases mA when increasing kVp to control produced heat. Each measurement have been repeated three times and the dose rate values are the average of those measurements.

Table 4.2: Output dose rates in air from X-ray tube at the centre of the field for various irradiation parameters measured by Unfors Xi R/F dosimeter

kVp	mA	Dose rate (mGy/s)	
		At 11 cm from Al filter	At 63 cm from Al filter
40	10	3.712	0.260
50	10	7.895	0.530
60	10	15.275	1.060
80	7	21.465	1.527
100	6	26.580	1.907
120	5	29.250	2.104
150	4	32.185	2.345

Table 4.3 shows the combination of kVp, mA and distances for energy dependence irradiations to avoid probable dose rate effects. As it can be seen in the Table, dose rates for different kVp just show small variations using selected mA and distances. It should also be noted that the same thickness of air layer was considered in approximation of beam qualities using SpekCalc program listed in Table 4.1.

Table 4.3: kVp, mA and distance conditions used for fibre irradiation in energy dependence test

kVp	mA	Distance (cm) From X-ray window (Al filter)	Dose Rate (mGy/s)
40	10	11	3.712
50	10	20	4.080
60	10	30	4.069
80	7	37	3.976
100	6	41	4.070
120	5	42	4.2075
150	4	45	4.204

10 samples were positioned on paper labels and irradiated for each kVp X-rays (40, 50, 60, 80, 100, 120 and 150 kVp) as well as gamma rays from Gammacell ^{60}Co source, as the method for the latter one was described in Section 3.2.2. Samples were then read at the same readout condition described in Section 3.2.3. TL yields for samples irradiated at different kVp were normalized to the response of samples irradiated by ^{60}Co gamma rays, where the results are shown in Figure 4.7 in comparison with theoretical prediction

as described before. Relatively good agreement is observed between theoretical and experimental results, however it should be noted that mean energy values for each kVp used to display experimental results on the plot are those derived from SpekCalc software, which are only approximated and perhaps not completely matched with the real output spectra from the current X-ray tube. This means that theoretical prediction of energy dependence by the ratio of μ_{en}/ρ can be used as a good estimation.

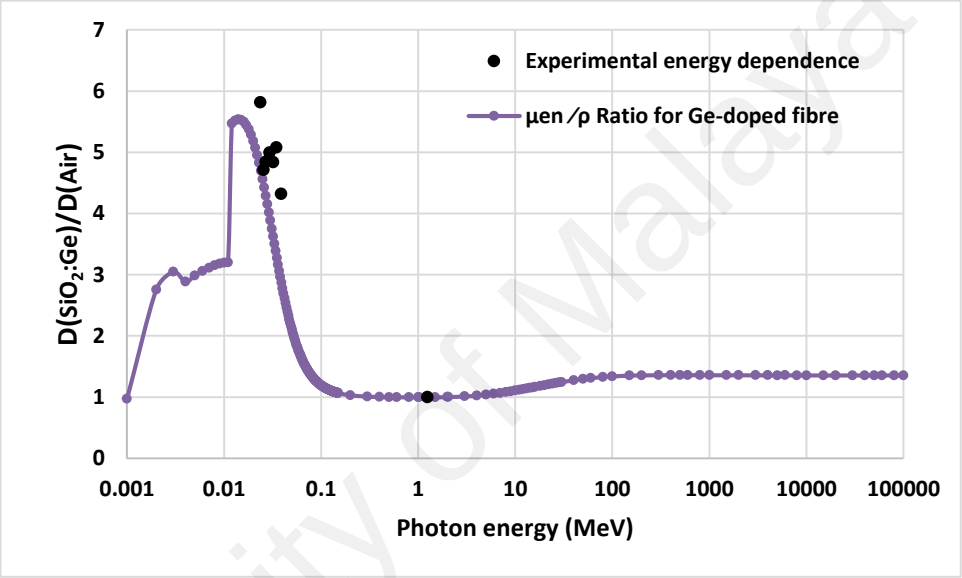

Figure 4.7: Experimental energy dependence in comparison with theoretical prediction for 4.9 % Ge-doped silica

4.5 Discussion and conclusion

However general equation of cavity theory (Equation 4.4) has been suggested to need some modifications (Almond & McCray, 1970; Horowitz et al., 1983), difference between calculated values for dosimeter response do not vary significantly (Horowitz et al., 1983). In addition, it has been shown that by considering photon spectra and mass energy attenuation coefficient of the mean energy instead of maximum energy, there is no need to apply any modifications to the original and simple Burlin expression (Miljanic & Ranogajec-Komor, 1997).

In addition to the approximations made in determination of the keV equivalent to a kVp another possible reason of relative difference between experimental results and theoretical prediction is the assumption of silica fibre size to be large enough compared to the range of secondary electrons in the fibre which is obviously not a quite valid assumption. Therefore Equation 4.4, the general form, is more reliable than the Equation 4.3 to give relative response. Considering Ge-doped SiO_2 as the cavity material for irradiation being made in air as the medium material, $\frac{D_c}{D_m}$ at a given energy (E) relative to the reference energy (^{60}Co gammas with average energy 1.25 MeV) can be calculated by Equation 4.5. This is equivalent to the experimental energy dependence value obtained at different kVp relative to ^{60}Co energy. Thus from the Equation 4.5, the value for d can be calculated for each kVp and for the current fibre (cavity) size, if d_0 be obtained theoretically for the reference energy (1.25 MeV) and be replaced in Equation 4.5.

$$\frac{(\frac{D_{SiO_2:Ge}}{D_{Air}})_E}{(\frac{D_{SiO_2:Ge}}{D_{Air}})_{1.25}} = \frac{\left[d\left(\frac{SP_{SiO_2:Ge}}{SP_{Air}}\right)+(1-d)\frac{(\mu_{en}/\rho)_{SiO_2:Ge}}{(\mu_{en}/\rho)_{Air}}\right]_E}{\left[d_0\left(\frac{SP_{SiO_2:Ge}}{SP_{Air}}\right)+(1-d_0)\frac{\left(\mu_{en}/\rho\right)_{SiO_2:Ge}}{\left(\mu_{en}/\rho\right)_{Air}}\right]_{1.25}} \tag{4.5}$$

Based on Burlin cavity theory (Burlin, 1966), in addition to cavity and medium material, d depend on the size of the cavity, its positioning in radiation field that determines the area exposed to radiation, and energy of the radiation which determines the range of particles in the cavity. The value for d at each incident energy can be calculated by Equation 4.6 where g and β are calculated using Equation 4.7 and Equation 4.8.

$$d = \frac{(1-e^{-\beta g})}{\beta g} \tag{4.6}$$

$$g = \frac{4V}{S}\rho \tag{4.7}$$

$$e^{-\beta R} = 0.01 \tag{4.8}$$

Where β is effective mass attenuation coefficient for electrons in (cm^2/g), g is the average path length of electrons across the cavity in (g/cm^2), V and S present the total volume and surface area of the cavity with mass density of ρ and R is the extrapolated range of electrons inside the cavity material. Equation 4.8 for calculation of β, proposed by (Burlin & Chan, 1967) is not unique and various empirical equations for calculation of β associated with some modifications in Burlin cavity theory have been suggested for different materials and different energy ranges (Miljanic & Ranogajec-Komor, 1997), however the best fit to experimental results have been shown to be obtained by Equation 4.8 and Burlin theory (Shiragai, 1984). Continuous slowing down approximation (CSDA) range was used as R in this equation, because it has been approved as a good approximation for such calculations (Miljanic & Razem, 1996). The values for CSDA ranges at different energies were obtained by interpolating from the values related to default energies extracted from NIST database (Figure 4.8).

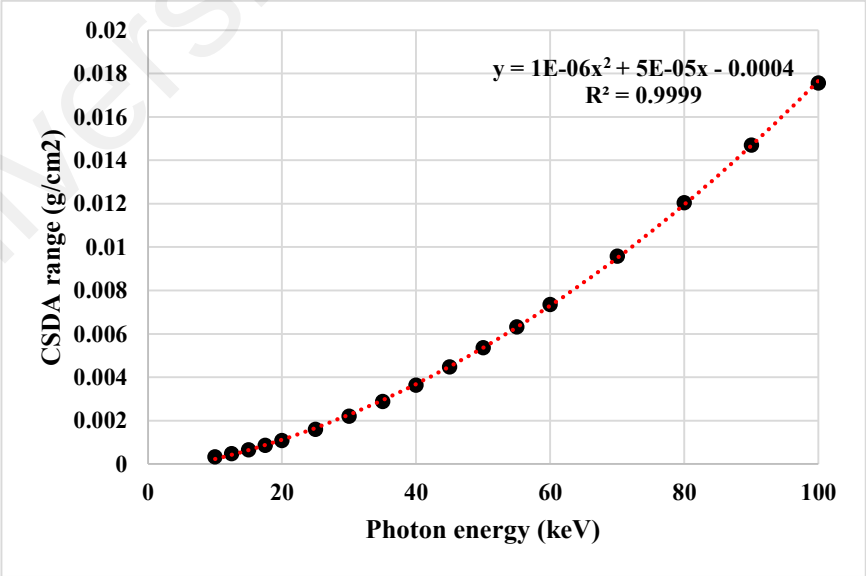

Figure 4.8: Interpolation of CSDA range of electrons in SiO_2:Ge for energy range of 10 to 100 keV from NIST default energies

Denominator in the right side of Equation 4.5 was calculated using Equations 4.6 to 4.8 and the ratio of SP and μ_{en}/ρ for 1.25 MeV photons, obtained from NIST database. To calculate average path length inside silica fibre using Equation 4.7, total size of the fibre and size of the fibre core were considered in separate calculations. The values 0.596 and 0.962 for d_0 were obtained by considering the volume of the whole fibre and the core of fibre respectively. Although, the main TL response of fibre is produced by fibre core, but dealing with cavity theory, where the changes in spectrum inside the medium caused by cavity are important, the total volume of the fibre must be considered. In addition for ^{60}Co photon energy and sub millimeter dosimeter sizes, the first value is in agreement with the expectation (Miljanic & Ranogajec-Komor, 1997), therefore total fibre size was considered as the cavity size in next series of calculations. By replacing $d_0 = 0.596$ and experimental obtained relative responses for various keV (mean energies of Table 4.1) in Equation 4.5, d was calculated for each mean energy. The *d* calculated by this method showed negative values in some cases, while $d_0 = 0.962$ gives negative d values in all cases. Negative d value is unacceptable since based on original definition in cavity theory, it should be a value between 0 and 1. This contradiction can be just caused by the wrong assumption of considering mean energies approximated by SpekCalc program as the alternative mono-energetic beam for kVp spectrum, which reconfirms previous reasoning about deviation from theoretical prediction in Figure 4.7. Then *d* values for various photon energies from 10 to 100 keV were calculated using Equations 4.6 to 4.8 and interpolated CSDA ranges. Using these d values, relative responses were obtained with results shown in Figure 4.9 in comparison with μ_{en}/ρ ratios.

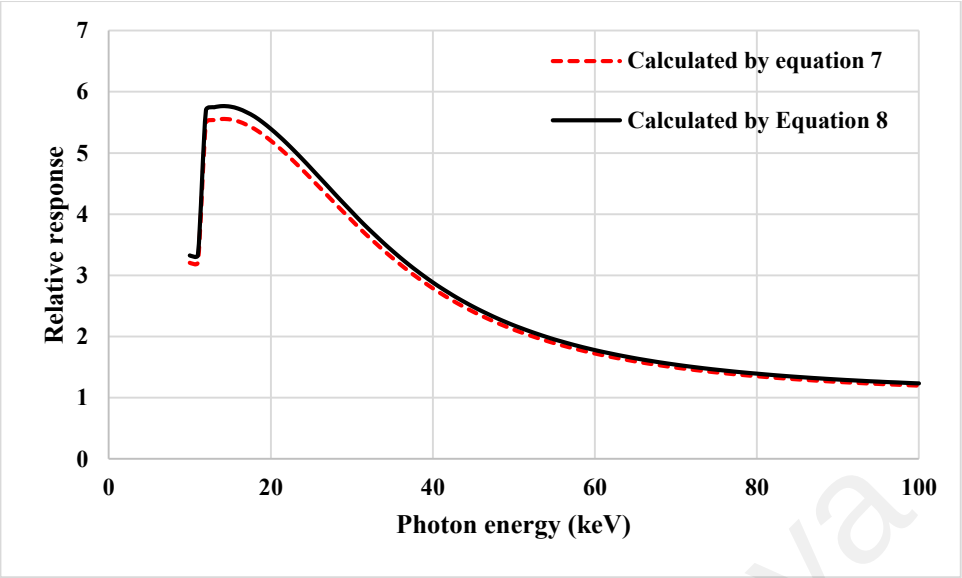

Figure 4.9: Calculated relative response for 4.9 % Ge-doped silica

These results confirm the suitability of the cavity theory expression for large size dosimeters to be applied to assess the energy dependence correction factors at each energy for the size and material of the current fibre dosimeter. The important issue is considering material composition of the sensitive part of the TLD (fibre core with Ge doping), but the total volume of the fibre not only sensitive part to calculate weighting factor (*d*). Figure 4.10 shows changes in calculated d with photon energy and diameter of fibre for 4.9 % weight Ge-doped silica. As it is observed, only for very small cavity thickness (fibre diameter) of 10 µm, contribution of the first term in Equation 4.4 (stopping power ratio) becomes considerable. With increasing the dosimeter thickness, predicted relative response approaches to the ratio of mass energy absorption coefficients. However these changes in *d* do not result in significant variations in the calculated relative response and the ratio of μ_{en}/ρ can still be used to estimate energy dependence of TLD.

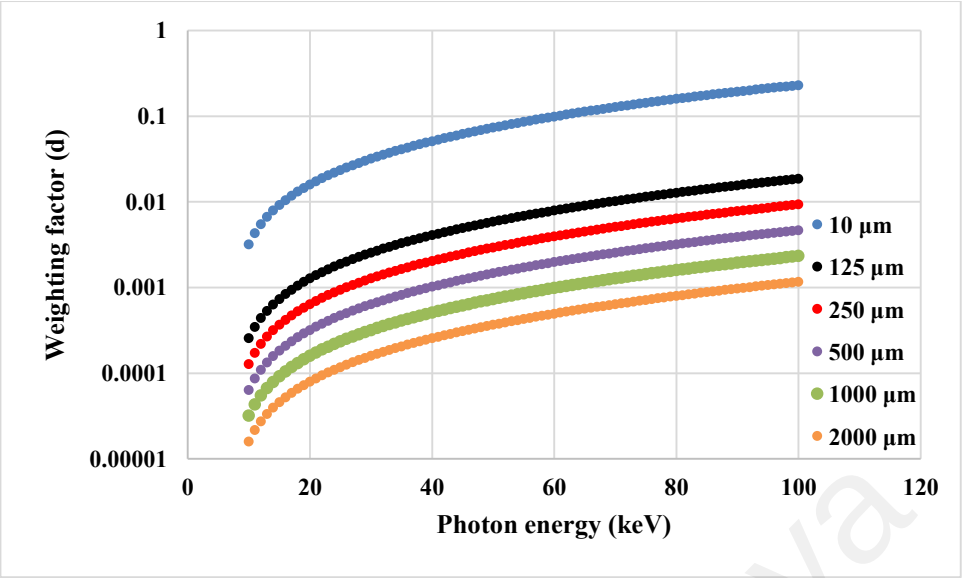

Figure 4.10: Calculated weighting factor for various fibre diameters

CHAPTER 5: ANGULAR DEPENDENCE

5.1 Introduction

Although much attention has been paid on silica fibre thermoluminescent dosimeters due to their adaptive nature and potential use in radiation therapy and other applications, practical dosimetry still require more detailed knowledge on different factors that may have a considerable influence on their accuracy. Most of the past investigations contain a general characterisation of these dosimeters including sensitivity and linearity with respect to dose and less attention has been assigned to the fibre response with respect to the beam angulation. The use of silica fibre TLD as a practical dosimeter involves the positioning of small pieces of fibre (usually 5mm length) on the flat phantom surface, uneven body skin or even different sites inside tissues for *in vivo* dosimetry applications. In complicated treatment fields, angle of beam incidence usually changes dramatically. Application in personal dosimetry or for quality assurance in diagnostic environment also causes sharp changes in the incident angle of beam. Such conditions, therefore demand the characterisation of the angular dependence behaviour of the dosimeter.

Variation in detector response caused by changes in angle of incidence have been reported in case of different dosimeters types such as ionization chambers, MOSFETs (metal oxide semiconductor field effect transistor), commercial TL dosimeters, OSL (optically stimulated luminescence) dosimeters and even more recently developed ones such as plastic fibre optic dosimeters. Physical shape, asymmetric dimensions and inherent characteristics of dosimeter due to the special designs cause the response of detector to be angular dependent. As some examples, several authors (Vohra et al., 1980;Jin et al., 1992;Guimarães et al., 2007) reported significant angular dependencies for $CaSO_4$, LiF and LiF/CaF_2 TLDs respectively, with addition of the filters which were used to diminish energy dependence. In an investigation by Dong et al. (2002) alteration of the angular dependence trend of TLD-100H (LiF:Mg,Cu,P) with changing in photon

energy was reported, and also asymmetric construction of MOSFET was suggested to be responsible for its angular dependence. Jursinic (2007) and Kerns et al. (2011) studied the angular dependence of disk-shaped OSLDs (0.2mm thickness with 7 &5 mm diameter respectively) in water equivalent phantoms, but did not observe any significant effect. These all suggest that angular dependence behaviour is affected not only by the physical symmetry of the dosimeter shape but also by the energy of radiation beam as well as the irradiation medium.

Regarding to the silica fibre TLDs, two reports were found that investigate the angular dependencies, (Noor et al., 2014; Entezam et al., 2016). They have studied the dependence of TL response to beam direction for fibres with cladding/core diameter of 116/9 and 270/42 μm respectively. Both works only studied probable angular dependence caused by asymmetric doping or microcrystalline structure of fibre, in a setup that just allowed rotating the gantry from 0 to 360 degree positions around the cylindrical samples with their axis positioned perpendicular to the beam direction (Figure 5.1).

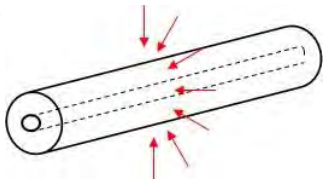

Figure 5.1: Angular dependence test setup in previous reports on fibres

But in practical dosimetry having a situation in which the beam reach to the fibre in a non-perpendicular angle is a quite probable issue which is not investigated yet. Since potential use of these detectors in both diagnostic (Issa et al., 2011) and therapeutic (Noor et al., 2014) energy ranges has been demonstrated, the effect of changing radiation incident angle with fibre axis for both kilovoltage (keV) and megavoltage (MeV) photon beams and also in different irradiation mediums is investigated in this study. Monte Carlo simulations are also used as the main tool to provide support for the experimental results.

5.2 Materials and methods

Ge-doped silica fibre samples (SMF-1) were prepared in 5 mm length pieces, as it was explained in Section 3.2.1. This was the choice for samples length, since it is the usual length adopted in all recent studies which perhaps affected by the planchet size of the TLD reader machine and also to provide an easy handling of fibres. Since the samples were pristine (i.e., without any pre-dose record and also suppose not to be irradiated more than once), a simple annealing regime of 400 °C for 1 hour was applied just to ensure the removal of low temperature peaks in the TL glow curve. Samples were then left to allow gradual cooling to ambient temperature.

5.2.1 keV irradiations using X-ray tube

In this study, X-ray photons produced by ERESCO X-ray generator described in Section 4.3.1 (shown in Figure 4.3) were used for keV irradiation of fibres. This machine can generate X-ray photon energies ranged from 10 kVp up to 200 kVp with the current up to 10 mAs. Fibre samples were irradiated using photons produced at 30 kVp with tube current of 10 mA to provide minimum irradiation time for this kVp. Since with this X-ray machine only an ionization chamber (model TM31013) was available which is not recommended for low keV measurements (because of the significant beam attenuation in the chamber walls), it was only used to check the stability and reproducibility of the X-ray tube output with time. This chamber has a flexible cable that allows the user for suitable positioning in different situations. Increased sensitive volume of 0.3 cm^3 in the chamber is designed to allow precise dosimetry in low level measurements. Relatively long irradiation time between 10 to 60 mins were examined to check consistency of the tube output. Fibre samples were also irradiated for these time durations later. A total of 10 samples were used for each measurement and fibres were positioned at 90° angle of incidence for this experiment. The meaning of different incident angles with geometry of SMF-1 are shown in Figure 5.2.

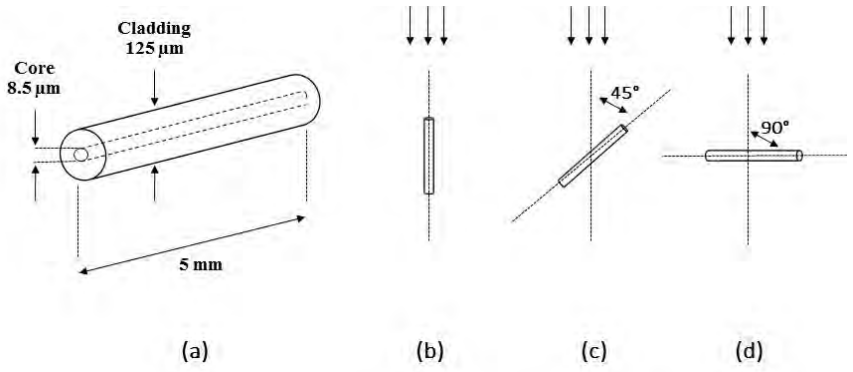

Figure 5.2: Dimensions of the SMF-1 fibre (a) and setup for angular dependence experiments (b-d)

Samples were then placed on paper labels and positioned on Styrofoam holders which were specially shaped to provide different incident angles at the same distance from the x-ray tube output window (schematically shown in Figure 5.3). Styrofoam holder provides free-in-air condition (identical to the simulation configuration mentioned in Section 5.2.3), since it is composed of H and C and has density of ~0.05 g/cm^3. Samples were then irradiated with the same irradiation parameters kV, mA and time, to evaluate their angular response.

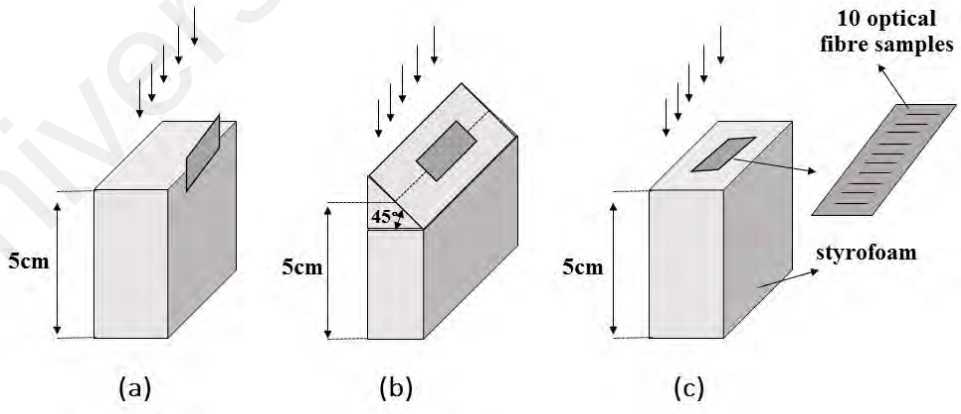

Figure 5.3: Schematic diagram of experimental setup for free-in-air irradiations, for both keV and MeV X-ray exposures. Incident angle is 0°, 45° and 90° for (a), (b) and (c) respectively.

5.2.2 MeV irradiations using medical linear accelerator (Linac)

Varian 2100 C medical linear accelerator (Varian Medical Systems, Palo Alto, CA) located at University of Malaya Medical Centre (UMMC) was used for megavoltage photon beam irradiations. This machine is able to produce 6 and 10 MeV photon beams as well as 6, 9, 12, 16 and 20 MeV electron beams with the possible dose rate ranged from 100 to 600 cGy/min. 6 MeV photon beam at a fixed dose rate of 600 cGy/min was used to irradiate fibres in the same free-in-air setup as described for keV irradiation. Source-to-surface distance of 100 cm and a field size of 10×10 cm^2 were adopted for irradiations. Beside from the free-in-air measurements, for MeV photons, Layered solid-water™ (Gammex, Middleton, USA) of dimensions 30×30×20 cm^3 and density 1.03 g/cm^3 was used to study in phantom and on-phantom situations to check the effect of incident angle at different irradiation mediums and charged particle equilibrium (CPE) conditions. Figure 5.4 shows the Linac irradiating fibres at 0° angle on the surface of a solid water phantom.

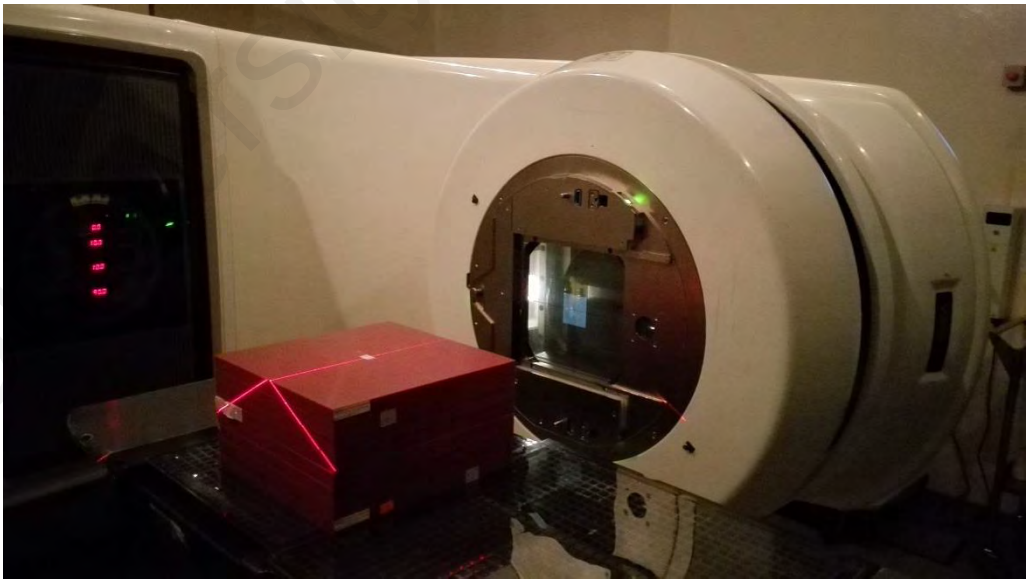

Figure 5.4. Varian 2100 C Linac irradiating solid water phantom

The schematic view of the setup to provide 0, 45 and 90 degrees incident angles is shown in Figure 5.5. Samples were placed at the isocenter and field size was adjusted to 10×10 cm^2 at SSD of 100 cm. To deliver a constant dose, in free-in-air and in-depth experiments, identical monitor units (100 MU) were delivered to the samples. However, the number of monitor units to provide the same dose on phantom surface were calculated using the Varian Medical Systems (Palo Alto, CA) treatment planning system (model Eclipse V13). This was because of different scattered radiation delivered to samples on the surface of the phantom at different incident angles. Samples were finally read using the same read out parameters described in Section 3.2.3.

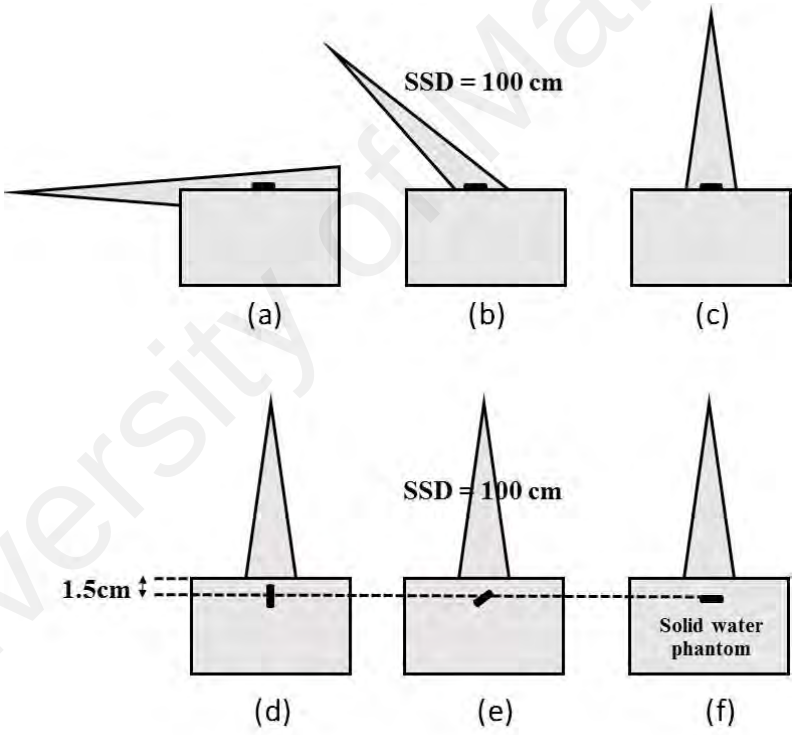

Figure 5.5: Experimental setup adopted for angular dependence tests at 6 MeV under (a-c) non-CPE conditions (phantom surface) and (d-f) CPE conditions (within phantom). Setup (d) and (e) were arranged using two sets of layered phantoms together and samples positioned between phantoms and irradiated one by one

5.2.3 Monte Carlo simulation

To support the evaluations obtained in the kVp and MeV measurements, Monte Carlo (MC) simulations using the MCNP (Monte Carlo N Particle) code were executed. The

MCNP code is known to be a multipurpose, widespread and powerful Monte Carlo tool for simulation of radiation transportation. Based on the accessibility, initially, version 4C of the code was used for the calculations presented in Chapters 5 & 6. However, following the availability of a newer version, MCNPX, it was used for rest of the simulations presented in Chapter 7. Also in few cases results of two versions, including spectrums and dose calculations, were compared against each other where no considerable differences were observed. The code provides different possibilities of calculating energy spectrum, particle fluence and deposited energy in any 3D cell of interest ("MCNPX user's manual, version 2.6.0," 2007). The MCNP input file includes the definition of cells, surfaces and complementary information which contains elemental compositions and densities, source description, tallies (for desired output definition) and variance reduction functions.

Photon irradiations at different incident angles were simulated to obtain the dose received by the silica fibre dosimeters under kVp and MeV irradiations. Since access to mono-energetic photon source with arbitrary energies is not possible, MC simulation is the preferred tool to provide insight into such phenomenon for different photon energies. The samples were positioned in three different angles between the fibre axis and direction of incident radiation namely 0, 45 and 90 degrees. For simulation of free-in-air condition for MeV photons at which the effect of field size is not important (because of the lack of scattered particles), photon beam was defined in circular shape that produced 1 cm diameter field size at 100 cm distance from the 6 MeV source. This was to allow sufficient numbers of interactions to be generated within the fibre, obtaining acceptable calculational uncertainty with the use of MCNP code defaults. This distance was decreased to 39 cm in the case of 30 kVp beam. The photon spectrum for 6 MeV beam from Varian accelerator was derived from (Sheikh-Bagheri & Rogers, 2002), however, spectrum for 30 kVp photon beam needed to include in the input file was calculated with

simulation of the X-ray tube structure based on the realistic specifications. Schematic view of the simulation geometry and details of the generator structure are presented in Figure 5.6 and Table 5.1 respectively.

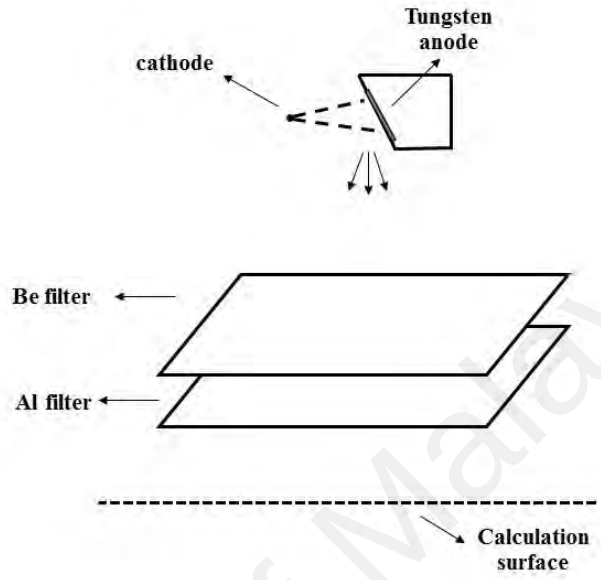

Figure 5.6: Schematic view of the X-ray tube simulation for calculation of 30 kVp photon spectrum

Table 5.1: Detailed specifications used in X-ray tube simulation

Nominal focal spot size	1 mm
Anode angle	20°
Target material	Tungsten
Be filter thickness	0.8 mm
Al filter thickness	2 mm
Initial electron energy	30 keV

Then calculated spectrum was used in the angular dependence simulations. The effect of field size for 30 kVp photons which are effectively attenuated in air was verified and the real field size (8×8 cm^2) was considered in simulations. The cylindrical shape fibre

sample with 5 mm length and 125 μm diameter including 8.5 μm core was placed free-in-air at the center of the field. The elemental composition of the fibre core and cladding based on elemental analysis presented in (Mahdiraji et al., 2015b) was used for MC simulation as detailed in Table 5.2.

Table 5.2: Elemental compositions and densities of SMF-1 used for Monte Carlo simulation

Atomic weights (%)	O	Si	Ge	Density (g/cm^3)
SMF-1 core	63.4	31.7	4.9	2.16
SMF-1 cladding	53.4	46.6	0	2.15

Addition of dopants to the silica structure has been approved as the main source of defects generation in fibre optics (Bradley et al., 2012; Yusoff et al., 2005), and it is recognized that thermoluminescence response of fibre mainly arises from the fibre core. Therefore, it was necessary to define the detached cells to acquire absorbed dose in the core and cladding parts of the fibre separately. However because of the very small core size, long calculational time are required. Different tallies are available in MCNP code to determine the calculation output. Tally *F8 was used to calculate the energy deposition in the core and cladding cells of the fibre, in the units of MeV and present the result per incident primary photon in the required cells. Unlike tally F6, tally *F8 does not use any track length estimation and is more reliable in case of micrometer cell sizes such as in this work. The energy cut off can be used to control calculation time, but due to the small fibre size, it was set to 0.001 MeV for both photons and electrons to guarantee the highest accuracy.

5.3 Results and discussion

Figure 5.7 shows the fibres response to 30 kVp irradiations being made at durations between 10 and 60 min that was performed to check the stability of the X-ray tube output with time. 30 kVp photon spectrum obtained from MC simulation is shown in Figure 5.8 in comparison with the approximated spectrum by SpekCalc software (described in Section 4.3.3), which is also in good agreement with published results by (Hernandez & Boone, 2014) for X-ray generator with the same target/filter combination. This spectrum was used as the primary photon spectrum for angular dependence simulations as described.

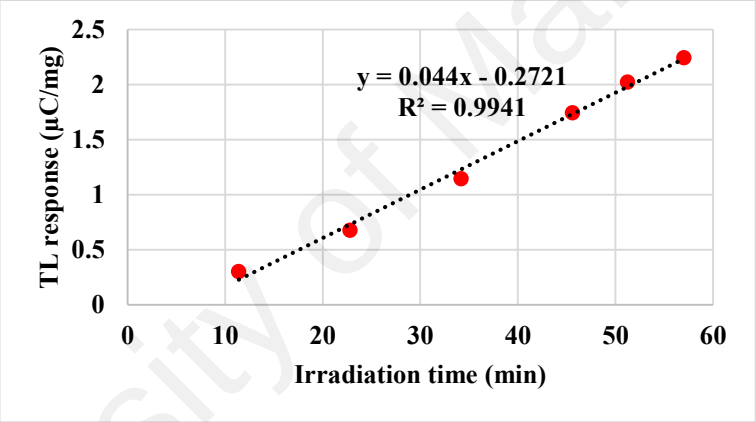

Figure 5.7: Calibration of fibre response for 30 kVp X-rays

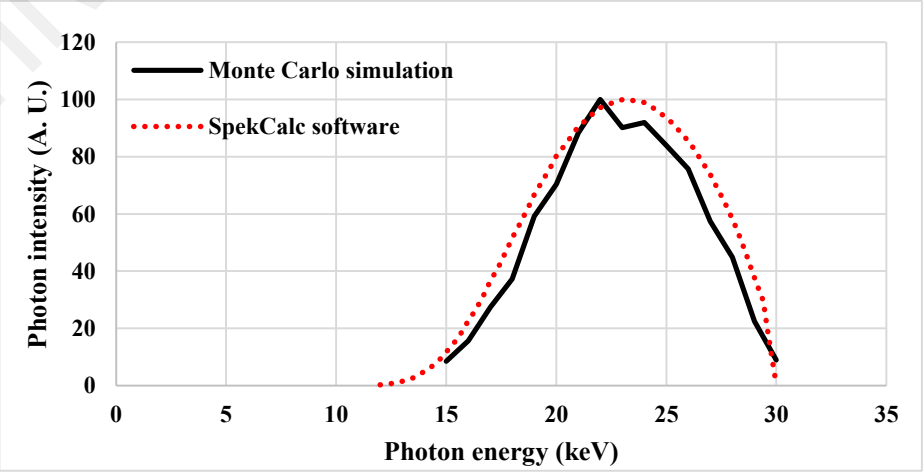

Figure 5.8: 30 kVp photon spectrum obtained from MC simulation compared to SpekCalc approximation

5.3.1 Effect of photon energy in free-in-air condition

Figure 5.9 and Figure 5.10 show the angular dependence of silica fibre TLDs in free-in-air condition at 30 kVp and 6 MeV photon energies, respectively. The simulation and experimental results are presented for comparison. Detector responses in both cases are relative to the response at 90° incident angle. The error bars indicate the uncertainties related to MC simulation as well as the variations among 10 fibre samples irradiated for each condition. The fibres responses show opposite trends on angular dependence to 30 kVp and 6 MeV photon beams, measurements and simulations agreed to within the uncertainties offered by photon source definition in simulations and incident angle (in experiments). At 30 kVp, fibre shows ~ 35 % less response in parallel condition (0°) to the beam direction relative to the normal positioning (90°), while for the case of 6 MeV beam, fibre shows ~20 % higher response at incident angle of 0° relative to 90°.

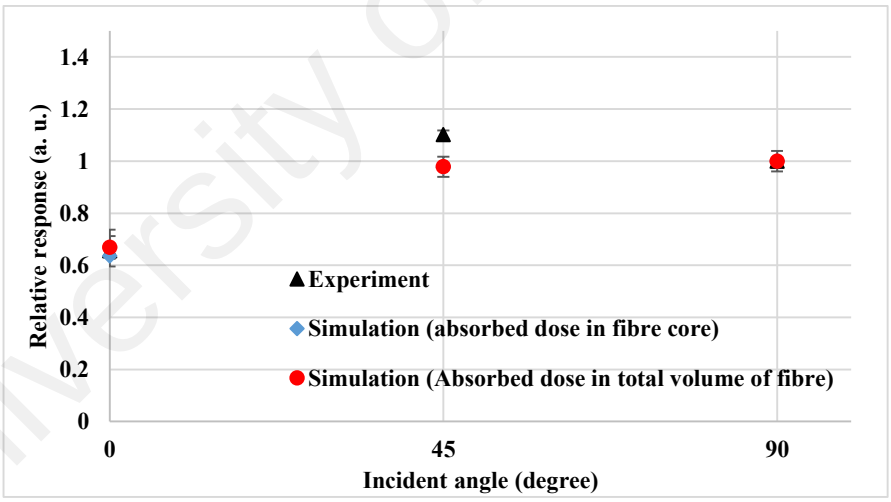

Figure 5.9: Comparison of angular dependence of fibres, simulated and from experiment conducted free-in-air at 30 kVp

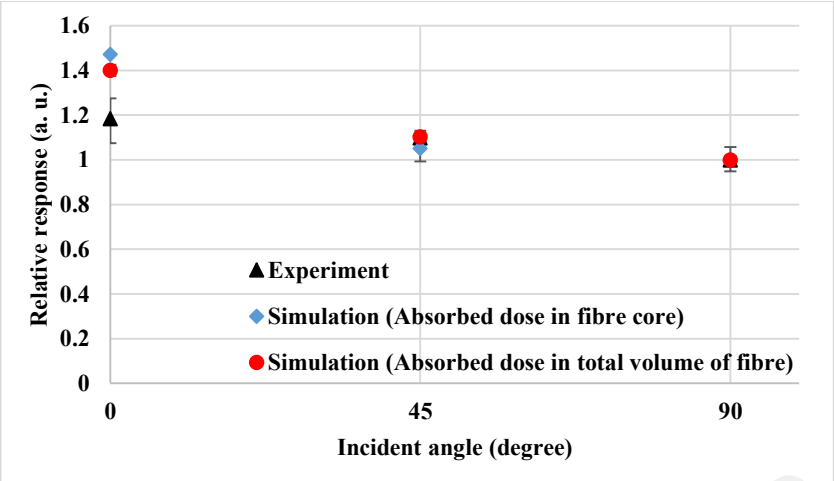

Figure 5.10: Comparison of angular dependence of fibres, simulated and from experiment made free-in-air at 6 MeV

Additional MC modeling was used to verify changes in detector response with angle of incidence for different beam energies. Various mono energetic photon beams 20, 30, 60, 80, 100, 500, 1250, 4000 and 6000 keV were simulated with the same free-in-air setup described before. Absorbed dose in the core and cladding cells were recorded individually in all cases. Figure 5.11 indicates the results of the additional MC modeling. In free-in-air condition, for low energy photons, absorbed dose in fibre increases with surface area subjected to irradiation from angle 0° to 90°. This is due to the short range of secondary particles inside SiO_2 for the case of low energy photons which resulted in less energy deposition inside the fibre when positioned in parallel to the beam direction. The estimated range of electrons through a given medium can be calculated by dividing Continuous Slowing Down Approximation (CSDA) range of electrons to mass density of the medium. Table 5.3 shows this approximation for silicon dioxide and electron energies ranged from 20 keV to 6 MeV. For example assuming 30 keV as the maximum electron energy produced by 30 kVp photon beam, electron would penetrate ~10 μm range inside fibre material. At an incident angle of 0°, the probability of energy deposition inside the fibre volume by such electrons would be much lesser than the fibre positioned at 90° at which larger cross section of the material is exposed to radiation. The measured response

at 45° shows an apparent greater response than that at 90°. Most probably, at the maximum photon energy of 30 keV this may not be sufficient to irradiate the entire cross sectional area of the fibre at 90° position compared to 45° position. As a result, the fibre core was directly exposed to 30 keV photons, being yet another observation pointing to the fibre core as the predominantly sensitive region of the fibre. For MeV photons, the electrons have much longer ranges than the fibre diameter and require a buildup region to establish charged particle equilibrium (CPE). Thus, with the fibre in 90° incident angle to the beam most of the produced secondary particles will deposit their energy beyond the fibre diameter and eventually decrease the dose response. Figure 5.12 and Figure 5.13 represent a schematic view of this situation for 30 keV and 6 MeV electrons, respectively.

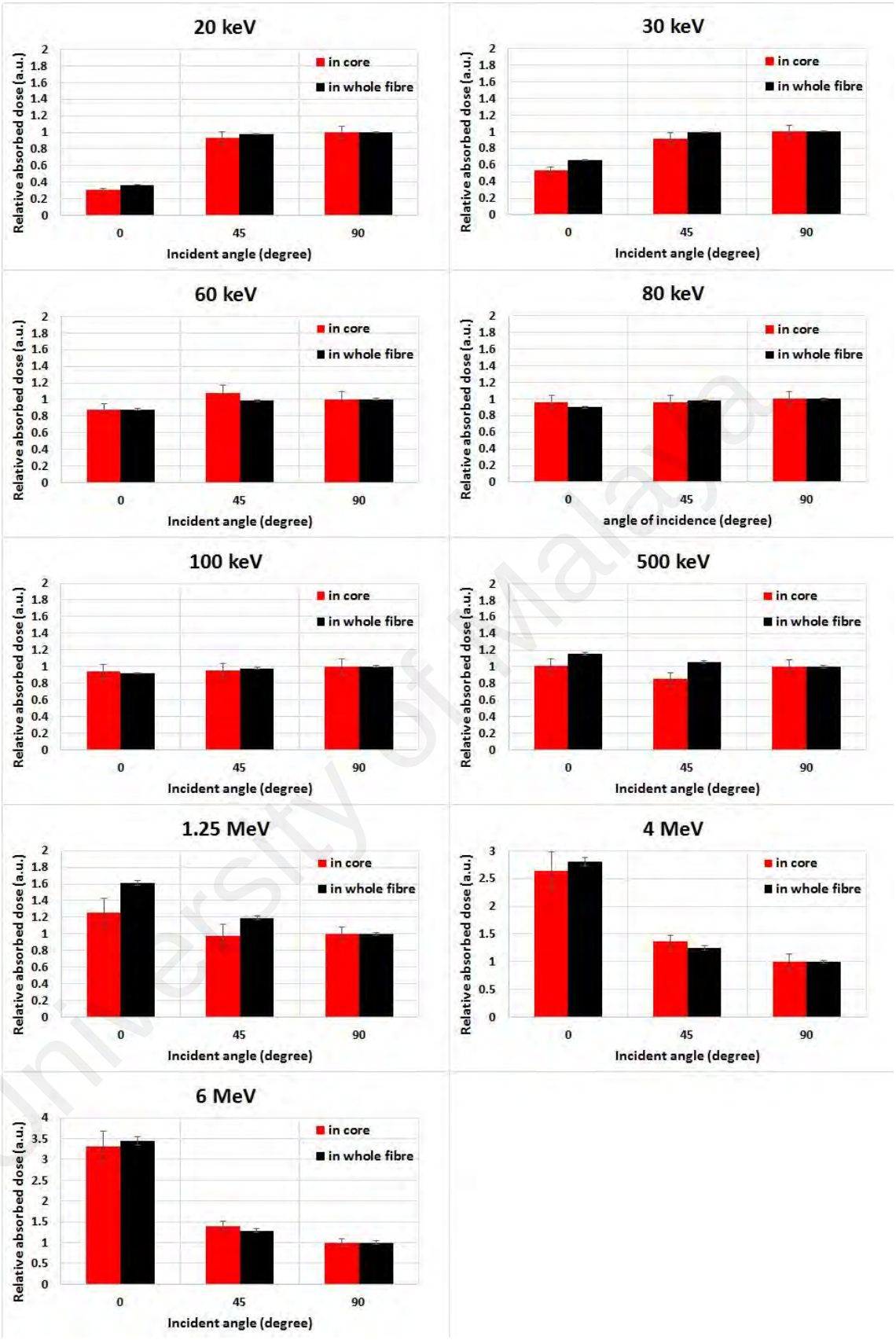

Figure 5.11: Angular dependence of fibre response for different mono-energetic beams (simulation results)

Table 5.3: Range of electrons with different energies inside silicon dioxide (extracted from ("Powers, Stopping, Ranges for Electrons (ESTAR)," 2015)

Electron energy (keV)	CSDA range (g/cm^2)	Approximate range in SiO_2
20	1.084×10^{-3}	5.04 µm
30	2.201×10^{-3}	10.23 µm
60	7.338×10^{-3}	34.13 µm
80	1.201×10^{-2}	55.86 µm
100	1.753×10^{-2}	81.53 µm
500	2.122×10^{-2}	98.69 µm
1250	6.817×10^{-1}	0.317 cm
4000	2.38	1.106 cm
6000	3.53	1.641 cm

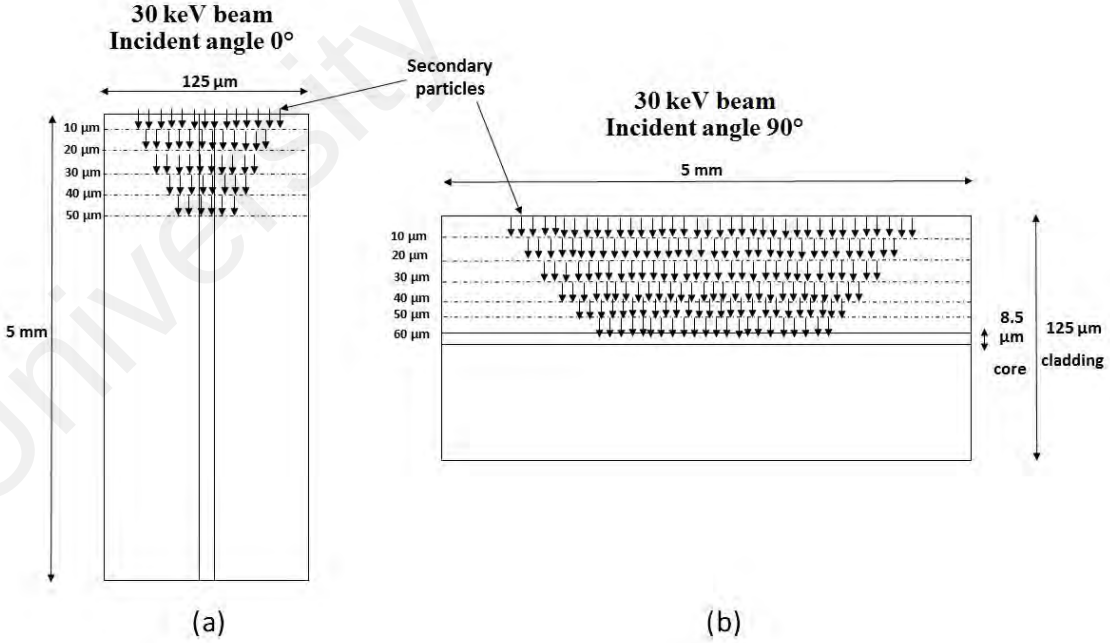

Figure 5.12: Optical fibre cross-section and energy deposition by a 30 keV photon beam at incident angles 0° (a) and 90° (b)

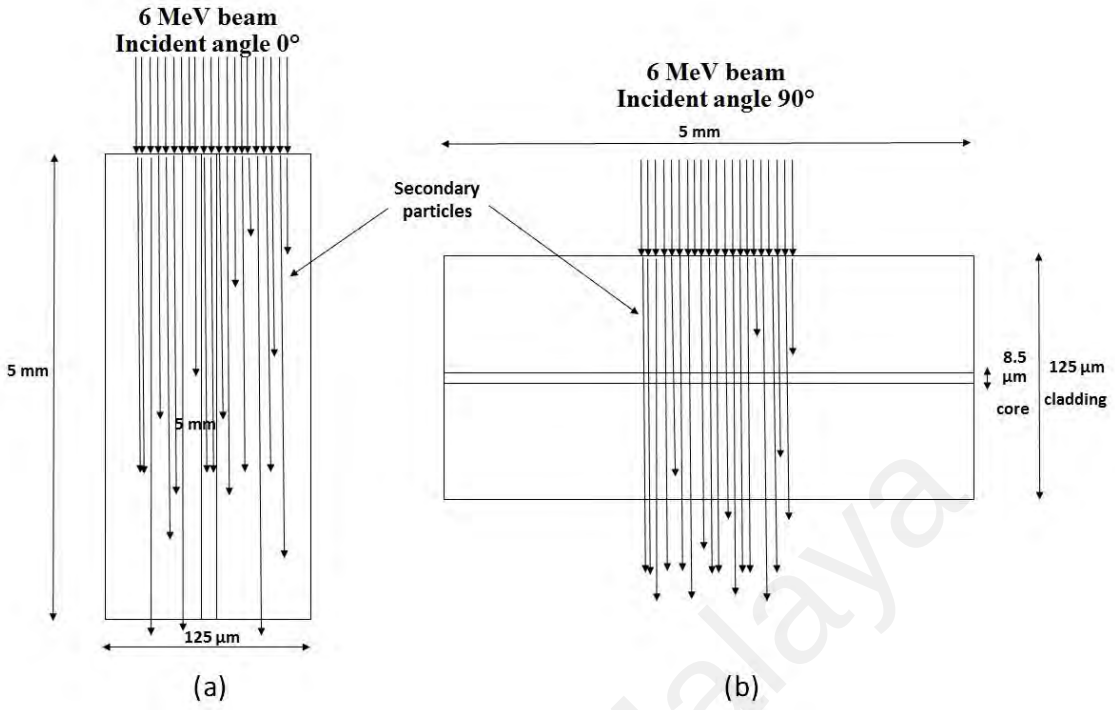

Figure 5.13: Optical fibre cross-section and energy deposition by 6 MeV photon beam at incident angles 0° (a) and 90° (b)

Figure 5.14 illustrates summery of the simulation results presented in Figure 5.11. It shows the response of fibre at 0° position relative to 90° position for different energy beams. Based on the simulation results, there would be a region of approximately between 100 and 500 keV in which angular dependence is insignificant due to the same portion of dosimeter volume affected by secondary particles at different incident angles. At MeV energies inverse trend of angular dependence emerges where dose response increases with photon energy. This is due to the lack of build-up region for high energy photons (MeV) in which, short cross section of fibre does not provide electron equilibrium condition. At 0° incident angle where photons have longer track length through the fibre, there are more opportunities for them to interact and deposit energy by the secondary electrons (Figure 5.13). This results is almost 3.5 times higher response at 0° incident angle for mono-energetic 6 MeV photon beam compared to 90°. For the case of a spectrum of photons such as 6 MeV beam produced in a Linac, different trends of various energy photons combined, eventuating the pattern displayed in Figure 5.10.

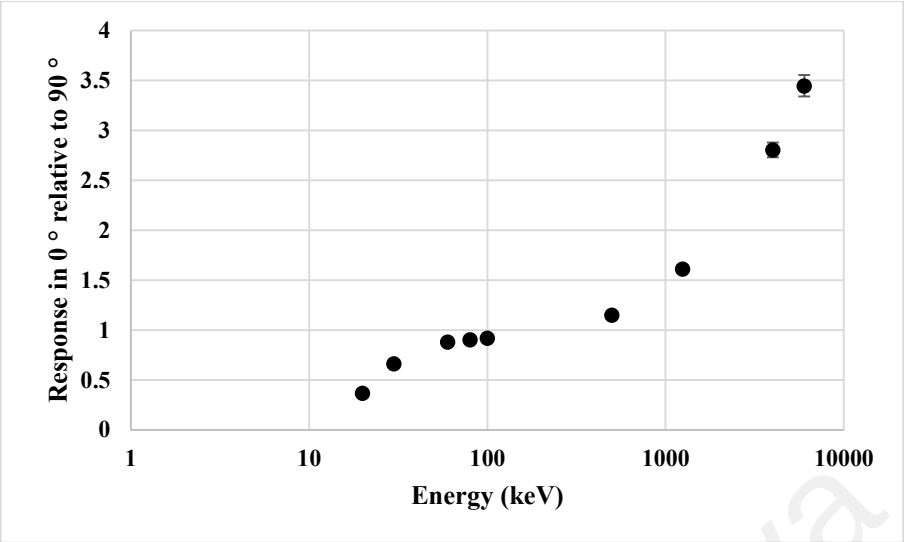

Figure 5.14: Change in angular dependence trend with energy of the mono-energetic photon beam (summary of Figure 5.11)

5.3.2 Effect of irradiation medium

Due to the micrometer cross section scale of the silica fibres, they are more sensitive to beam quality relative to a sensor with larger dimensions. Therefore irradiation medium may have a significant effect on the fibre response and angular dependence as well. Thus, different experimental setups were designed with fibres positioned at various incident angles from X-ray beams on the surface and inside the phantom at depth of maximum dose (1.5 cm for 6 MeV) as shown in Figure 5.5. MC simulation was also performed for these cases. Unlike models in the previous section, the real field size (10×10 cm^2) was defined in MC simulations to consider scattering effects due to the presence of the phantom. In order to decrease the calculation time reasonably, total fibre volume was defined as one cell. This assumption was valid since simulation results in Section 5.3.1 showed similar trends for both absorbed dose in the fibre core and the total volume of fibre. Despite eliminating small scoring volume of the core cell and considering one monolithic cell, introduction of phantom increased calculation time to 120 hours by using the available system (Intel Core i7 Processor/8GB RAM) in case of on-phantom models.

Angular dependence of fibres at on phantom surface and in-depth situations are demonstrated in Figure 5.15 and Figure 5.16, respectively.

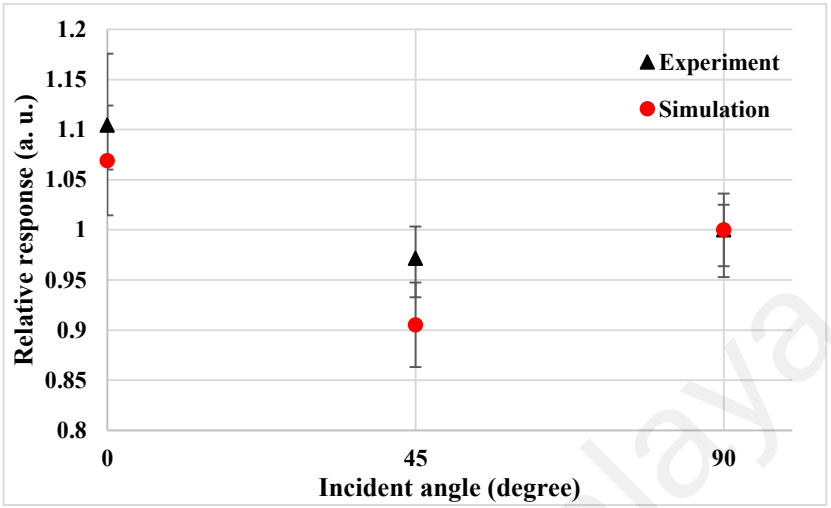

Figure 5.15: Angular dependence of fibre response to a 6 MeV photon spectrum (on phantom surface)

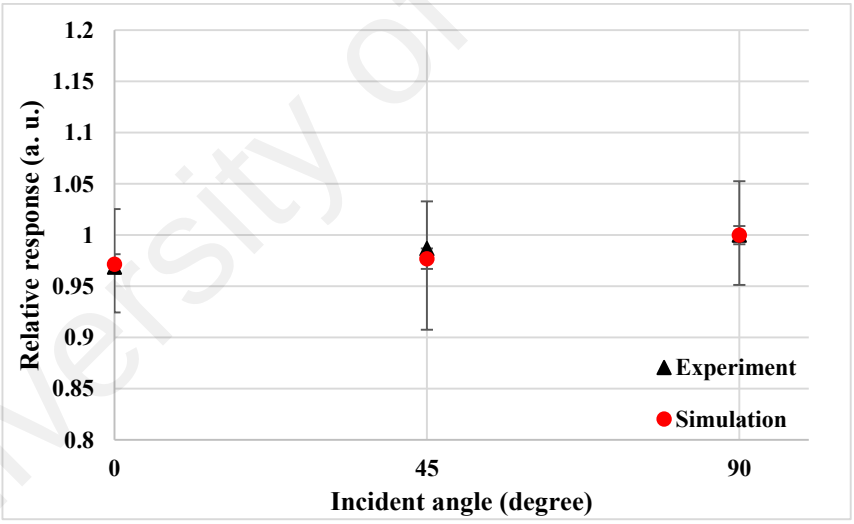

Figure 5.16: Angular dependence of fibres to a 6 MeV photon spectrum (inside phantom at 1.5 cm depth)

As it is expected for the case of phantom surface, the effect of incident angle decreases to 10 % compared to that free-in-air (20 %) in the presence of phantom, the fibre response remaining greater at 0° relative to that at 90° (Figure 5.15). This is almost certainly due to an appreciable amount of scattered radiation from the phantom at 0° incident angle, enhancing the low energy part of the spectrum and eventually decreasing the free-in-air

angular dependency. Similarly in the case of 45° incident angle, reduction of backscattered radiation is responsible for the decrease observed in response relative to 90°. MC simulation predicts nearly identical ratios for the absorbed dose in fibre at 0° and 45° positions relative to 90° incident angle.

For irradiations made in the phantom (Figure 5.16) at the depth of maximum dose, with electron equilibrium achieved, the trend of angular dependence is changed. In this condition the cross-sectional area of fibres subjected to radiation determines the absorption efficiency. Therefore a greater response is observed at the incident angle of 90°, being only 3.1 % greater than that at 0° (Figure 5.16). Simulation results show strong agreement with the experimental results in these cases (less than 1 %).

5.4 Conclusion

Results of this study showed the changes in angular dependence of silica fibre TLDs with beam energy. Simulation results showed an almost angle-independent dose absorption in fibre at photon energies ranged from ~100 keV to ~500 keV. Response of SMF-1 TLD was shown to be around 35 % and 20 % for 30 keV and 6 MeV angular dependent, respectively, when irradiated free in air. The micrometer cross section of fibre, lack of CPE condition and scattered radiations are mainly responsible for the observed directional dependence. In general, during irradiation, an irradiated dosimeter of larger cross section may receive greater absorbed dose and accordingly show greater response. Results of this study suggest to include another term in the general expression for response to take account of the dosimeter dimensions. A dosimeter of small dimensions positioned within a photon field, with the radiation incident on the short dimension will result in minimum response, and the small dimension being insufficient to provide build-up in the higher energy MeV photon beam. A 125 μm diameter optical fibre displayed significant angular dependence free-in-air and in the on surface condition, can be used

accurately with only 3 % angular dependence in depths beyond the build-up region for radiotherapy photon beams. Application of such fibres in radiotherapy normally does not necessitate free-in-air measurements, while other applications such as personal or diagnostic dosimetry which demand in-air measurements also need a flat response dosimeter in terms of energy of radiation. Since the response of silica fibres is energy dependent, a filter designed to reduce the energy dependence would be desirable. Since the main TL response generates from the fibre core where the Ge is doped, the angular dependency observed in SMF would be due to that of very small core of about 8.5 μm. Thus, the angular dependency is expected to be further reduced by using a fibre with larger core size and symmetric dimensions. With development of advanced and tailor made silica fibres, it is possible to provide for fibre dosimeters that are custom designed with optimized parameters in order to practically suppress such angular dependence.

CHAPTER 6: GAMMA IRRADIATOR DOSE MAPPING

6.1 Introduction

Following characterisation process of GDSF dosimeters presented in Chapters 3 to 5, some potential applications of such material will be studied in Chapters 6 to 8. The dosimetric advantages of these TLDs have been shown which include excellent linearity over wide range of doses (referred to results in Chapter 3), relatively good sensitivity compared to common TLDs (Mahdiraji et al., 2015b), low fading (Noor et al., 2012), high spatial resolution and possesses non hygroscopic nature. Due to the aforementioned advantages, these TLDs have been used in numerous dosimetric applications. For instance Issa et al. (2011) reported the use of GDSF for X-ray therapy at energies 90 kVp and 300 kVp and for depth dose measurement in water where good agreement was observed between GDSF and ionization chamber measurements. GDSFs were also suggested for MeV external radiotherapy (Noor et al., 2014), brachytherapy (Issa et al., 2012), intensity modulated radiotherapy (IMRT) (Noor et al., 2010) and etc. This chapter presents the first application of GDSF in this thesis, specifically on the potential use of this dosimeter for dose mapping in a gamma irradiator.

A practical TL dosimetry system can provide relative or absolute doses following proper calibration and correction. Industrial gamma irradiation facilities with different shape of active parts, normally have a container called “sample chamber” in which, dose distribution may change point by point, depending on source geometry, carrier system and shielding structure. Several earlier studies showed dose distributions in different type of irradiators using Monte Carlo codes and/or dosimetry systems. For instance, Oliveira & Salgado (2001) and Sohrabpour et al. (2002) reported dose mapping for UTR and IR-136 irradiation facilities, respectively. MCNP code has been used in both works, while the results of simulation in the latter one were also benchmarked with poly-methyl-meth-acrylate (PMMA) dosimetry.

Gammacell 220 (GC-220), equipped with ^{60}Co γ-ray emitters, is widely used in various fields of radiation researches generally effects of radiation dose on different materials, specifically biological samples in medical, biological and agricultural studies. Since the machine has a cylindrical shape sample chamber with 20.6 cm length and 15.2 cm heights, and materials with different dimensions are placed in the sample chamber for irradiation, distribution of dose rate inside the chamber at different sites should be identified. In those applications where the accuracy of the delivered dose is not critical, user may consider the nominal dose rates calculated simply by exponential decay law. However, for precise use or calibration purpose in dosimetry researches, exact dose rate at each point must be recognized. Furthermore, correction factors needed to consider the effect of scattered radiation while examining an energy dependent dosimeter, demand awareness about energy spectrum of photons inside the irradiator. Since experimental measurement of the photon spectrum inside the sample chamber is not straight forward, Monte Carlo simulation is usually used for this purpose.

Only a very limited number of previous investigations reported the dose distribution inside the GC-220 sample chamber (see for example (Raisali & Sohrabpour, 1993) and (Hefne, 2000)). The first study reported the use of EGS4 code combined with Fricke dosimeters, while the second one utilized MCNP code to obtain dose rates in some regions of interest inside the chamber. This Chapter investigates the feasibility of the use of sub-millimeter diameter GDSF TLDs to obtain dose distribution inside the chamber of a GC-220 gamma irradiator and elucidates the reliability of measured doses by Monte Carlo dosimetry system where dose distribution is calculated by MCNP code.

6.2 Materials and methods

6.2.1 TL dosimetry using silica fibres

Procedure of sample preparation and annealing was the same as explained in Chapter 3. The mass of 5 mm length sample by considering the average mass of 10-20 pieces of fibre was 0.132 mg but precise measurement of mass for each single fibre sample was not possible with the available electronic scales (precision 10^{-5} g). Since the variations in fibres length (and mass) can cause an uncertainty in the reading of samples irradiated with the same dose, a screening process was followed. A total of 100 pieces of 5 mm length fibre arranged in 5 groups (20 samples in each group) were irradiated to a sample dose of 1 Gy and then measured by TLD reader device. Samples with readings in the range of ±1.5 % were selected for dose mapping experiment and were placed on small pieces of sticky papers and positioned in predefined points on the plane passing through the center of cylindrical sample chamber of GC-220. Very low density Styrofoam holder (used so as to not affect the existing dose distribution), was applied in fixing to it a transparent plastic sheet that actually retained the fibre samples, with the fibres positioned at 1 cm intervals (Figure 6.1). Delivered dose in both the radial and axial directions on this plane was measured by the fibre TLDs. The coordinate axes are also shown in Figure 6.1. Materials that are required to be irradiated by gamma rays, are normally positioned on the bottom surface of the Gammacell sample chamber. Therefore, the dose distribution on this surface is also needed. Figure 6.2 shows the fibres arrangement on the bottom surface to obtain dose rate ratios on this plane of the irradiator. Using this arrangement, for each distance from the center point on the bottom plane, 6 samples were irradiated in equal positions. 4 samples were also used at the center point and the average of their readings was used to calculate dose rate ratios relative to the central point.

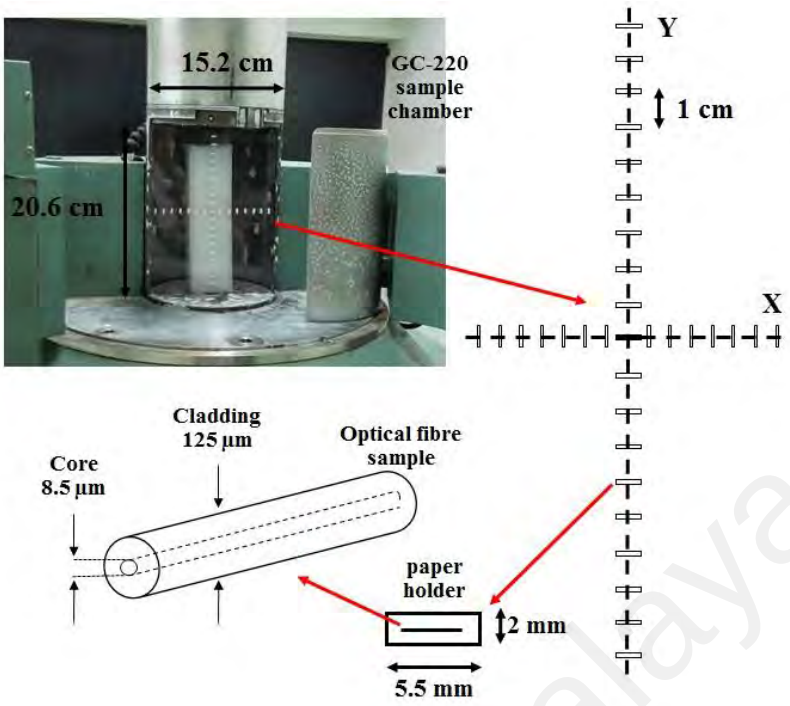

Figure 6.1: Arrangement of GDSFs on the vertical and horizontal axes passing through the central plane of the sample chamber

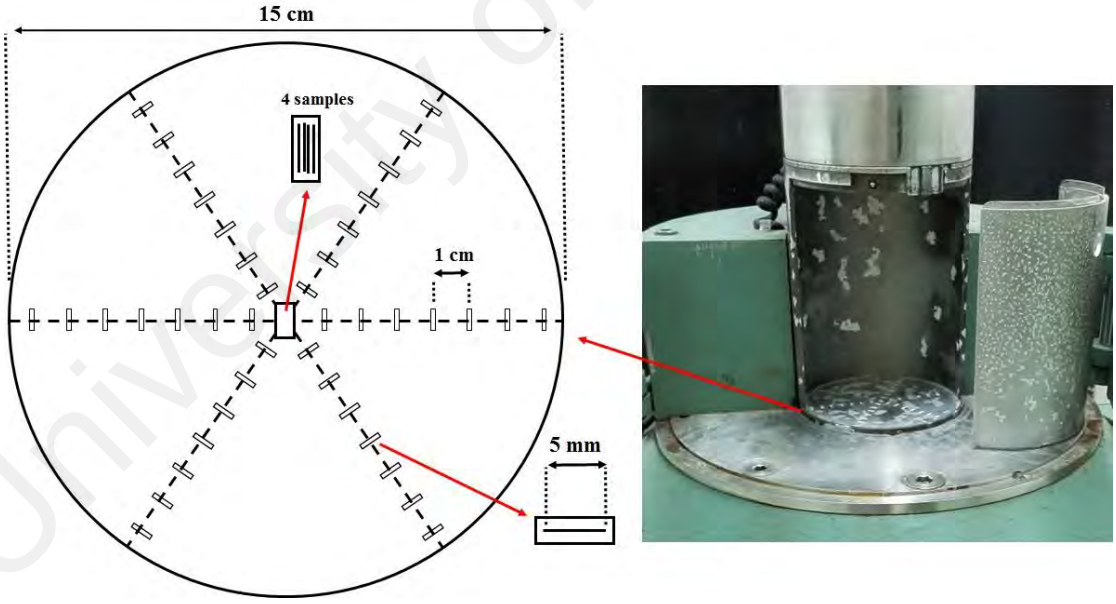

Figure 6.2: Fibre dosimeters positioned on the bottom surface of the sample chamber for dose measurement

Dosimeter samples were arranged as described and irradiation time was adjusted to deliver 20 Gy nominal dose at the central point of the machine. Nominal dose rate calculated by decay law at the time of experiment was 2.15 Gy/min. Time temperature

profile (TTP) for reading samples using the Harshaw 3500 TLD reader, was set at preheat temperature of 50 °C, maximum temperature of 400 °C with heating rate of 25 °C/s as selection of these was discussed in Chapter 3.

6.2.2 Monte Carlo simulation of GC-220

MCNP code was used in this study to calculate dose distribution inside the Gammacell 220. Geometry of all internal components of Gammacell 220 was derived from the instruction manual ("Instruction manual Gammacell 220 Cobalt 60 irradiation unit," 1968). The Gammacell includes 48 cylindrical elements each 1 cm diameter and 20.3 cm length encapsulated in a stainless steel rack resulting in a geometry of cylindrical shell having 10.45 cm radius for radioactive source. Steel layer is not the only layer placed between the gamma source and material to be irradiated inside the machine, since sample chamber has a 4 mm thickness aluminum wall that also affects the spectrum of particles reach to the chamber volume. The entire cell is well shielded with sufficient thickness of lead and access tube is also included lead-filled steel cylinders in both upper and lower drawers provided acceptable radiation protection for machine user while moving the sample chamber upward and downward. Figure 6.3 shows the GC-220 irradiator together with the geometry modeled by MCNP code.

Atomic weights and mass densities were also entered into the MCNP input file to describe material specifications. The predominant Cobalt 60 gamma ray lines (1.1732 and 1.3325 MeV) with the same probability and isotropic distribution were defined to complete the description of rod shaped sources. Two series of models were run to obtain needed parameters, the first models to calculate energy spectrum of the photons. Photon spectrum was calculated once in the whole volume of the sample chamber and then in a spherical cell with 2 cm radius at the center of the sample chamber. Tally F4 was used for photon counting in 20 keV width energy intervals ranged from 0 to 1340 keV to cover

the total expected photon energies. The same models were also run using electron counter for electron spectrum calculation.

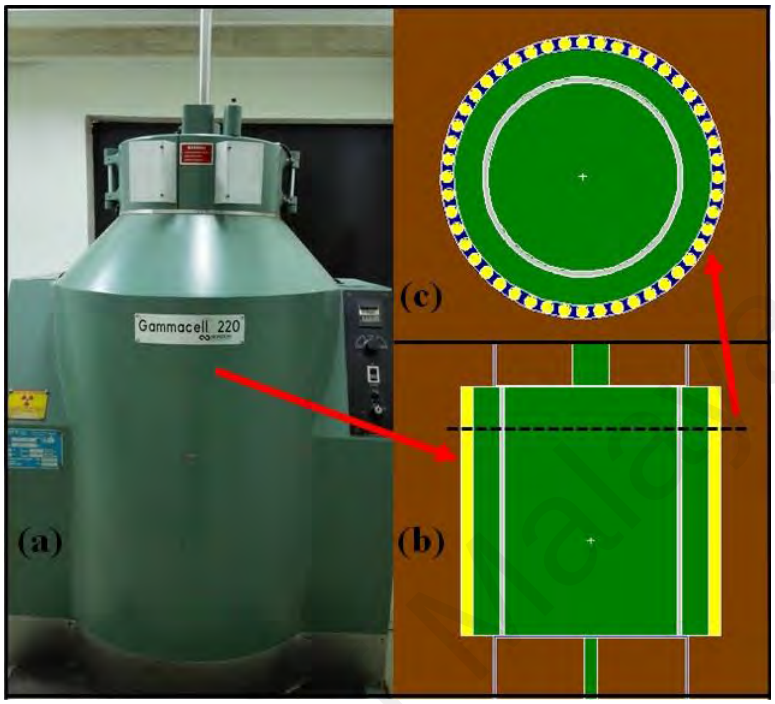

Figure 6.3: (a) Gammacell 220 irradiator, (b) geometry of the sample chamber modeled in MCNP and (c) cross sectional view of the ^{60}Co rods

To calculate the dose rate in specific positions on vertical and horizontal axes, the second series of models were constructed. 2.5 mm radius spherical detectors were used to obtain point by point energy deposition on central plane and calculate relative doses. These detectors were placed in steps of 1 cm at different radial and axial distances ranged from 0 to 7 cm and 0 to 10 cm, respectively. Dose rates were also calculated upon the radial line on bottom surface of the chamber using hemisphere shaped detectors arranged from 0 to 7 cm. Tally *F8 was used to calculate the dose rate, and energy cut-off 10 keV was considered for both photon and electron transportations. The use of greater or lower energy cut-off values were also examined, and it was confirmed that lower amount results in higher calculation time making the simulation impractical, while assuming larger cut-offs leading to larger calculation uncertainties. Model was executed by tracking 1.5×10^8 number of initial photons for particles spectrum with related calculation error less than 5

percent presented by the code. In case of absorbed dose calculations, to acquire sufficiently low calculation error of between 1 and 3 percent by the code, the number of initial photons was 8×10^8, thus proportionally longer calculation time was needed.

6.3 Results and discussion

As explained in Section 6.2.1, 100 samples of GDSF were irradiated to choose samples with uniform response for dose mapping purpose. Figure 6.4 indicates the TL yields from all samples which are normalized to the average value of readings. Variation in samples length and inhomogeneity in concentration of trapping centers along the fibre length resulted from fabrication process (fibre pulling and doping) are mainly responsible for such variations observed in TL response (Abdul Sani et al., 2014; Mahdiraji et al., 2015b; Noor et al., 2010).

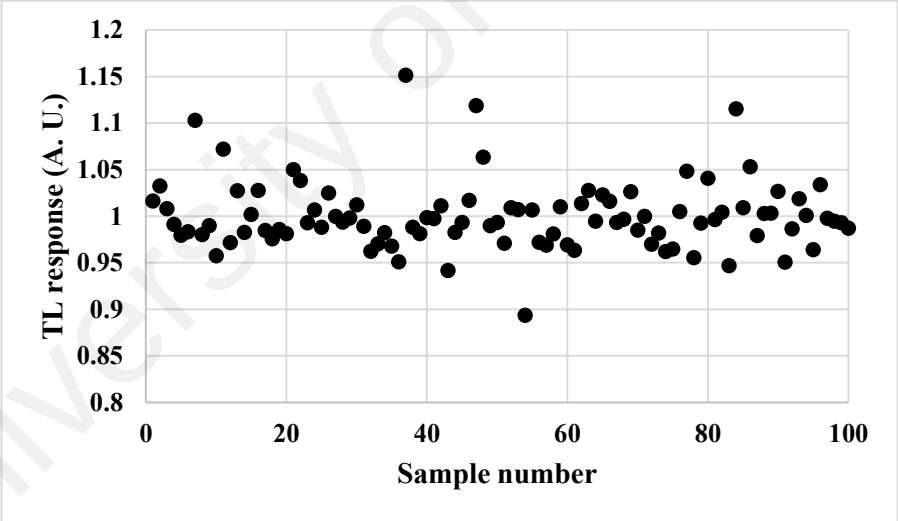

Figure 6.4: Result of screening of 100 GDSF (TL response of samples are normalized to the mean value of readings)

6.3.1 Comparison of measured and calculated dose distributions

Dose rates measured by silica fibre TLDs on central plane of GC-220, in horizontal (radial direction) and vertical (axial direction) axes are shown in Figure 6.5 and Figure 6.6, respectively. The results of MC simulation are also shown for comparison.

Simulation and experimental results are in agreement with maximum difference of 6.7 % at X = 3 cm for horizontal axis and 4.8 % at Y = - 8 cm for vertical axis. Dose rate on radial axis at the center of sample chamber is minimum compared to the edges near the chamber wall where it is almost 20 % greater. The center point of the sample chamber which has the minimum dose on radial direction is the point with maximum dose in axial direction. Dose rate changes along the axial direction of chamber is even more than radial direction with 22 % and 26 %, respectively at Y = 1 and Y = 20 compared to Y = 0.

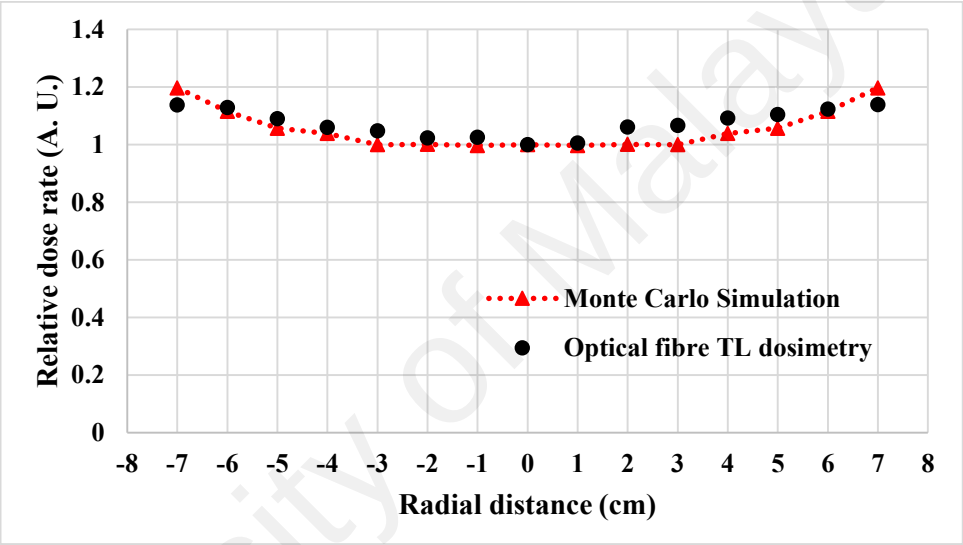

Figure 6.5: Radial dose rate on central plane of GC-220 sample chamber (Y = 0)

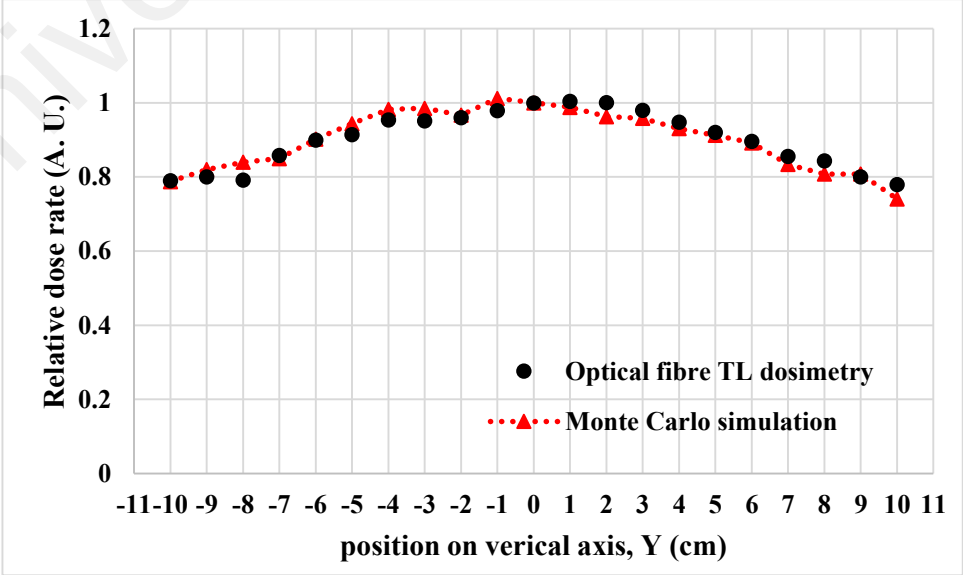

Figure 6.6: Axial dose rate on central plane of GC-220 sample chamber (X = 0)

The trend for dose rates ratios measured and calculated in central plane is similar to those reported in the literature (Hefne, 2000; Raisali & Sohrabpour, 1993), however current results with 1 cm spatial resolution confirmed the literature data, also provided more points than the literature. These additional points particularly in case of vertical axis dose rates show some non-uniformity which has not reported before. Since TL dosimetry show the same trend of increment and reduction in dose rates predicted by MC simulation, it is evident that changes of dose rates are not very smooth as it had been reported in previous mentioned reports. These results also reveal that the structural difference of GC-220 inside the upper and lower drawers, which can be seen in Figure 6.3, and also the main shielding of the machine which is not symmetric, cause approximately 4 % lower dose rate at the upper part relative to the lower part of the sample chamber. This is reasonable, since the diameter of hollow cylinder designed in the shielding of upper part is larger than that of lower region, subsequent reduction of backscatter radiation may decrease the dose at upper points. This issue has not been discussed in previous reports as well.

Dose rate ratios on the bottom surface of the sample chamber shown in Figure 6.7, indicate more uniformity on this plane. The maximum dose points obtained from the agreement of experimental and simulation results are located at X = ± 3 cm with about 7 % higher dose rates which are decreased to 5 % at 4 cm and remained constant by further increasing the distance from the center point of the bottom surface. This result is practically useful, because samples are normally positioned on this plane for irradiation.

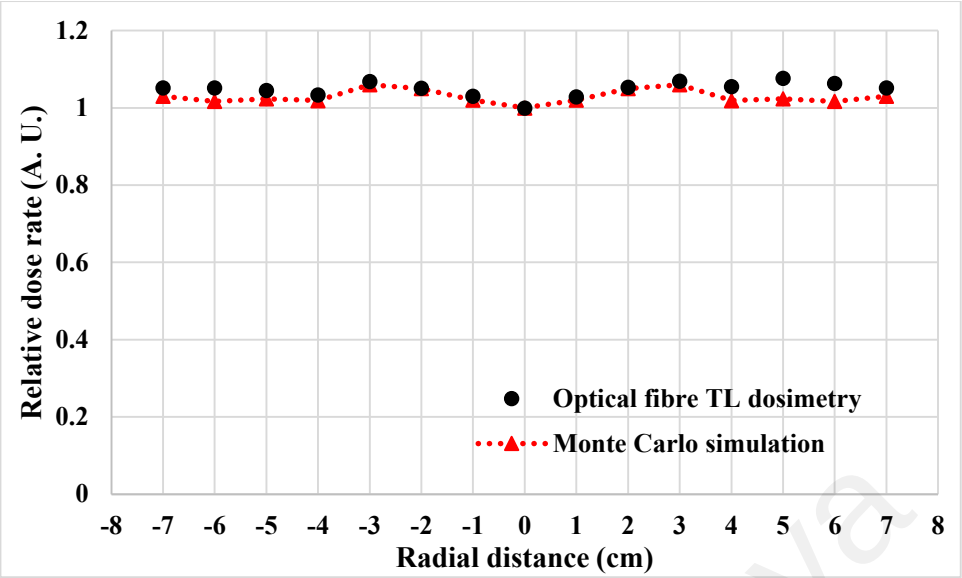

Figure 6.7: Radial dose rate on bottom plane of GC-220 chamber (Y = -10)

6.3.2 Photons and electrons spectrums obtained by MC simulation

Since the response of silica fibre dosimeter is energy dependent, another important analysis is regarding to the spectral distribution of particles inside the sample chamber that can potentially affect the dosimeter response if significantly changed in chamber volume. Therefore, photons spectrum was calculated in air inside the GC-220 sample chamber at two scoring volumes, once at the whole volume of sample chamber and another time in the middle height on central axis and in an air-filled sphere. The obtained spectrum is shown in Figure 6.8.

Photon intensities received to the spherical cell is quite identical with the spectrum obtained for the whole sample chamber volume, which means that consideration of this spectrum in any part of the sample chamber is a valid assumption. Spectrum includes a low energy part with a peak at around 200 keV. This peak with intensity of almost 12 % of the ^{60}Co gamma lines, is composed of photons attenuated by steel layer around cobalt rods, aluminum wall of the chamber and backscattered radiation from outer lead shield. Spectrum of photoelectrons calculated using tally F4 is also shown in Figure 6.9.

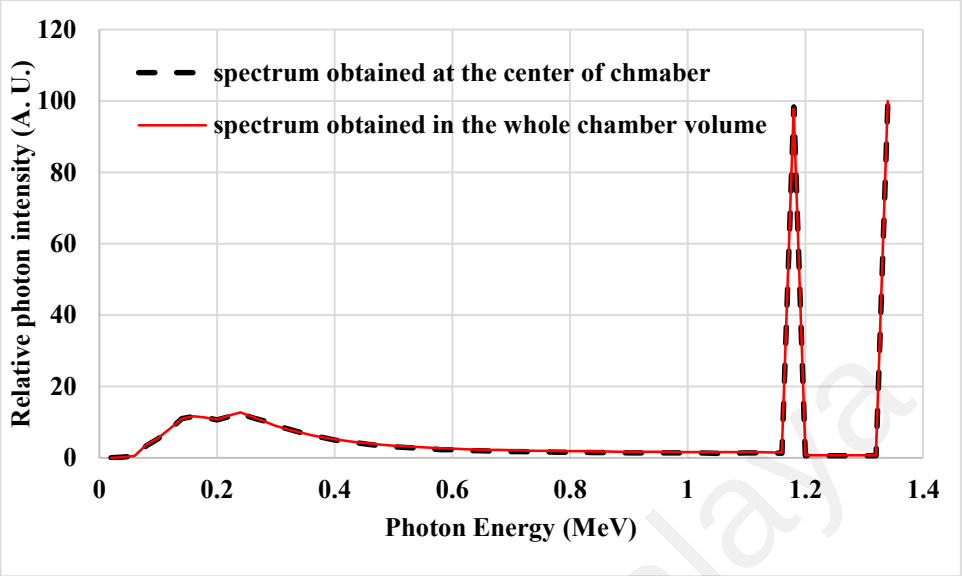

Figure 6.8: Spectrum of photons scored inside GC-220 sample chamber showing existence of a low energy part around 200 keV

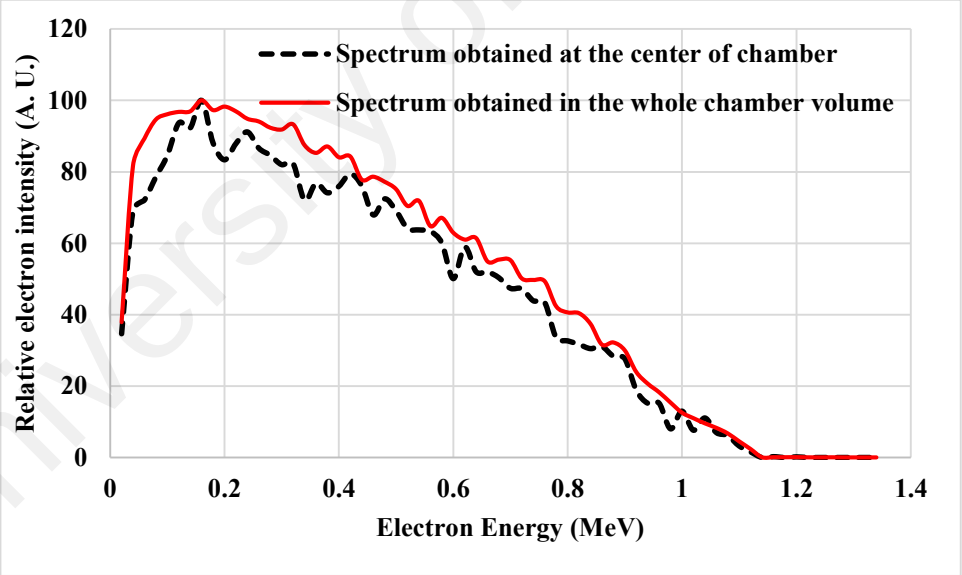

Figure 6.9: Electron spectrum scored inside GC-220 sample chamber

Electrons spectrum is somehow the same as the low energy part of the photon spectrum with the same peak at around 200 keV and gradual decrease in intensity for higher electron energies. Electrons intensity is negligible after 1.1 MeV. Fluctuations observed in the electron spectrum specially for the one obtained at the center of the chamber (less

than 15 %) is due to the increase in calculation uncertainty owing to a lesser number of particles reaching to the scoring volume. The total flux of electrons calculated per emitted photon from ^{60}Co source is only 1.1 % of photons flux counted in the sample chamber. Obtained spectrum for photons is in good agreement with the published data (Raisali & Sohrabpour, 1993), however, electrons spectrum is not reported before. These spectrums and contribution of both photons and photoelectrons should be considered for correcting dosimeter response particularly for dosimeter materials with high effective atomic numbers that show higher response in the keV energy region. Since this irradiator is also used in dosimetry studies, calculated spectrum would be practically useful for response corrections.

6.4 Conclusion

Gammacell 220 was accurately modeled by MCNP code and radiation spectrums for both the photons and electrons were obtained inside the sample chamber. Since the response of an energy dependent dosimeter show a significant variation in MeV region compared to keV range, recognition of these spectrums is useful for correction of detectors response in dosimetry studies. Micrometer diameter silica fibre TL dosimeters were used for dose mapping inside a gamma irradiator in this study and measured values were compared with the simulation results. Since photon spectrum was obtained to be identical in the entire chamber volume, no correction for energy response of fibres were needed over the volume of sample chamber. Dose rates calculated on both radial and axial directions and also on bottom surface of the exposure chamber showed good agreement with the result of silica fibre TL dosimetry. Dose mapping has been reported here with higher accuracy and precision than the literature data. The ability of fibre dosimeters for such dose mapping study has clearly been shown by the precision of the obtained results. Dose rate on the central plane of the CG-220 and on vertical axis (X = 0) was found to be 22% and 26% lower, respectively at lower and upper points compared with the maximum

dose rate at the center. On radial axis at the center of the chamber (Y = 0), dose rate was found to be higher at the corners (near the chamber wall) by ~20 %. The dose rates are more uniform on the bottom surface of chamber (Y = - 10) and vary by less than 7 %. User of the irradiator should be aware of inhomogeneity of dose distribution in the sample chamber; otherwise the estimated doses would be erroneous.

CHAPTER 7: INTRABEAM SYSTEM DOSIMETRY

7.1 Introduction

Intra Operative Radiation Therapy (IORT), a relatively recent treatment modality, is attracting interest as a result of the inherent advantages relative to other methods of radiation therapy. This technique provides patient convenience, reducing the number of treatment fractions that are more conventionally used in external beam radiotherapy with just single session IORT irradiation being required. Generally in brachytherapy, survival of normal tissues necessitates a source with rapid dose-rate fall-off. The INTRABEAM X-ray source (XRS) manufactured by Carl Zeiss Surgical (Oberkochen, Germany) is one such type of device, introduced initially for partial breast cancer radiotherapy (Kraus-Tiefenbacher et al., 2003), being later also used to treat other cancers such as spinal metastases (Schneider et al., 2011), brain tumours (Seddighi et al., 2015) and prostate cancer (Buge et al., 2015). This treatment modality benefits from the biological effectiveness of low energy photons (Brenner et al., 1999) in addition to other general advantages of the IORT method (Ebert & Carruthers, 2003). Thus said, the elevated delivered dose per treatment fraction necessitates accurate monitoring of dose to organs at risk. A prime example is in regard to skin dose, of importance not least because of the inherent cosmetic aspects of breast IORT. In view of the dominant special characteristics of the INTRABEAM system, primarily in regard to the photon field, with associated changes in beam quality and dose-rate gradient, the dosimetric task of working at a nominal operating voltage of 50 kVp is complex. Beam hardening occurs with depth into tissue and even within the body of spherical applicators used for breast irradiation. Use of the INTRABEAM XRS system also gives rise to a rapid dose-rate fall off from the tip, prevailing over a distance into tissue of some 4 to 5 cm. Both factors demand a dosimeter of size as small as possible in order to reduce uncertainties in dose assessment resulting from the inherent volume-averaging effects (Fogg et al., 2010; Soares et al., 2006).

Furthermore, dosimetry of the INTRABEAM system requires a non-hygroscopic dosimeter for *in vivo* measurements.

GDSFs have been proposed as high spatial resolution dosimeters, with various tailor-made sizes available, down to ~100 μm outer diameter that offer sensitivities covering a wide range of dose as well as reusability, providing for a range of clinical radiation applications (Bradley et al., 2012). The ability of these fibres to be used as TL dosimeters in radiotherapy and also non-medical applications has been studied in various publications [see for instance (Abdul Rahman et al., 2014; Jafari et al., 2014)]. With regards to their potential application in brachytherapy, Issa et al. (2012) studied the use of GDSFs with keV and MeV photons in comparison with Monte Carlo simulation results and reported 3 % and 1 % agreement, respectively. Palmer et al. (2013) reported the use of GDSFs for high dose-rate (HDR) brachytherapy dosimetry in comparison with two other dosimeters, EBT3 films and PRESAGE polymers, pointing to a problematic noise to response ratio and a consistent over response at low doses. It was believed that part of the problem was due to the lack of a suitable stabilization process for the GDSF. In this research, the dosimetric characteristics of these fibres had potentially been significantly improved by a proper annealing regime and pre-dose treatment, as described in Chapter 3 of this thesis.

Therefore in this Chapter, the aim is to characterize the GDSFs and to investigate their dosimetric utility for the INTRABEAM system dosimetry. Firstly, the GDSFs was calibrated to obtain the relationship between TL responses and absorbed dose. The probable effects of changes in photon spectrum and dose-rate variations on TL response were subsequently investigated and verified. Additionally, depth-dose curves obtained using the GDSF TLDs were compared against reference measurements made using an ionization chamber (IC). The feasibility of GDSF for skin dose measurement was then

examined by validating measurements made on a water phantom surface against Gafchromic EBT3 films and Monte Carlo simulations. Last but not least, the GDSFs were used to assess the skin doses incurred by three breast cancer patients undergoing IORT in an operation setup.

7.2 Materials and methods

7.2.1 INTRABEAM system X-ray source (XRS)

Electronic brachytherapy sources has recently gained popularity because of their inherent advantages compared to radioactive brachytherapy sources such as offering a constant dose rate at a fixed distance from the source and avoiding potential risks from the handling of radioactive sources. One of the low keV X-ray systems became commercially available recently, is the INTRABEAM system (Carl Zeiss Surgical, Oberkochen, Germany) that is able to generate isotropic dose distribution in a tumour cavity subsequent to lumpectomy as a particular example of that so called IORT. This system has various shaped applicators enable the user to produce different dose distributions based on the treatment need. System is equipped with a stand allowing to position the XRS within the patient with 6 degrees of freedom (Figure 7.1).

Figure 7.1: INTRABEAM system stand with the XRS attached with spherical applicator (picture taken from 9th ZEISS INTRABEAM System User Meeting Abstract Booklet, 2015)

The INTRABEAM IORT XRS includes a 10 cm long, 3.2 mm outer diameter tube, made from mu-metal for magnetic shielding, with the exception of 1.6 cm end part which is made from beryllium to provide a quasi X-ray transparent window, terminating in the form of a hemispherical cap (Yanch & Harte, 1996). This needle shaped tube is attached to an electron gun that generates the electrons which are then accelerated through the evacuated tube. This produces bremsstrahlung and characteristic X-ray with mean energy of 20–30 keV which is markedly less than that of the maximum energy of 50 keV. Electrons strike the very thin gold target (presumably chosen to be of a thickness optimal in stopping the majority of electrons, generating maximal bremsstrahlung and characteristic lines from this high atomic number target) deposited on the inner layer at the end of the tube. Based on manufacturer's data, electrons reaching the gold target have a Gaussian energy distribution of full width at half maximum (FWHM) of 5 keV (Clausen et al., 2012). The outer surface of the tube is coated along its whole length with a thin

layer of chromium nitride (CrN) (Bouzid et al., 2014), providing both for durability and biocompatibility (Keshtgar et al., 2014). The resulting bremsstrahlung X-ray spectrum with a maximum energy of approximate 50 keV eventuates an almost isotropic dose distribution showing maximum angular variation of 15 % (Yanch & Harte, 1996).

The INTRABEAM system was initially introduced with cylindrical, spherical and needle applicators (Keshtgar et al., 2014) and then was later equipped with superficial (flat) applicators that are capable of converting spherical dose distributions to flat circular shapes (Schneider et al., 2014). The system of interest in treatment of the post-lumpectomy primary breast tumour bed includes eight different diameter spherical applicators made of polyetherimide, ranging in diameter from 1.5 cm to 5 cm in 0.5 cm increments. Figure 7.2 (A) shows the smallest and largest size spherical applicators, while the console and quality control devices associated with the X-ray source (XRS) are shown in Figure 7.2 (B). For the smaller size applicators (diameters from 1.5 to 3 cm), an aluminum attenuator is placed between the applicator body and the XRS probe (Eaton, 2012). This intentional beam hardening (removal of very low energy photons from the treatment spectrum by the aluminum) is sufficiently performed by the applicator body itself when larger applicator sizes are being utilized (Keshtgar et al., 2014).

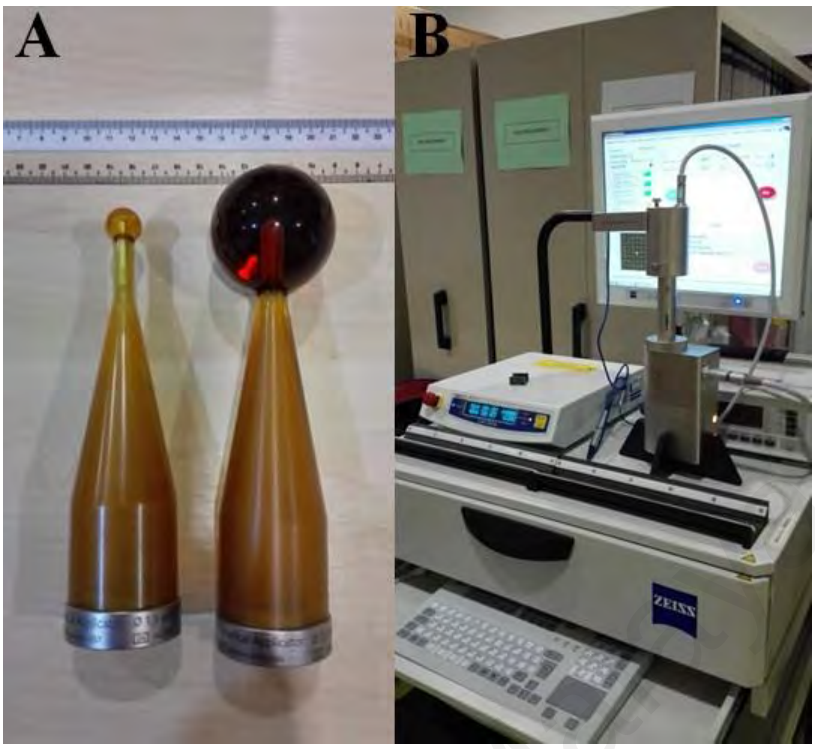

Figure 7.2: A) Smallest and largest size spherical applicator of INTRABEAM system (1.5 cm and 5 cm diameter) B) INTRABEAM XRS attached to the control console and PAICH (PAICH is mounted for the output check)

7.2.2 INTRABEAM system water phantom and ionization chamber

INTRABEAM system has a specific water phantom with possibility of mounting of the XRS for QA purpose. The water phantom is equipped with a sub-millimeter knob having 0.01 mm precision that allows changing of distance between ionization chamber housing and the tip of the XRS or applicators. Accuracy in positioning was a very important need in this study, since the effects of phenomenon happening in present photon field with distance, including dose rate and beam quality changes, on fibre response might be considerable. Walls of the phantom are made from lead glass in order to provide enough shielding for the user. Water phantom has horizontal and vertical plastic housings designed for positioning of ionization chambers (IC) to measure depth doses and to check the XRS output isotropy respectively. The space embedded in the wall to accommodate IC cable, is also well shielded by steel covers for radiation protection. Figure 7.3 shows the INTRABEAM water phantom, its knob and the way XRS is mounted on the phantom.

The ionization chamber was of model type PTW TN34013A (PTW, Freiburg, Germany) with a 0.005 cm^3 sensitive volume (Figure 7.4).

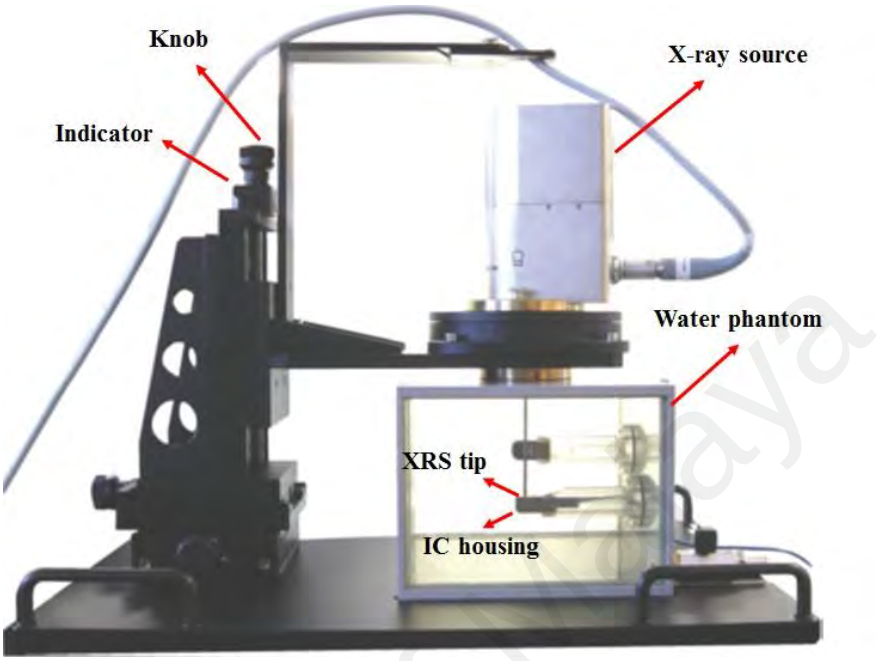

Figure 7.3: INTRABEAM water phantom provided for in-house QA procedure (picture taken from INTRABEAM® water phantom manual)

Figure 7.4: PTW TN34013A Ionization Chamber

7.2.3 EBT3 Gafchromic film

The Gafchromic EBT3 film (Radiation Products Design Inc., USA) is composed of an active layer of 28 µm thickness sandwiched between two matte substrate of clear polyester each with 125 µm thickness. It is recommended for the dynamic dose range of 0.1 to 20 Gy and its energy dependence is minimal in the range of 100 keV to MeV energies (EBT3 film instruction manual). The EBT3 films (cut into 20 mm × 20 mm)

were placed at a source to detector distance (SDD) of 10 mm in the water phantom. The films were irradiated to known doses of 1 to 20 Gy at selected intervals. The films were scanned 24 hours after irradiation to allow for post-irradiation colour changes, using an Epson 10000 XL flat-bed scanner (Epson America Inc, Long Beach, CA). The films were scanned in transmission mode, at a resolution of 75 dots per inch (dpi) and 48-bits RGB format. The images of scanned film were saved as TIFF format to avoid compression and loss of data. All the images were analyzed using the ImageJ 1.47 software (National Institution of Health, USA). A calibration curve relating the pixel value and the doses was established. EBT3 film was used for surface dose measurement and comparison with doses measured by GDSFs.

7.2.4 Preparation of GDSF samples

Single mode fibres (SMF-1) characterized in Chapters 3 to 5 were used in this study. Preparation of 5 mm samples was as described in Chapter 3. Based on the findings in Chapter 3, a pre-dose of 100 Gy (from GC-220) was applied to the fibres, to stabilize the TL response of samples. The fibres were then annealed in a pre-heated furnace at 500 °C for 60 minutes followed by immediate cooling. These are important preparatory steps in use of GDSFs, as pristine or non-irradiated samples potentially show deviation from a linear fit (in the past an over-response has been observed) from low to high doses (also can be seen in the results reported by Issa et al. (2011) and Noor et al. (2010)). In this circumstance, a unique calibration equation (obtained for pristine samples) may result in overestimation of dose at very low dose regions, as reported by Palmer et al. (2013). After irradiating the GDSF samples, the TL response of samples were read and recorded using a Harshaw 3500 TLD reader by linear heating from 50°C to 400 °C with a heating rate of 25 °C/s. A 24 hours relaxation time was given between irradiation and reading of all samples to provide similar fading.

7.2.5 Calibration of GDSFs

A total of five prepared GDSF samples were placed on small sized (~ 2.5 × 8 mm) paper labels (Figure 7.5-A and B) and attached to the upper surface of the horizontal chamber housing (Figure 7.5-C). The water phantom has a screw equipped with an indicator to adjust the distance between the source and chamber housing, providing a precision of 0.01 mm. The location of the XRS tip was adjusted to provide for tip to samples separation of 10 mm. Subsequently, irradiation doses were given, ranging from 1 Gy to 20 Gy at the position of the samples. Based on the recorded calibration data (for absorbed dose values in water), the duration of irradiation was determined by the system control console, and checked real time by the internal radiation monitor (IRM).

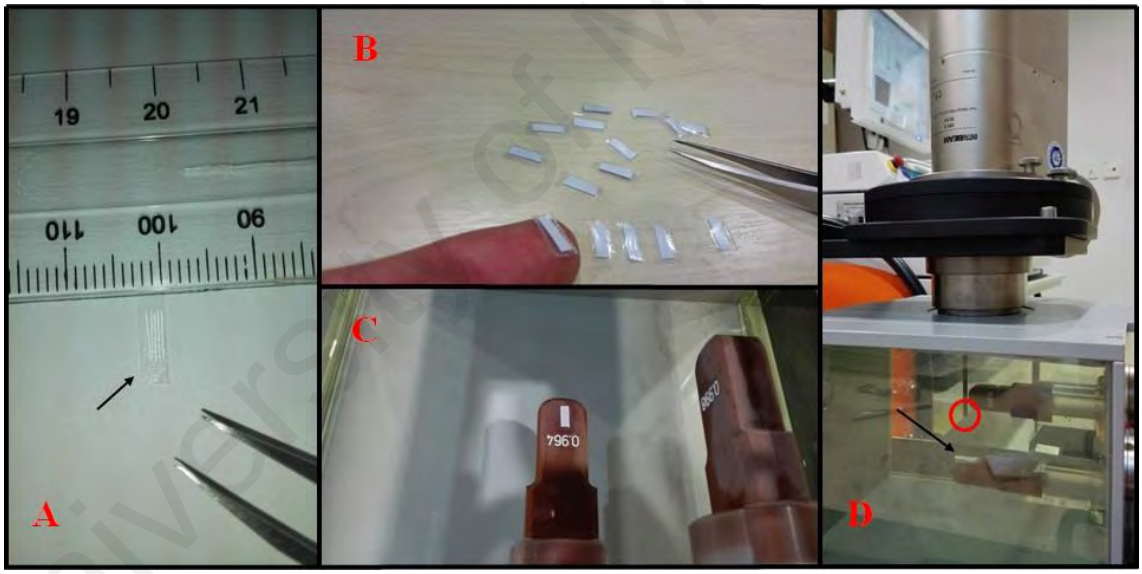

Figure 7.5: Experimental setup for positioning (A, B and C) and irradiating (D) GDSF (black arrows show the location of GDSFs and red circle shows the XRS tip)

To examine the effect of beam quality and dose-rate changes on GDSF response, the irradiation depth in water was changed stepwise over the range 3 to 45 mm, the operational depth of the XRS and the range for which reference depth-dose data from factory measurements are available. The distance between XRS tip and GDSF samples was changed to provide depths of 3, 4, 5, 6, 7, 9, 10, 15, 20, 25, 30, 35, 40 and 45 mm in

water. Then, a dose of 1 Gy (dose to be delivered to water) was applied to the GDSF samples at specified depth.

The probable effect on GDSF TL response of the presence of a spherical applicator placed over the XRS tip (the size of applicator being dependent on the size of excised tumour lump) was assessed, comparison being made with the results from irradiations conducted with the bare tip and probe arrangement. These irradiations were performed in water with the fibre samples positioned on the surface of the applicators. Irradiations were made at the tip of all spherical applicators with sizes of 1.5, 2, 2.5, 3, 3.5, 4, 4.5 and 5 cm diameters. For the largest and smallest applicator sizes (5 and 1.5 cm), several doses ranging from 1 to 20 Gy were irradiated, while for other applicators, only one irradiation of 10 Gy was applied to fibres on the applicator surface.

7.2.6 Depth dose measurement

In order to measure depth-doses in water, groups of 5 GDSF samples were positioned on the upper surface of the chamber housing, ready to provide for sequential irradiations at various depths ranging from 3 to 45 mm. With this arrangement, the irradiation dose of 20 Gy (dose to water) at a depth of 3 mm was given, effectively resulting in different doses to each sample group. The samples were then read-out and application made of the calibration equation described in the previous section in order to calculate the dose-rate at each depth. The resulting depth-dose curve was compared against the factory commissioning data, measured using the IC.

7.2.7 Monte Carlo simulations

The main issue regarding the use of GDSFs for dosimetry of the INTRABEAM system is energy dependence of the TL response of these fibres due to the predominance of photoelectric effects at low keV energy and non-tissue equivalence of fibre material as discussed in Chapter 4. To characterize the effect of changes in beam quality with depth

in medium (water or tissue) and provide the correction factors for energy dependence at various situation such as presence of different size applicators as well as depth in tissue (distance between irradiation and measurement points), Monte Carlo simulations were conducted.

Version X of the MCNP code ("MCNPX user's manual, version 2.6.0," 2007) was used in this study, due to the accessibility and useful possibilities of the code as described in Chapter 5. The INTRABEAM XRS was simulated based on the accurate geometrical and compositional data provided by the manufacturer (Carl Zeiss, Germany). Geometry is the first thing to be defined using cells to determine volumes and surfaces to specify cells. Then proper elemental compositions and densities are used to fill volumes to complete geometry definition. Accurate description of the electron source is usually the most basic issue, of high importance in simulation that needs high accuracy but then often a number of approximations and further detailed verifications are needed. Clausen et al., (2012) have investigated the impact of radius of the electron beam hitting the gold target of the IORT system. It was reported that effective points of incidence of the diverged electron beam to the target, which agreed with the available experimental dose distribution, were obtained with a value of the radius that ranged from 0.6 to 0.7 mm and from 0.7 to 0.8 mm, with weighting factors of 1.05 and 1.55 respectively. The same electron beam lines were used in the current study with the Gaussian energy spectrum as provided by manufacturer (shown in Figure 7.6).

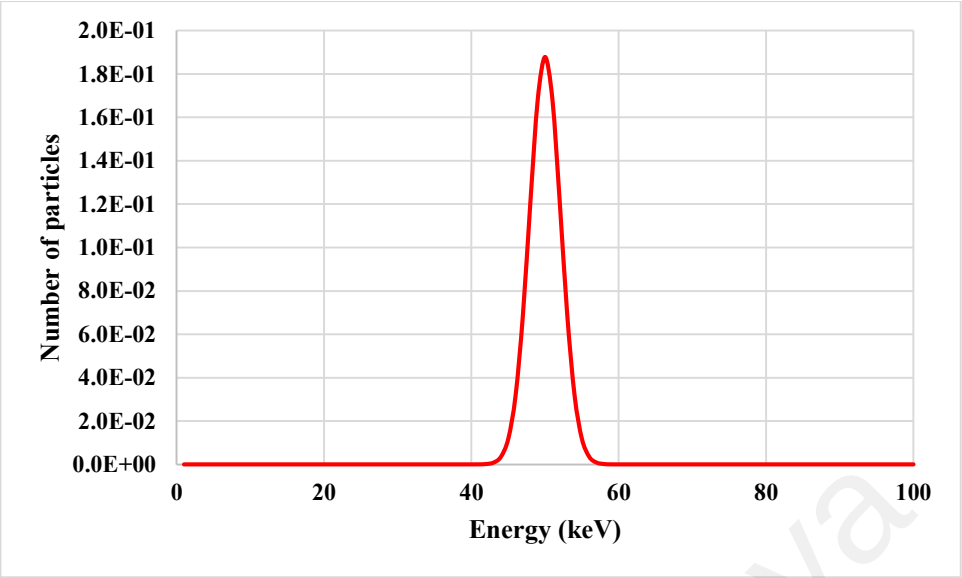

Figure 7.6: Gaussian energy distribution of primary electron beam considered in MC simulation

The first series of models were simulated to obtain the energy spectra at different surfaces, including different depths in water and the various applicator surfaces. Photon counts in 0.2 keV energy bins, from 0 to 63 keV (the maximum electron energy of the Gaussian distribution), were performed using tally F4. Energy cut off for both electron and photon transportations in all simulations was set at 1 keV to ensure maximum accuracy. Other than the XRS tip, the photon spectra were calculated at different depths in water to investigate the changes in beam quality. As can be seen in Figure 7.7, 1 × 1 cm^2 area scoring planes were positioned at 5 mm intervals from the tip of the XRS.

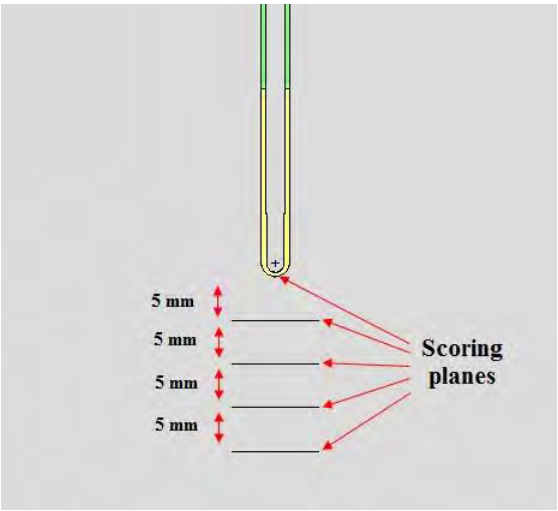

Figure 7.7: Intrabeam bare probe simulated in water and relevant surfaces to acquire photon spectra

The contribution of each primary electron to generate a photon passing through the XRS exit plane was 0.0129 which indicated that only 129 photons will be emanated from XRS for every 10^4 initially emitted electrons. Subsequently, calculation of dose distribution by tracing initial electrons becomes impractical, since the calculation time increases. This is because an extremely large number of photon interactions, of the order of a few hundred millions, is necessary to obtain dose calculation uncertainty within the acceptable range. Thus, for the purpose of acquiring absorbed dose in the second series of simulations, a photon source with the calculated spectrum from the first series and with an isotropic emission was positioned on the outer surface of the XRS tip instead of the electron source definition. Tally *F8 which is equivalent to the detector pulse height was used to calculate dose at this stage. This tally calculates the energy deposition in cells of interest, by all photons and electrons, in terms of MeV per initial emitted particle from the source. Depth doses in water were calculated using deposited energies in cylindrical cells of 1 mm length and 1 mm radius positioned on the symmetry axis of the beam, with their flat-surfaces faced to the source. A low energy cut off of 1 keV for both electrons and photons was set. This is the minimum possible tracking level in MCNPX code that allows obtaining minimum relative error for dose, eventuating in maximum accuracy.

Simulations were continued with increasing the number of primary particles (electrons for the spectrum simulations and photons for the dose simulations) until acceptable calculation uncertainties were obtained. Depth dose calculation in water were performed for the bare probe and also for spherical applicators. Figure 7.8 (A) shows 4.5 cm applicator and scoring cells for dose calculation in water, while Figure 7.8 (B) demonstrates the internal structure of smallest applicator (1.5 cm diameter) with respective materials. For validation purpose of calculated data, depth dose data produced by the INTRABEAM XRS and spherical applicators as measured by the PTW TN34013A ionization chamber (IC) in water was taken as the benchmark to be compared to MC simulation results.

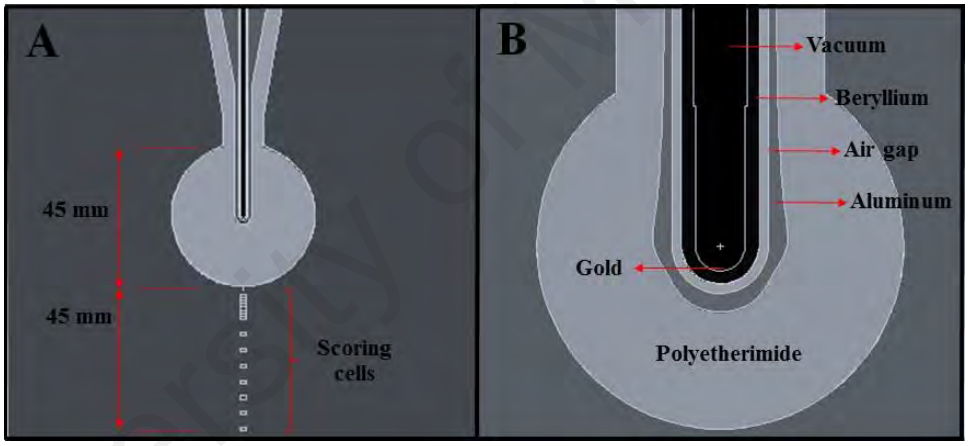

Figure 7.8: (A) 4.5 cm spherical applicator and scoring cells to calculate depth doses, (B) structure of 1.5 cm applicator

7.2.8 Surface dose measurement using the water phantom

This part of the study was aimed at measuring the dose on the water surface of the water phantom, with benchmarking against Gafchromic EBT3 film measurement results and Monte Carlo (MC) simulation. This serves as a validation of the GDSF measurements, prior to the conduct of clinical skin-dose measurements made in three actual IORT procedures, as previously referred to. In the measurement, EBT3 film was cut and positioned on the surface of the water phantom and in the vicinity of the applicator

stem using very thin transparent PVC sheet (Figure 7.9 (A)). This identical setup was simulated within the MNCP software with circular shaped water cells (1 mm width) arranged on the surface 0–40 mm distance from the applicator stem (Figure 7.9 (B) and (C)). Since the goal of simulation and measurement of surface dose is to evaluate and imitate the absorbed dose to skin, and skin dose should be calculated relative to the prescription dose at applicator surface. The thicknesses of water layer were identical for both cells, i.e. the cell around the applicator surface and every cells of interest (those in which dose is calculated). The cell thickness for the current model was set to 80 μm, to be made comparable with the thickness of epidermal layer of skin (ICRP, 1992). A greater thickness of the order of 1 mm was also examined, the outcome of which showed the smaller thickness to better reproduce the experimental results.

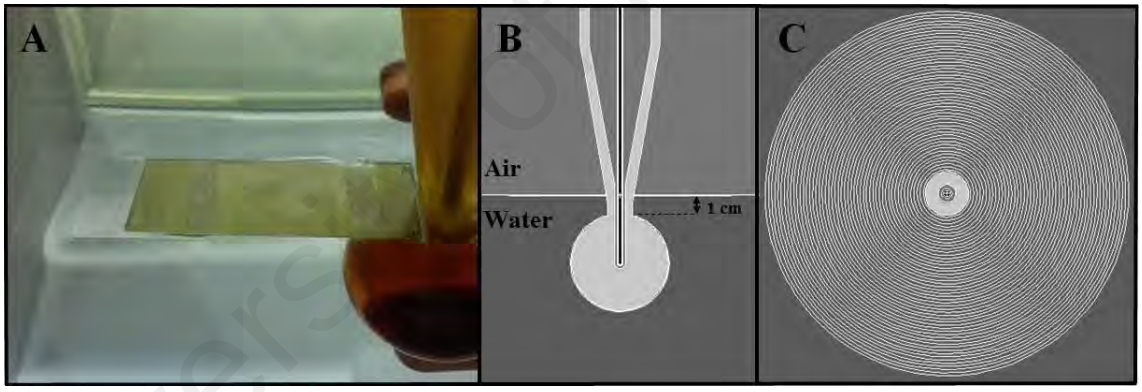

Figure 7.9: (A) Experimental setup for EBT3 film positioning on water surface (B) MCNP modeled geometry of INTRABEAM 5 cm applicator in water phantom (C) ring shape water voxels for surface dose determination

A screening process was performed similar to that described in Section 6.2 in order to select GDSF samples offering response variation to within ±1%, allowing point dose measurements in the absence of any need for averaging over several fibre samples. Figure 7.10 shows a schematic of the experimental setup for the surface dose measurement, where the applicator neck was positioned 1 cm from the water surface. GDSF samples

were arranged at 3 mm intervals on a thin polyethylene sheet that was attached to the applicator stem to remain fixed on the water surface.

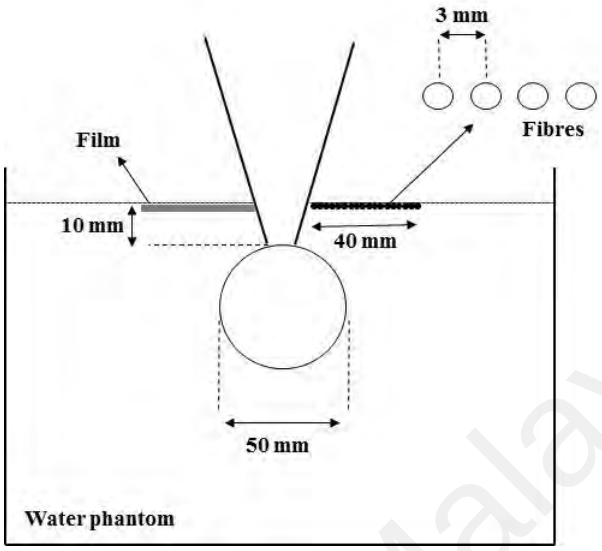

Figure 7.10: Schematic view of the experimental setup for surface dose measurement in water phantom using EBT3 film and GDSFs

7.2.9 *In vivo* skin dose measurement during IORT of breast cancer

Skin dose measurement was performed on three patients undergoing IORT during breast conserving surgery at the University of Malaya Medical Centre under the TARGIT-B trial (Vaidya, 2014), with case 1 using the 4 cm diameter spherical applicator and cases 2 and 3 using the 5 cm applicator. Dose was prescribed to 20 Gy to the surface of the applicator for all three cases. GDSF TLDs were arranged on paper labels and sealed in sterile envelopes that were subsequently positioned at multiple locations on the skin around the patient breast. The experimental setup and fibre arrangement for skin dose assessment for case 1 is shown in Figure 7.11. For this case, the GDSF TLDs (5 samples at each point) were positioned at six locations including points at distances of 1.5 and 5 cm from the applicator stem in the superior, inferior and medial directions (Figure 7.11-B). In addition, an array of GDSF TLDs were positioned at separations from the applicator stem of 0.5 to 6.5 cm at 2 mm intervals in the lateral direction (Figure 7.11-C).

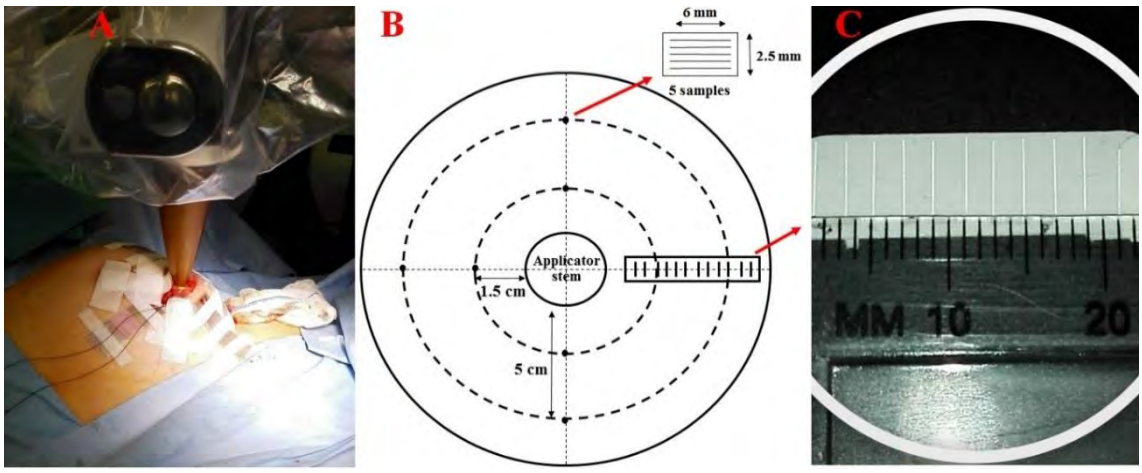

Figure 7.11: A) Clinical setup for skin dose measurement by GDSFs, B) Locations of GDSFs around the applicator stem. C) Magnified view of fibre TLDs arranged at 2 mm intervals

For IORT cases 2 and 3, the groups of GDSF TLDs were similarly positioned on small paper labels and an effort was made to place them as close as possible to the applicator stem (the edge of the skin) to measure the maximum dose to the patient skin which was expected to be at nearest points to applicator stem from the result of surface dose measurements in water phantom. The arrangement and the positioning of samples on the breast skin for case 3 (which is also similar for case 2), is depicted in Figure 7.12. This section of the study was approved by the medical ethics committee of the University of Malaya Medical Centre (MECID No: 201512-1958).

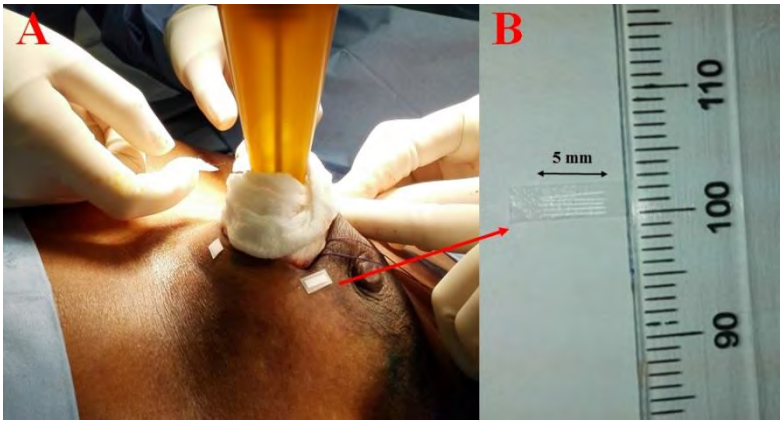

Figure 7.12: A) Positioning of GDSFs on breast skin; B) arrangement of GDSF TLDs on paper labels

7.3 Results and discussion

7.3.1 X-ray energy spectrum and beam hardening

Measured spectrums for different electron accelerating potentials of similar IORT sources have been reported (Beatty et al., 1996; Ebert & Carruthers, 2003). However, different measurement conditions including detector efficiency, measurement medium as well as different coating materials of the initial version of XRS (Yanch & Harte, 1996) do not allow direct comparison of these spectrums with current results. The X-ray spectrum obtained in this work was calculated at the tip of the XRS probe in water which is displayed in Figure 7.13. This spectrum has a range of up to approximately 50 keV with two distinct characteristic X-ray lines originating from the Gold and Chromium elements present at the probe tip. The shape of the spectrum is in good agreement with previous simulated spectrums (Bouzid et al., 2015; Nwankwo et al., 2013; White et al., 2016) calculated using Geant4 Monte Carlo code.

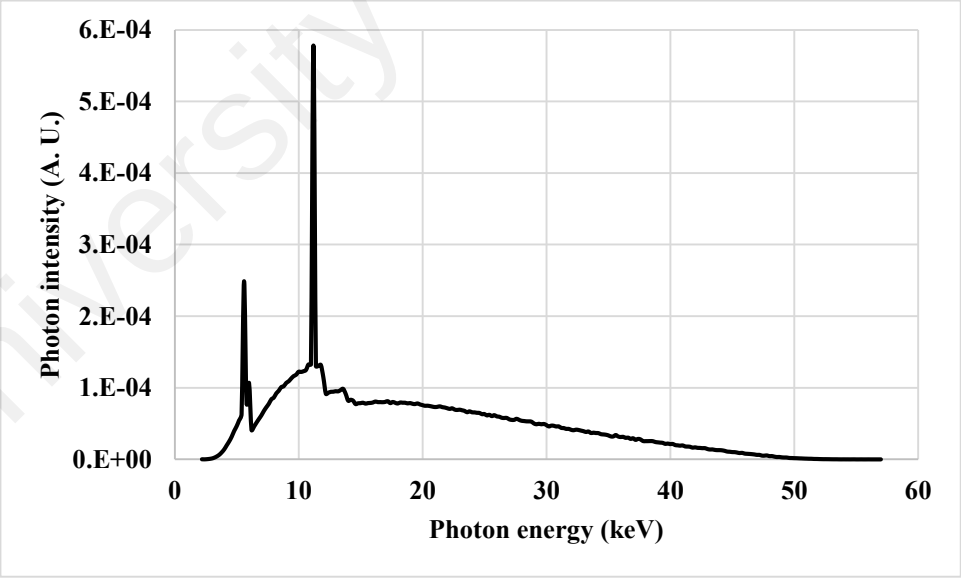

Figure 7.13: X-ray spectrum produced in simulation of the XRS operating at nominal energy of 50 kVp. The lower energy characteristic X-ray lines (5.4 and 6 keV) and the greater energy peaks (10.4, 11.8 and 13.6 keV) are relevant to chromium (the biocompatible coating) and gold (target) respectively (in agreement with characteristic X-rays of mentioned elements (Thompson & Vaughan, 2001))

Figure 7.14 (with logarithmic scale) demonstrates the photon spectrums at the tip of the XRS bare probe compared to those attenuated by different thicknesses of water between the tip and scoring plane (Figure 7.7). Larger fluctuations were observed in the photon spectrums scored at deeper depths due to the increase in photon calculation uncertainties as less particles reach the scoring planes at larger distances from the source. It should be noted that these spectrums were acquired by tracing primary electrons striking to the target, not by definition of photon source at the XRS tip.

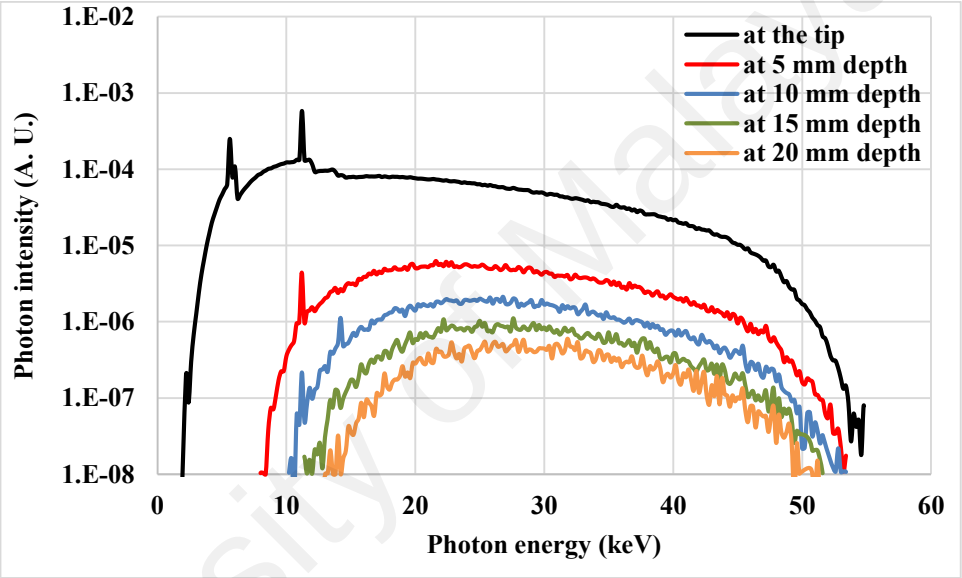

Figure 7.14: X-ray spectrum at XRS tip and different depths in water obtained by MC simulation

Photon spectrums on the surface of different size applicators were obtained using the procedure described in Section 7.2.7 with the difference that the photon spectrum calculated at the XRS tip was considered to be the initial source. The comparisons of these spectrums to the one acquired at the probe tip are shown in Figure 7.15. Photons with energy below 20 keV are attenuated effectively by the applicators in the way that the intensity of photons with energy less than 8 keV is almost zero.

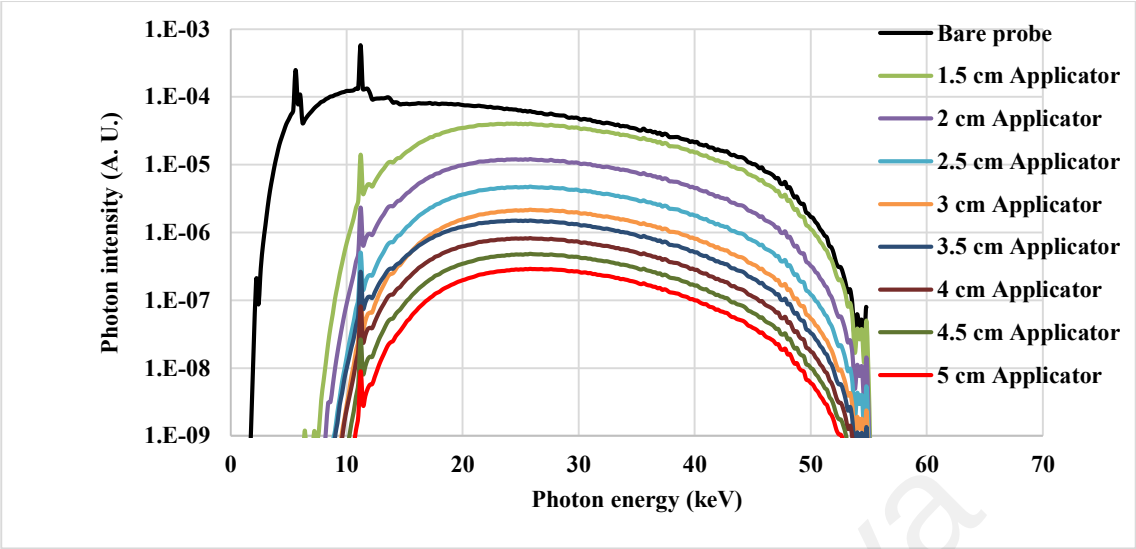

Figure 7.15: X-ray spectrum at XRS tip compared to that of various size applicator surfaces obtained by Monte Carlo simulation

To make a quantitative evaluation of beam hardening effect of the applicators, beam quality can be presented by the mean energy of each spectrum that characterizes the spectral distribution of the radiation field by the distribution of fluence with respect to energy (Khan, 2003). These mean energies were calculated using Equation 7.1, where E_m represents the mean energy of the spectrum, and $N(E_i)$ is the number of photons acquired in the E_i energy bin, and i varies from the minimum (m = 1) to the maximum value (n = kVp, here is the maximum electron energy of the initial Gaussian distribution) of the energy spectrum.

$$E_m = \frac{\sum_m^n N(E)_i E_i}{\sum_m^n N(E)_i} \tag{7.1}$$

Table 7.1 shows the calculated mean energies of the bare probe spectrum at different depth in water and Table 7.2 at the surface of various size applicators. These mean energies are in agreement with the effective energy of the Intrabeam source 20 - 30 keV reported in (Keshtgar et al., 2014). As expected, beam hardening happens for the bare probe spectrum in water and mean energy increases from 19.3 keV at the tip of the XRS

needle to 30.1 keV at 20 mm depth in water. The mean energy of the photon field at the surface of applicators does not change significantly for different applicator sizes which ranges from 27.7 to 28.7 keV. Mean energy shows small increments from 27.7 keV for 1.5 cm applicator to 28.7 keV for 3 cm applicator and from 27.9 keV for 3.5 cm applicator to 28.7 keV for 5 cm applicator. This is caused by the presence of aluminum attenuator in four smaller size applicators which is not present in four larger ones.

Table 7.1: Mean photon energies of the XRS spectrums (bare probe) obtained at different depths in water

Scoring plane		**Effective photon energy (keV)**
Tip of the X-ray source		19.3
5 mm	Depth in water	26.7
10 mm		28.1
15 mm		29.2
20 mm		30.1

Table 7.2: Mean photon energies of the XRS spectrums obtained on the surface of various applicator sizes

Scoring plane		**Effective photon energy (keV)**
On the surface of	1.5 cm applicator	27.7
	2 cm applicator	28
	2.5 cm applicator	28.4
	3 cm applicator	28.7
	3.5 cm applicator	27.9
	4 cm applicator	28.2
	4.5 cm applicator	28.4
	5 cm applicator	28.7

7.3.2 Dose response linearity of GDSFs

Figure 7.16 shows the TL response of GDSFs as a function of absorbed dose, covering the dose range 1 to 20 Gy. Irradiations were made with the bare XRS probe in water, with samples located at 10 mm distance from the probe tip. It should be noted that each point in the graph is represented as the mean value of the TL responses of five fibre samples in which the range of variations among samples TL yield are shown by error bars. The GDSF TL responses to 50 kVp X-rays have been compared against the respective responses to a 6 MeV generated photon beam from a Varian 2100C medical linear accelerator as well as ^{60}Co gamma rays delivered using GC-220. The dose-response shows high degree of linearity ($R^2 = 0.99$) for all three photon energies. The GDSF TLDs show greater response to low keV X-rays (by some several times) compared to that obtained in the megavoltage-generated/MeV photons range, a matter underpinned by the considerable photoelectric energy dependence of the silica-based fibres, resulting in elevated absorption at photon energies below some 100 keV due to the dominance of photoelectric effects in this range. The low energy 50 kVp X-rays of an XRS system suffer change in beam quality as the beam hardens in travelling deeper into water or tissues (the lower end of the bremsstrahlung spectrum being preferentially absorbed). The effect of these changes in beam quality to the response is further evaluated in the next section.

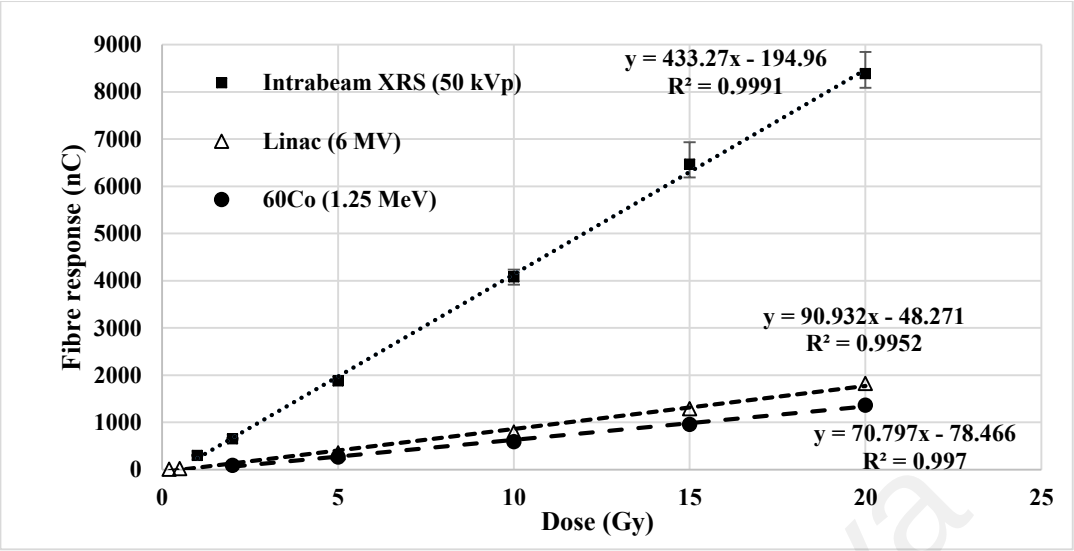

Figure 7.16: GDSF TL dose response with the INTRABEAM photon source compared to the responses obtained with the MV-generated/MeV photon beams

7.3.3 Effect of irradiation depth on TL response

To investigate the effect on fibre response of beam quality variations at different depths, the same dose of 1 Gy (to water) was applied to GDSF samples at depths ranging from 3 to 45 mm, as described in Section 7.2.5. Beam hardening will occur to the spectrum of 50 kVp generated photons as they travel in the attenuating medium (the applicators and water or tissue in the present study), thereby increasing the mean energy of the spectrum (as can be seen in Table 7.1 and Table 7.2). With the relatively low photon energies of the INTRABEAM XRS suffering attenuation as described, there will be an expected effect on TL response of the GDSF TLDs in the low keV, as shown in Chapter 4, yielding increase or decrease in TL response proceeding to deeper points in the water. Figure 7.17 shows the result for the delivery of a constant dose of 1 Gy, applied to different depths. A variation of ± 4.2 % (1SD of 2.3 %) was observed in the TL responses across all depths investigated with the maximum and minimum at 5 and 35 mm depths respectively without showing any increasing or decreasing trend within the uncertainties. This observation could be due to the decrease in dose-rate of the XRS X-rays with depth and coupled with dose-rate dependency of the TLDs. The XRS system used in this study gives rise to a

marked dose-rate fall-off, a desired feature of the system for brachy-IORT applications, from 33.9 Gy/min at 3 mm distance from the source to 0.068 Gy/min at 45 mm depth in water. The effect of dose-rate changes on TL response of GDSF has been reported by (Abdul Rahman et al., 2011) in the range of 1 to 6 Gy/min for megavoltage photon and electron beams. In this range, the GDSF TLDs showed a limited 2.4 to 3.9 % dependence on dose-rate, with higher responses at lower dose-rates. This phenomenon is known as reciprocity law failure, sometimes also as the Schwarzschild effect (see for instance, (Djouguela et al., 2005)). Since, in this case, the dose-rate and beam quality were both changing with increasing depth in water, it was not possible to distinguish their respective effects on GDSF TLD responses. However it will be investigated in more detail in the coming sections.

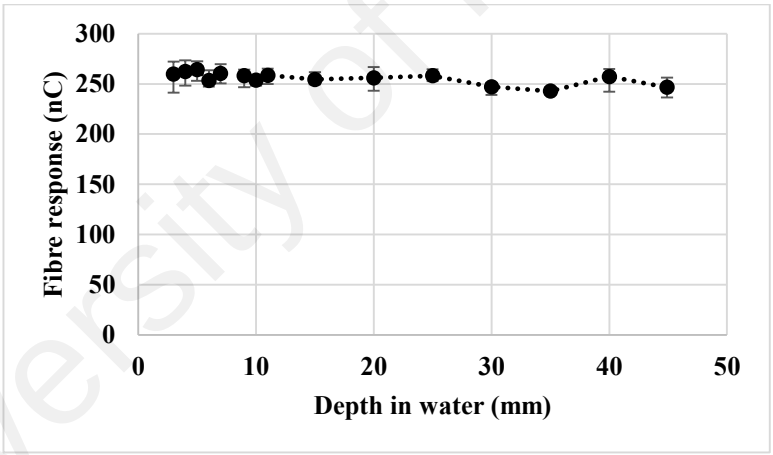

Figure 7.17: GDSF TL response for 1 Gy delivered dose versus depth of measurement in water

7.3.4 Depth dose determination

Figure 7.18 shows the depth dose data for the bare probe measured by ionization chamber (IC) in water for two available XRS units (XRS 1 and XRS 2) in UMMC (University of Malaya Medical Center). Comparison was made against the MCNP calculated depth dose data which have been normalized to the maximum value at 3 mm depth. It was observed that simulation results conformed well to the dose fall off in water

for the XRS 2. However, a systematic difference was noted between the simulated and the XRS 1 depth dose data. This difference in the output dose rate of different sources has been reported elsewhere (Armoogum et al., 2007) and this can be due to the difference in the structures of X-ray generator including electron source, beam deflector as well as the gold target. Since the target has a micrometer scale thickness (Clausen et al., 2012), the difference between manufactured and ideal target thicknesses can be a plausible reason for this observation. This means that the calculated photon spectrums may also be somehow different for any individual XRS.

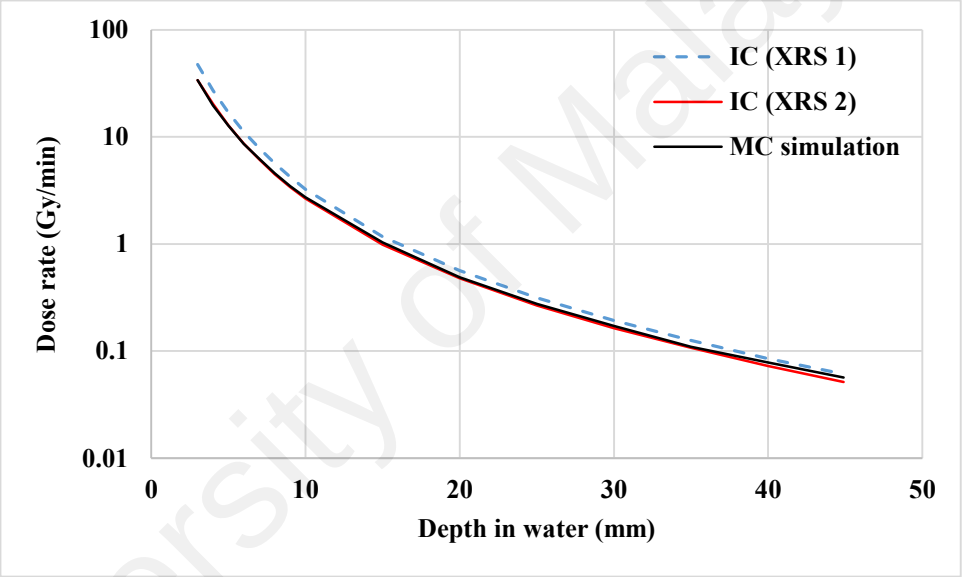

Figure 7.18: Depth dose fall off calculated by MCNP versus measured one by IC for two different XRS

Based on the calibration equation obtained (Figure 7.16), the TL responses were directly converted to dose, and the end results are presented in Figure 7.19. Comparison was also made with depth-dose values measured with the IC and MC simulation. It should be noted that irradiations for depth dose measurement were carried out using XRS 2. No correction was applied for effect of depth (including both dose-rate and beam quality effects). Depth doses measured by the GDSF TLDs were in the range of 0.028 Gy to 21.1 Gy and agreed to a mean of within 6 % with IC measurements. Maximum deviation of

11 % was observed from the IC measurement at 8 mm depth in water where the dose rate fall-off is very rapid. Dose measured by GDSF are slightly lower than the IC measurement at all points except for the first 3 points closer to the XRS tip.

Plausible reasons for such deviation are the effect of energy dependence as described before as well as the positioning procedure of fibres samples on the chamber housing. Additionally, the thickness of the paper labels to which the TLDs are affixed was not accounted, a situation that prevails for all of the investigations reported herein.

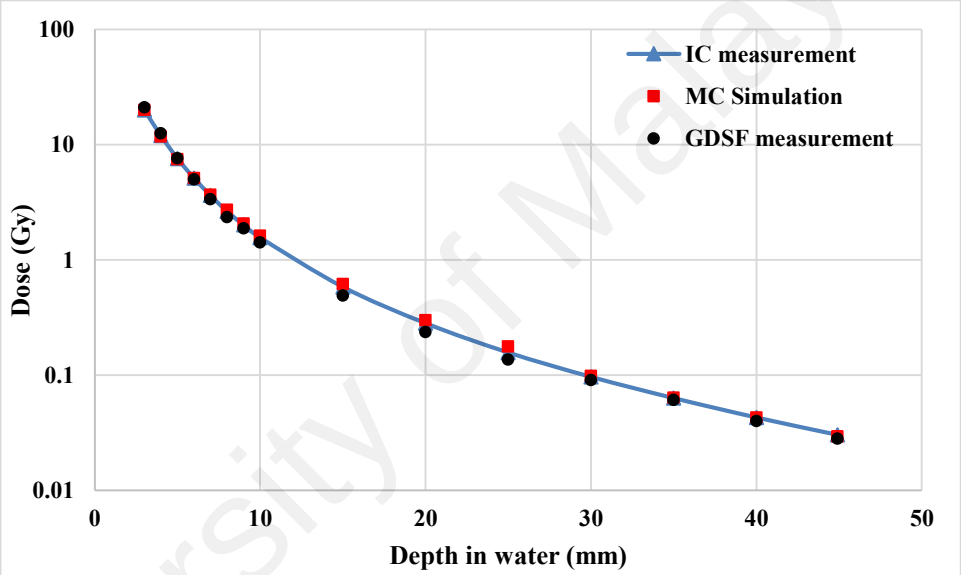

Figure 7.19: Results of depth dose measurement in water using GDSF compared to IC measurements and MC simulations

7.3.5 Calibration for applicators

Over the dose range 1 to 20 Gy, Figure 7.20 shows the results of calibrations made on the surfaces of the largest and smallest spherical applicators. Comparison was made with the previous linear fit obtained for the XRS probe in the absence of any applicator. At identical dose values, the GDSF TLDs on the surface of the small applicator resulted in greater responses compared to that obtained with the large applicator, with differences of between 25 and 32 %, depending on dose. At 10 mm depth in water, the TL yields

recorded for the bare probe irradiation were lower than that of the 1.5 cm applicator but greater than that of the 5 cm applicator.

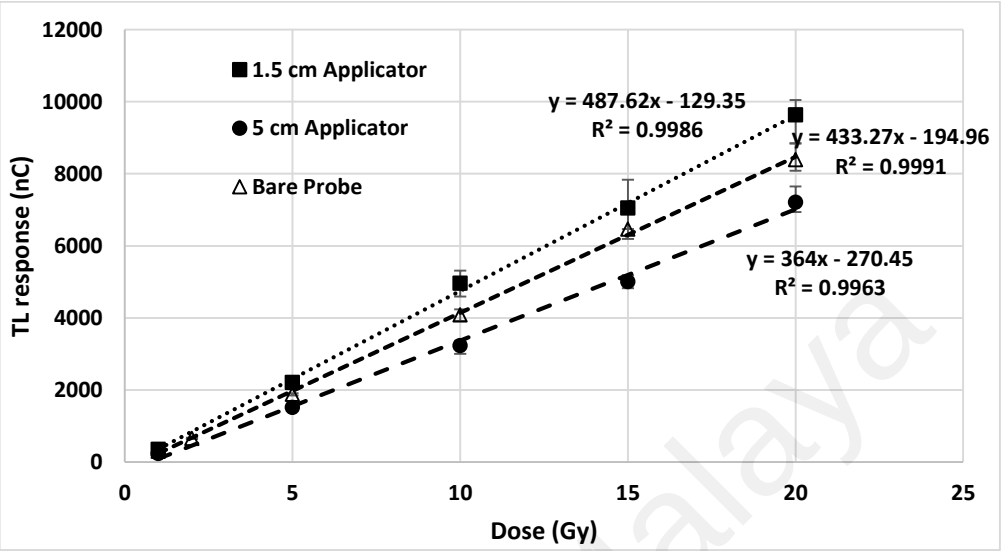

Figure 7.20: Dose response of GDSF irradiated at 10 mm distance from the XRS probe compared to those of on applicators surface

Simulation results in Section 7.3.1 had proven small changes in beam quality at the surface of spherical applicators depending on the applicator size. This can be the possible reason for the difference in GDSF TL responses for large and small applicator sizes. This difference can also be due to the dose-rate dependence of TL response.

Table 7.3: Dose rate at the surface of the range of spherical applicators calculated by the Intrabeam system based on calibration measurements

Applicator diameter (cm)	Dose-rate on surface (Gy/min)
1.5	3.17
2	1.89
2.5	1.23
3	0.85
3.5	1.15
4	0.83
4.5	0.57
5	0.43

Table 7.3 shows the dose-rates on-surface of different size applicators. Larger applicators demonstrate lower dose-rates on the surface as expected, but it should also be noted that the four smaller applicators have an aluminum attenuator which are not present in the four larger applicators. As was explained in Section 7.2.5, this part of the study was extended by irradiating the GDSF TLDs to the same dose of 10 Gy, for fibres positioned on the surface of all applicators. Table 7.4 presents the ratio of TL response of the GDSF TLDs irradiated on each applicator surface relative to that on the 1.5 cm applicator. As can be observed, TL response in general decreases with increasing applicator diameter. Since applicator diameter has the inverse relation with dose rate, it should be clarified whether variations in TL response are related to dose rate or not.

Table 7.4: Ratio of the TL response of GDSF to 10 Gy dose, measured on the surface of various spherical applicators relative to that of the 1.5 cm applicator

Applicator diameter (cm)	Relative TL response
1.5	1
2	0.91
2.5	0.89
3	0.87
3.5	0.83
4	0.8
4.5	0.84
5	0.82

Chen & Leung (2000) have theoretically shown the possibility of both increase or decrease of the TL response with increasing dose-rate, an observation that has also been reported experimentally. For instance, for a somewhat similar TL material, CVD (chemical vapor deposition) diamond, Wrobel et al. (2006) reported higher response at lower dose-rates, although Zaragoza et al. (2010) reported the converse trend. The first group used 45 kVp X-rays for dose-rates ranging from 0.7 to 100 Gy/min, while the second group utilized ^{60}Co gamma rays, with dose-rates in the range 2.4 to 20.67 Gy/min. The possibility that the dose-rate effect on TL response could be a complicated function of dose and energy of irradiation cannot be discounted.

7.3.6 Verification of dose rate and beam quality effects

In order to verify effect on fibre TL response of dose rate, two different experiments were designed. In the first experiment, the ERESCO X-ray tube generating photons at nominal energy of 50 kVp was used to be compared with the photon spectrum produced by INTRABEAM XRS. Description of the X-ray tube and estimated output photon spectrum is presented in Chapter 4. Same kVp of 50 kV was used while various dose rates were produced by changing tube current (mA) and distance from X-ray tube output window (Al filter). Changes in the spectrums of X-ray caused by different air thicknesses between source and fibre samples is assumed to be insignificant, since short distances ranging from 10 to 60 cm were used. The dose rates at each condition (distance and mA) were measured using the Unfors ionization chamber (described in Chapter 4) and the same dose were applied to various groups including 10 fibre samples using different dose rates. Figure 7.21 presents the results of fibre TL responses in terms of applied dose rates.

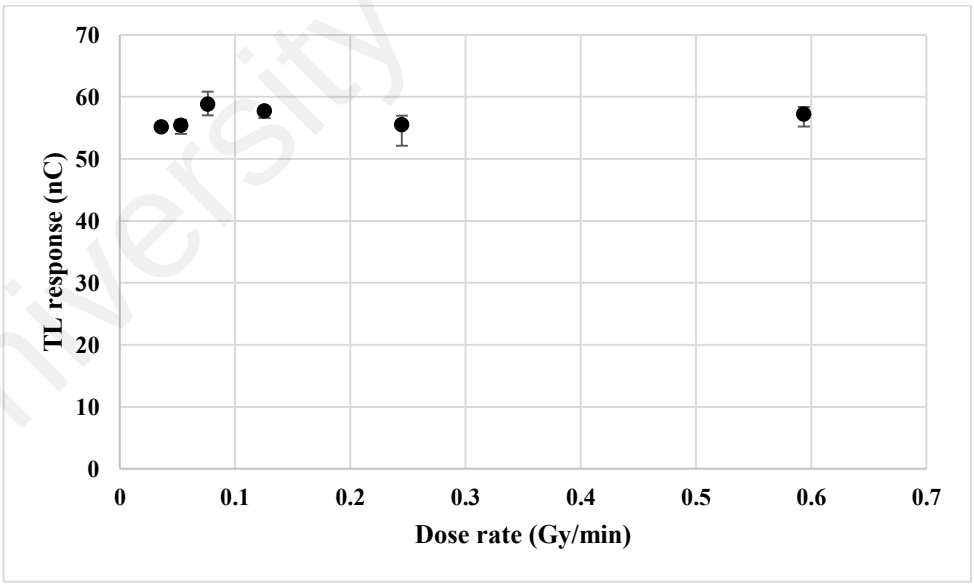

Figure 7.21: Experimental results to evaluate dose rate effect on TL response of fibres using 50 kVp photons from ERESCO X-ray generator

Since the dose rates produced by X-ray tube do not cover the range of dose rates from XRS with applicators (Table 7.3), 6 groups of fibres, each including 10 samples were irradiated in another experiment with various dose rates ranging from 1 to 6 Gy/min using a Novalis Tx medical linear accelerator (Varian Medical systems, Palo Alto, CA). Samples were irradiated using 6 MeV photon beam at the reference condition i.e. at 1.5 cm depth in solid water phantom and with source to surface distance of 100 cm and at the centre of the field size 10 × 10 cm^2. The results are shown in Figure 7.22 with error bars showing the associated variations in TL response among 10 samples.

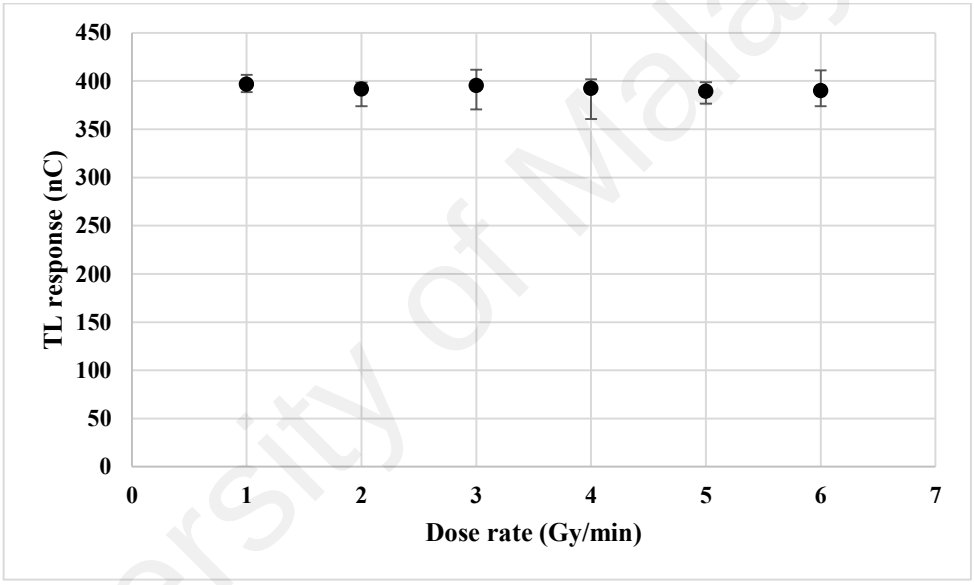

Figure 7.22: Experimental results to evaluate dose rate effect on TL response of fibres using 6 MeV photons from linear accelerator

From the results obtained from both experiments, it can be concluded that change in dose rate at least in the range from 0.04 to 6 Gy/min does not have a considerable effect on TL response of the current GDSF and variable results obtained on applicator surfaces cannot be due to the dose rate effect. Therefore MC simulation were used to confirm the effect of beam quality on absorbed dose in present situation.

In simulation, Ge-doped silica fibre was positioned on the surface of various size applicators from 1.5 to 5 cm diameters. In each simulation, photon spectrum inside the fibre volume was calculated in addition to the absorbed dose to fibre. Photon spectrums obtained are shown in Figure 7.23 where the mean energy of the spectrums shows small variation from 28.1 to 29.1 keV for 1.5 to 3 cm applicator and from 28.3 to 29.2 keV for 3.5 to 5 cm applicator.

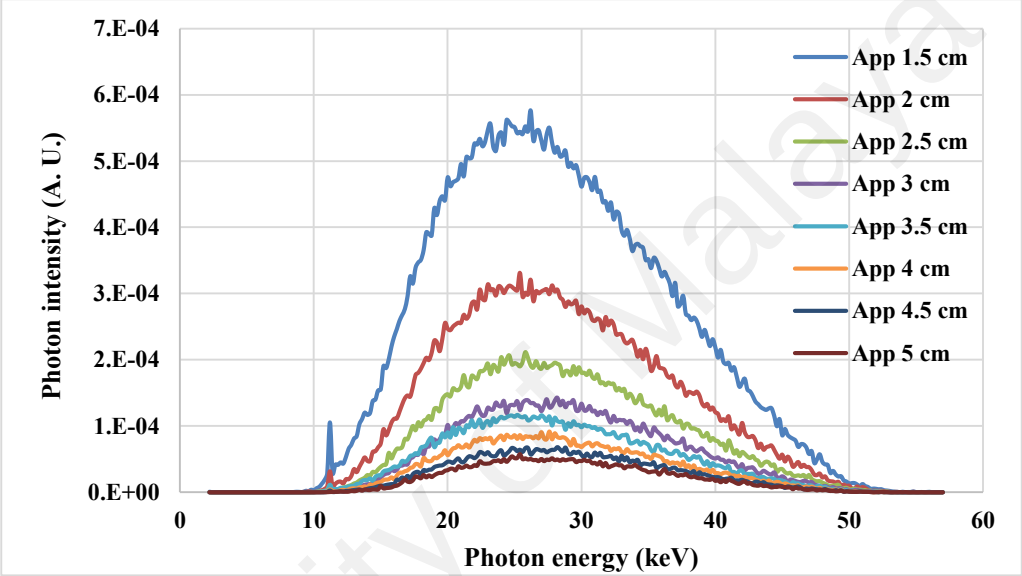

Figure 7.23: Photon spectrums calculated inside silica fibre located on the surface of different size applicators

Absorbed doses in fibre volume filled with water were also recorded in another series of simulation (each taking around 24 hours calculation time). As discussed in Chapter 4, the ratio of absorbed dose in dosimeter to absorbed dose in medium (water) can give an estimation of energy dependence of the dosimeter material, thus Equation 7.2 were used here to obtain relative response of fibre on the surface of various size applicators relative to the 1.5 cm applicator. This ratio is equivalent to the experimental values presented in Table 7.4. Figure 7.24 demonstrates a comparison between experiment and simulation results along with associated uncertainties. Experimental error bars show the variation among TL response of 5 samples irradiated at each case, while simulation error bars show

quadratic summation of MCNP calculated uncertainties for absorbed doses in fibre and water, at which their ratios represent relative response. Relatively large uncertainties observed from MC simulation are due to the small fibre volume that does not allow enough number of interactions and dose deposition inside fibre. It should also be mentioned that the absorbed dose in total volume of fibre (including both fibre cladding and the fibre core (where doped with Ge)) was calculated, as the size of fibre core (8.5 μm diameter) did not allow dose calculation with acceptable uncertainty. This can be a possible reason of relative observed differences between calculated and measured ratios. However mean energies of the calculated spectra inside fibre showed just small variations, with the agreement between the trends observed from MC simulation and measurement confirms the effect of beam quality changes on response of fibres located on applicators surface. Therefore experimental ratios presented in Table 7.4 will be used in conversion of TL response to absorbed dose in the coming sections.

$$Relative\ response = \frac{\left[\frac{Dose_{fibre}}{Dose_{water}}\right]_{App\ X}}{\left[\frac{Dose_{fibre}}{Dose_{water}}\right]_{App\ 1.5}} \qquad (7.2)$$

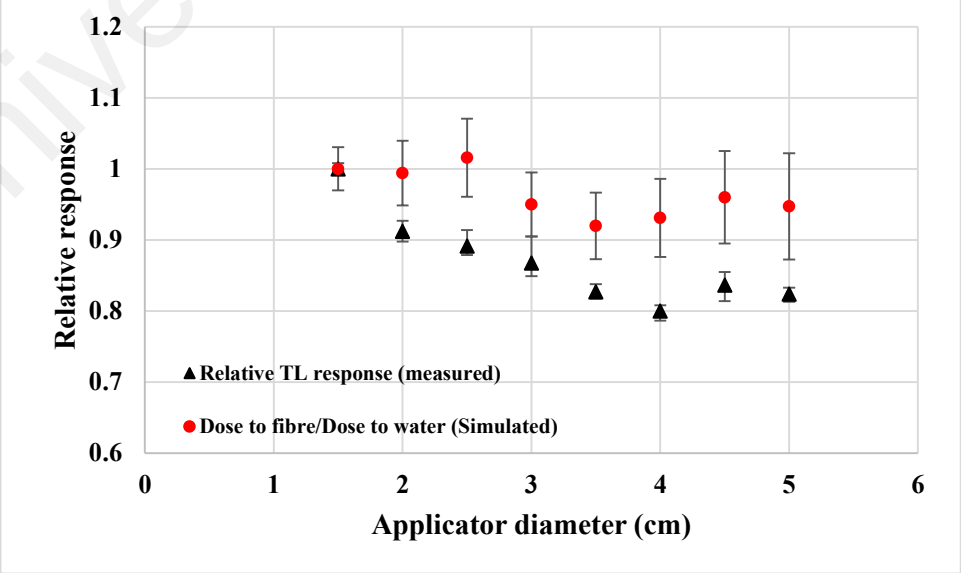

Figure 7.24: Relative TL responses measured on applicators surface compared to relative deposited dose calculated by MCNP code

7.3.7 Surface dose measurement using water phantom

Surface dose measurements were made in water for the setup shown in Figure 7.10, performed using EBT3 film, GDSFs and the MCNPX code. The results of absolute dose values in Gy recorded by all three of the evaluation techniques as a function of distance for a 5 cm applicator are shown in Figure 7.25. To convert TL responses to dose, the calibration equation obtained at the surface of the 5 cm diameter applicator (Figure 7.20) was used, without applying any correction for the distance of separation between the applicator surface and point of measurement. Surface dose from simulation was calculated using Equation 7.3, where E_n and M_n are the deposited energy (in MeV) and mass (in g) in cell n, whereas E_0 and M_0 are related to the same quantities in the reference cell around the applicator which receives the prescribed dose (20 Gy in this experiment). The ring shaped water cells have 1 mm width and 80 µm thickness.

$$\frac{E_n/M_n}{E_0/M_0} \times 20\ \text{Gy} \tag{7.3}$$

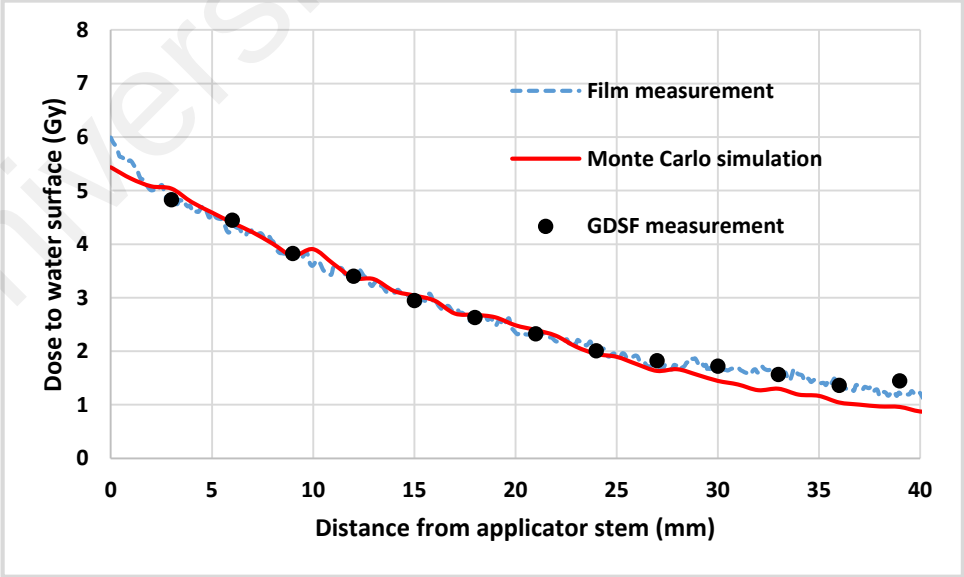

Figure 7.25: Surface dose measurement by GSDF TLDs compared to EBT3 film and MC simulation results

The maximum difference percentage between film and GDSF measurements was 6.6 % except for the point at the tail of the plot (at 39 cm distance) in which the difference was increased to 20 %. The deviations of film and GSDF measurements from MC simulation results, at distances smaller than 24 cm, were less than 5.6 % and 4 % respectively. However, the deviations increased to 27.2 % and 50.6 % for film and GSDF measurements respectively at 40 mm distance. Since both measurements showed relatively large discrepancy with MC results at the farthest points from the applicator this may be interpreted as a result of increasing uncertainty of MC calculations with increasing distance between the scoring cells and radiation source, caused by the decreasing numbers of particles reaching to the scoring cells. The observed difference may also possibly due to the uncertainty in positioning of the film and fibres at a fixed position on the water surface. The film and fibres were attached to the stem of the applicator and it is thought that the most distal part of the both holders may have entered into the water to a small extent and thus received a greater dose than predicted from the simulation.

7.3.8 *In vivo* skin dose measurement during IORT of breast cancer

For measurement of skin doses, the GDSFs were arranged on paper labels and were positioned on the breast skin at four positions subsequent to the insertion of the spherical applicator in the lumpectomy cavity. Assuming emission of photons from the XRS tip to be isotropic (Yanch & Harte, 1996), positioning of the fibres on the skin surface point to the fibre axis are normal to the radiation field. As such, no consideration has been made with regard to the angular dependence of fibre response, as discussed in Chapter 5. Furthermore, prior reports (Entezam et al., 2016; Noor et al., 2014) have demonstrated directional independence of response in situations in which the fibre axis was positioned normal to the radiation field. Table 7.5 shows the results of skin dose measurements for three patients (measurement sites are shown with their abbreviations). Figure 7.26 shows the decreasing trend of skin dose with increase in distance of the GDSF TLDs from

applicator stem on the lateral side for case 1 measurement. It should be noted that TL yields of samples for cases 2 and 3 were directly converted to absolute dose by using the calibration equation obtained for the 5 cm applicator, while for case 1, a coefficient obtained for the 4 cm applicator (Table 7.4) was used to correct the dose for the applicator size. Results did not point to any overdosing of skin, at which 6 Gy is usually being acknowledged to be the skin dose limit (Geleijns & Wondergem, 2005). Estimation of uncertainties related to *in vivo* dose measurements by GDSF TLDs in IORT of the breast by the method used in this study and the source of related uncertainties are presented in Table 7.6.

Combined uncertainties related to INTRABEAM system dosimetry using other types of TL dosimeter have been reported to be up to 12.7 % [Soares et al., 2006] for depth dose assessment and 16.6 % [Fogg et al., 2010] and 17 % [Eaton et al., 2012] for in vivo measurements, all greater than current estimations. This is mainly due to the greater thickness of the more conventional forms of TLD (with consequent volume effects) and calibration of the dosimeter using other radiation sources in those studies.

Table 7.5: Results of skin dose measured by GDSFs for three patients undergoing breast IORT

Case 1			**Case 2**		**Case 3**	
Distance from applicator stem			**Distance from applicator stem**		**Distance from applicator stem**	
	1.5 cm	5 cm	< 0.5 cm		< 0.5 cm	
Sup.	2.31 ± 0.09 Gy	0.63 ± 0.02 Gy	Sup.	5.26 ± 0.20 Gy	Sup.	5.47 ± 0.34 Gy
Inf.	3.13 ± 0.08 Gy	2.00 ± 0.07 Gy	Inf.	3.88 ± 0.17 Gy	Inf.	5.96 ± 0.11 Gy
Med.	3.19 ± 0.05 Gy	1.00 ± 0.04 Gy	Med.	3.81 ± 0.10 Gy	Med.	3.92 ± 0.12 Gy
Lat.	Shown in Figure 7.26		Lat.	3.39 ± 0.02 Gy	Lat.	4.88 ± 0.33 Gy

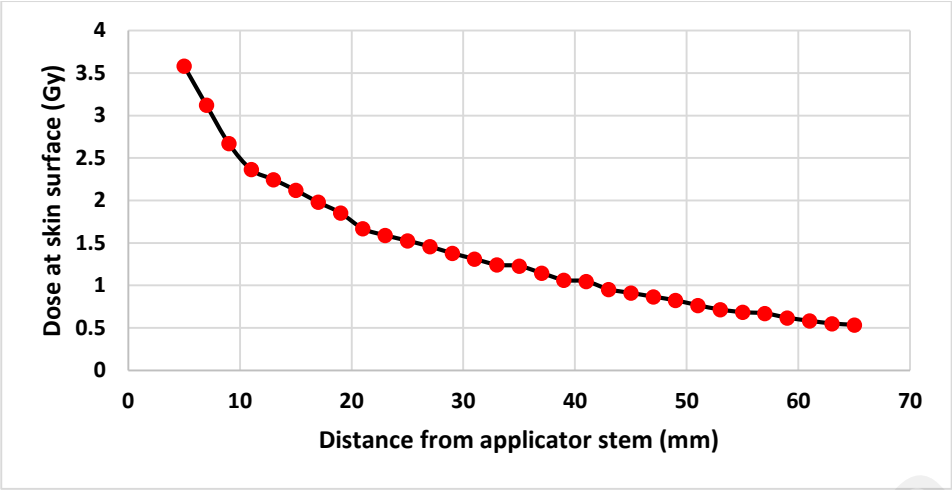

Figure 7.26: Breast skin doses measured on lateral side for case 1

Table 7.6: Determination of total uncertainty for *in vivo* dose measurements by GDSF TLDs in this study

Source of uncertainty	Estimated uncertainty (%)	Description
Positioning	9 - 10	As suggested by [Beatty et al., 1996] and [Fogg et al., 2010]
TLD reproducibility	1.2	Based on results of Chapter 3
Calibration	1.5 - 3.5	Uncertainty in the slope of linear fit - Figure 7.20
Energy dependence	2.3	Changes in beam quality with depth - Figure 7.17
Correction for applicators	0.8 – 3.5	For various applicator size - Table 7.4
Total uncertainty	**9.5 – 11.5**	**Based on one standard deviation (SD)**

7.4 Conclusion

Simulation using the MCNP code was performed on an INTRABEAM IORT x-ray source and related spherical applicators diameter ranging from 1.5 to 5 cm. The detailed specification data for simulation was provided by the manufacturer. Photon energy spectra calculated on the surface of all of the applicator sizes showed the mean energy of the output X-ray spectrum from the XRS tip to be obtained at 19.45 keV. Beam hardening due to the applicators increased the mean energy value minimally as a function of applicator size, ranging from 27.8 keV to 29 keV. As such, the variability of the beam quality is similar for all applicators in terms of distance from applicators surface. Spectra

related to all spherical applicators have been presented here for the first time. Calculated spectra were found to be in good agreement with previous published data. Dose-distance data obtained from simulation was then compared with the reference depth dose obtained with IC measurements and the accuracy of the model for dose calculations was verified. EBT3 film was used to measure exit dose from the water surface and results were in good agreement with calculated dose.

Then, the feasibility of the use of GDSF as a TL dosimeter for *in vivo* dose measurement in IORT of the breast using the INTRABEAM XRS system and spherical applicators was investigated. The TL response of the GDSFs showed excellent linearity over the dose range used in IORT. Despite the high atomic number of the silica-based GDSFs and non-tissue equivalency, the perturbation effect caused by such fibres is not significant due to their small size. The depth of measurement can affect the GDSF response because of changes in quality of photon beam. The effect of beam quality changes on dose assessment in water when dose was delivered using the bare probe was found to be ± 4.2 % with 2.3 % SD. The dose-rate changes caused by the use of the applicator have shown to result in no effect to the TL yield of Ge-doped silica fibres. The same dose on the surface of the 5 cm applicator resulted in a response that was lowered by 26 % compared to that of the 1.5 cm applicator which was due to changes in photon spectrum by applicators. In conclusion, GDSF TLDs can be used for *in vivo* dosimetry in low keV photon IORT, with a combined uncertainty of 9.5 to 11.5 %.

CHAPTER 8: HIGH DOSE DOSIMETRY

8.1 Introduction

High dose is a common term referred to the absorbed dose in the range of 10^2-10^6 Gy (Chen & McKeever, 1997) while ultra-high dose has also been used recently by some researchers (Alawiah et al., 2016; Obryk et al., 2011). High dose irradiation has been found many industrial applications, because it can sterilize products, annihilate microorganisms or improve functional properties of some materials (Negron-Mendoza et al., 2015). Polymer products such as cable jackets, car tires, pipes, disposable medical products and packaging materials as well as the food products are the most common materials being irradiated globally (Ehlermann, 2016a; Negron-Mendoza et al., 2015).

Dosimetry is a crucial task and of importance in such applications for safe delivering of radiation dose to the products. The amount of dose delivered needs to be assessed and controlled accurately, as non-sufficient absorbed dose would not fulfill the purpose of irradiation process, while higher doses may result in functional (reduced performance in the specific application) or even structural damage to the irradiated product. Radiation doses needed to deliver to the polymer products are mainly in the range of 25 to 30 kGy (Standardization, 2013) while for food processing lower dose around 10 kGy is usually applied. A general list of usual applied dose for foods which are categorized as low dose (< 1 kGy), medium dose (1 - 10 kGy) and high dose (> 10 kGy) can be found in (Ehlermann, 2016b).

There are several suitable dosimetry options which are sensitive in the dynamic range from below kGy to MGy doses. Some examples include Gafchromic films, Poly-methyl-meth-acrylate (PMMA), Opti-chromic dosimeters, Alanine dosimeters and Radiochromic films with the high threshold detection of 1, 3, 20, 100, 1000 kGy, respectively (Kuntz & Strasser, 2016; Soliman & Abdel-Fattah, 2013). TL materials have also been studied

as potential dosimeter for high dose dosimetry application. Most of the common phosphor TL materials show saturation at below 10 kGy, and their dose-response linearity range is limited to very low dose levels (Chen & McKeever, 1997). Numerous studies examined the properties of different TL materials under high dose irradiation. For instance Alawiah et al. (2016) reported the critical dose limit of 10 kGy for TLD-100 under electron radiation. Natural Opal demonstrated saturation dose of below 10 kGy (Antonio et al., 2016), while Sahare et al. (2007) studied TL properties of K3Na(SO4)2 : Eu nanocrystalline powder and demonstrated a linear TL response of up to 70 kGy.

In TL dosimeters based on silica fibre, different elements have been reported as doping in the silica structure giving different properties to the glass media (Sahini et al., 2014; Yusoff et al., 2005). Silica fibres have mostly been studied in terms of their sensitivities and among all doping elements, Ge-doped fibres have been proven as the most sensitive ones (Benabdesselam et al., 2013b; Mahdiraji et al., 2015b) whether in the form of cylindrical, flat or photonic crystal fibres (PCF). TL response of Ge-doped fibres in the dynamic gamma dose range of 1 Gy to 1 kGy is reported in Chapter 3. GDSF has also been evaluated at high electron doses by Alawiah et al. (2015), and the saturation has been reported to be around 5 kGy.

Most of the previous studies in the literature are mainly focused on the examinations of these silica fibre TLDs for medical dosimetry applications with maximum dose of several tens Gy. Except than a few number of studies (as mentioned), TL response of different doped silica fibres to high dose radiation has not been studied extensively. Since initial observations showed that less sensitive fibres i.e. the fibres without considerable response in low dose (below 100 Gy) can show enough sensitivity at higher dose range (where the high sensitive fibres start to be saturated), the idea for this study was formed. The purpose of study in this chapter is therefore to evaluate the thermoluminescence

response of different types of silica fibres including various doping materials with different concentrations. This work can possibly introduce a potential silica based TL dosimeter showing suitable dosimetric characteristics for high dose dosimetry application.

8.2 Materials and methods

8.2.1 Silica fibre samples

Different commercially available or tailor-made (by Flexilicate Sdn. Bhd., Malaysia) silica fibres with different pulling conditions and doping materials were selected for this study based on the primary criteria that they have not shown enough sensitivity at low dose applications (in the range of a few Gy and below). Selected fibres included P-doped, Al-doped, Er-doped, Al-Tm-doped, ultra-high numerical aperture (UH NA) fibres, borosilicate and two non-doped fibres, quartz (crystalline silica) and suprasil F300 (a low defect high purity amorphous silica medium). P-doped fibres with three different concentrations of 1.3, 3.6 and 7.8 mol % and Al-doped fibres with concentrations of 2, 4 and 5.1 mol % were tested, and will be named with their doping concentrations hereafter. Among all fibre types, the Ge-doped fibre (4.9 weight %) has the highest sensitivity to radiation and its properties are presented in Chapters 3 to 5. The fibre preforms for P, Al and Al-Tm-doped were manufactured by Telekom Malaysia and Multimedia University (Cyberjaya, Malaysia) using the modified chemical vapor deposition (MCVD) process. All fibre samples excluding Er-doped and ultra-high NA fibres were drawn by Flexilicate Sdn Bhd (University of Malaya, Kuala Lumpur, Malaysia). Er-doped fibre is a commercially available fibre mainly designed for optical amplifiers. Fibre samples had different diameters ranging from 125 μm to 570 μm. Samples were prepared for dosimetry by cutting into 5 mm pieces and subject to a pre-annealing treatment of 400 °C for 1 h in order to remove the probable turbulence in their glow curves by stabilizing the trapping structure.

8.2.2 Sinagama

Besides Gammacell 220 (located at University of Malaya Physics Department) which was used for irradiations at doses below 2 kGy, Sinagama which is a ^{60}Co industrial radiation plant (located at Malaysian Nuclear Agency) was used for doses above 2 kGy in this study. Dose rates at experiment time were 2.15 and 46 Gy/min for GC-220 and Sinagama respectively.

8.2.3 ALURTRON

ALURTRON model NHV EPS-3000 located at Malaysian Nuclear Agency (shown in Figure 8.1), which is an electron accelerator device for industrial radiation processing, was used to irradiate fibre sample with 2 MeV electron beam to doses ranged from 5 to 100 kGy. This irradiator can produce a range of electron energies with very high dose rate, and the irradiation time is adjusted by changing the speed of conveyor belt carrying the samples. Electron beam size was fixed with 120 cm length and 15 cm width. As example when the current was adjusted 10 mA, a constant high dose rate of 1.3 kGy/s was produced.

Figure 8.1: Output window of ALURTRON electron accelerator for industrial radiation processing

Irradiated samples were read with TLD reader Harshaw 3500 (Thermo Fisher Scientific Inc, U.S.) adopted with WinREMS software to generate the TL glow curves obtained from the samples. Time temperature profile (TTP) was selected based on the detailed explanations as discussed in Chapter 3. The pre-heat temperature and maximum temperature were set to 50 °C and 400 °C, respectively. Considering the heating rate 25 °C /s and 4 s post annealing, total reading time of 20 s was spent for each sample. In this chapter each point in all plots/figures represent average TL response of 5 fibre samples with error bars illustrate the variations among the TL responses of 5 samples for each dose.

8.3 Results and discussion

8.3.1 Comparison of fibres in terms of sensitivity

Sensitivity of a TLD material is generally defined as the intensity of TL signal produced by TLD per unit absorbed dose (Chen & McKeever, 1997). Sensitivity comparison can be made between two TLDs when all parameters related to the irradiation process as well as the TL measurement system (PMT properties and readout procedure) are constant. Silica fibres may show different sensitivities based on their composition, doping elements, doping concentration, pulling process and in general all parameters that affect defect structure of fibre (Mahdiraji et al., 2015a; Yusoff et al., 2005). Table 8.1 shows the TL responses of fibres under investigation when irradiated to 100 Gy test dose from ^{60}Co photons by the Gammacell 220 irradiator. TL yields in nC are normalized to the mass of fibres in mg. A significant difference in the sensitivity of fibres, in the order of 10^4 fold is recognizable.

Table 8.1: TL sensitivity of different silica fibres to dose

Fibre type	TL sensitivity (nC/mg.100Gy)	Fibre type	TL sensitivity (nC/mg.100Gy)
Ge-doped	62978	Er-doped	5.4
P-doped-1.3	7.2	UH NA	46.34
P-doped-3.8	12.03	F300	6.6
P-doped-7.6	66.88	Al-Tm-doped	221.66
Al-doped-2	7.07	quartz	736.39
Al-doped-4	8.61	borosilicate	7.08
Al-doped-5.1	8.7		

Based on the response to this initial test dose, the most and least sensitive types of fibres: Ge-doped and Er-doped samples both having the same diameter 125 μm, were irradiated using ^{60}Co gamma rays ranging from 1 to 20 kGy. Figure 8.2 demonstrates a comparison between the sensitivity of these two fibres. Although Er-doped fibre was reported to show TL response even at low dose ranges (Abdulla, 2003; Alawiah et al., 2015), Er-doped fibre used in this study, did not show any detectable TL response when irradiated to radiotherapy doses (a few Gy). Conversely, the Ge-doped fibre used here, showed high sensitivity at low doses as reported in previous chapters. Very significant difference in the response and sensitivity of fibres are noted using two different units employed on the vertical axis scales in the left (for Ge-doped fibre) and right (for Er-doped fibre) sides of the plot. It is observed that Ge-doped fibre has been completely saturated at 5 kGy, while Er-doped fibre still show increase in response until 20 kGy.

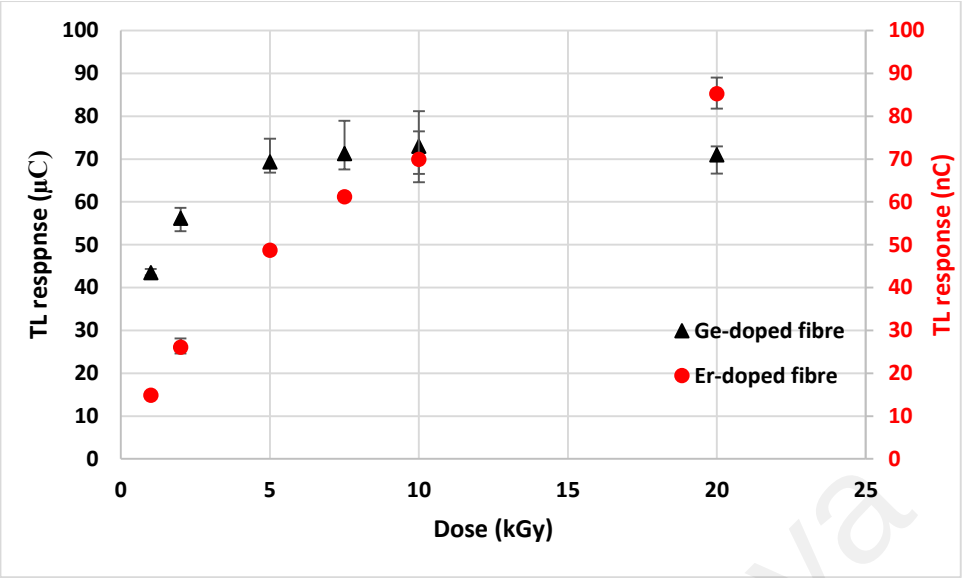

Figure 8.2: TL response of Ge and Er-doped fibres in ultra-high dose levels. Different units are used on vertical axes to show the order of sensitivity for these two fibre types. Left and right vertical axes are related to Ge and Er-doped fibres respectively.

8.3.2 Comparison of response to electron and photon doses

Since two different sources of high dose radiation (ALURTRON and Sinagama) were available, in order to recognize the probable effect of different source parameters such as radiation types (electron and gamma), dose rate and energy of radiation on TL yield from the fibres, a linearity test was performed. Two different fibre types, including Er-doped and UH NA fibre (with different order of sensitivity) were irradiated with both ^{60}Co gamma rays and 2 MeV electrons particles for doses from 1 to 20 kGy. As shown in Figure 8.3, it is observed that the sources type does not affect the fibre TL response significantly with a modest maximum difference of 10 % between points on TL/dose plot. Since the TL response of silica based materials to electron beam is expected to be higher than the photon radiation at the same dose and dose rate (Alawiah et al., 2015; Hashim et al., 2010), current result is likely to be due to the dose rate difference (46 Gy/min for Gamma source compared to 78 kGy/min for electron source). This effect is in agreement with the general reciprocity law for dose rate effect reported at radiotherapy dose rates

(Abdul Rahman et al., 2011). However the influence of such high dose rates on TL response, has not been investigated thoroughly.

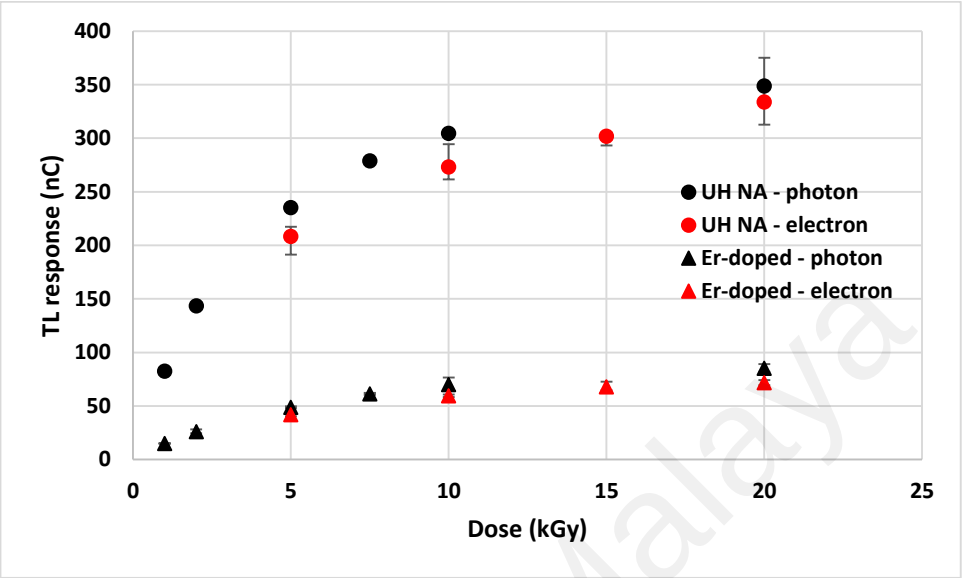

Figure 8.3: Comparison of the TL response of two fibre types to photon and electron doses

8.3.3 Linearity test for other samples (P-doped, Al-doped, F300, Al-Tm-doped, quartz, and borosilicate)

In the first evaluation, gamma rays from the ^{60}Co irradiator (Gammacell 220) were used to irradiate fibres from 100 Gy to 2 kGy with a dose rate of 2.15 Gy/min. Samples (5 samples per dose) were read at the previously explained reading condition. The quartz fibres showed complete saturation within the dose interval of 0.5- to 1.0 kGy (Figure 8.4) while the P-doped samples and one of the Al-doped samples (the one with the greatest Al concentration, at 5.1 mol %) showed evidence of a decrease of TL responses within the dose interval of 1 to 2 kGy, trending slowly towards saturation (Figure 8.5). As such, they were not considered for further testing at the more elevated doses of interest. Figure 8.5 also shows the correlation coefficient of each linear fit.

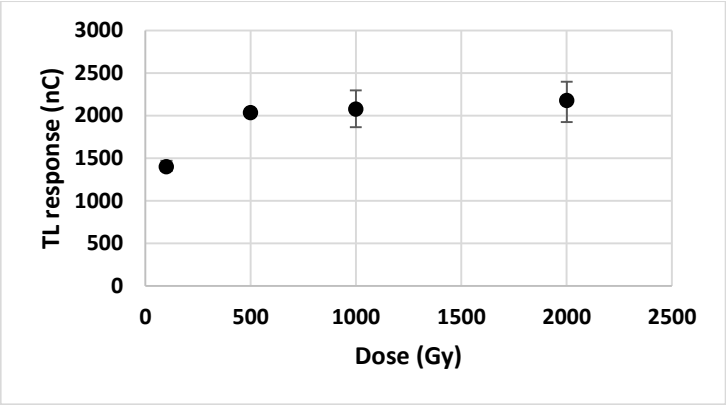

Figure 8.4: Saturation of quartz within the dose interval 0.5- to 1.0 kGy

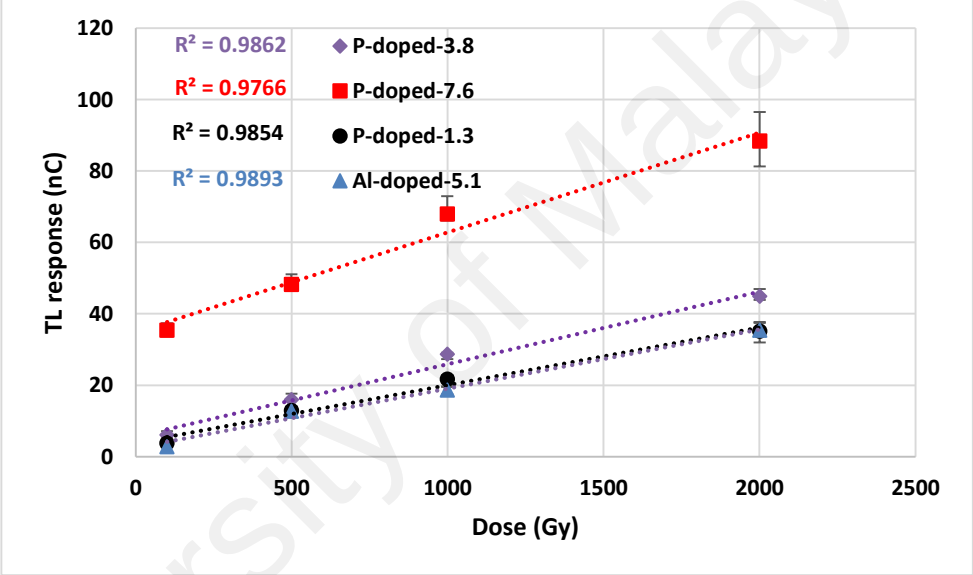

Figure 8.5: Deviation from linear fit observed in TL responses of P-doped fibres and Al-doped-5.1 from 1 to 2 kGy

Other samples that did not show any deviation from linear response until 2 kGy, with correlation coefficient better than 0.99 were selected to be tested at higher doses. These included fibre types Al-doped-4, Al-doped-2, Er-doped, UH NA, F300, Al-Tm-doped and borosilicate. They were irradiated to doses from 5 kGy up to 100 kGy by the electron source. TL yield from these samples are shown in Figure 8.6 and Figure 8.7 in two different scales in order to accommodate the significant differences in sensitivity of these fibres. From Figure 8.6 and Figure 8.7, it can be noticed that saturation level for UH NA occurs around 40 kGy, for types Al-doped-4, Er-doped, F300 and Al-Tm-doped around

60 kGy and for Al-doped-2 at 80 kGy. Borosilicate fibres show excellent linearity of response, up to around 100 kGy.

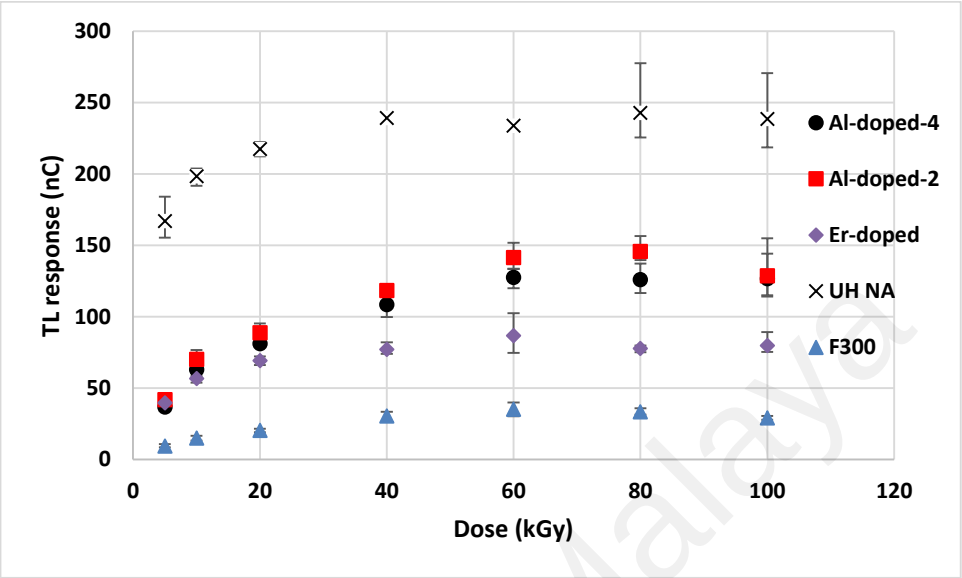

Figure 8.6: Fibre samples with saturation level below 100 kGy

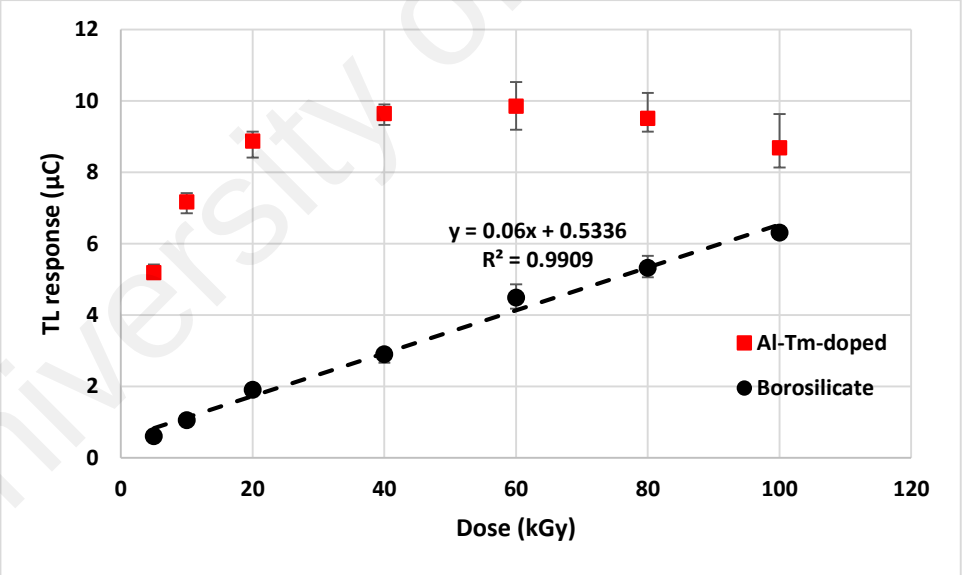

Figure 8.7: Dose-response linearity of borosilicate fibre compared to a saturated high sensitive fibre

8.3.4 Glow curve comparison

Glow curve of a thermoluminescent material can reveal the parameters related to charge transfer process between trapping and recombination centres. The temperature at

TL peak position (T_{max}) is usually an indicator showing the suitability of the material as a dosimeter, since deeper traps result in more stable retention of charge carriers and lower fading. Glow curves related to all 13 samples investigated in this study, for a test dose of 1 kGy from photon source, are shown in Figure 8.8. To be able to demonstrate all glow curves in the identical scale, all curves are normalized to their maximum values which are assigned as 100 in the plots. Glow curve of several samples (Al-doped, P-doped, F300 and quartz) follow the same pattern with a thin and well-defined single peak at temperature around 180 °C. Other samples, however, demonstrate different shape glow curves for instance Al-Tm-doped with a significant part located at temperatures higher than the reading temperature 400 °C. This fibre and borosilicate fibre were then read with maximum temperature of 500 °C in another experiment to ensure that the glow curves become completed (as shown in Figure 8.9). Shape of the glow curve for Er-doped fibre is quite different with Er-doped fibres reported in the literature at low doses (Abdulla, 2003; Alawiah et al., 2015). Glow curve for Ge-doped and borosilicate fibre show some similarity in shape with a single but broadened TL peak, and also in T_{max} position which is around 260 °C. It should be noted that, no difference was found between the glow curve of fibres from any types irradiated with photons or electrons for a specific dose.

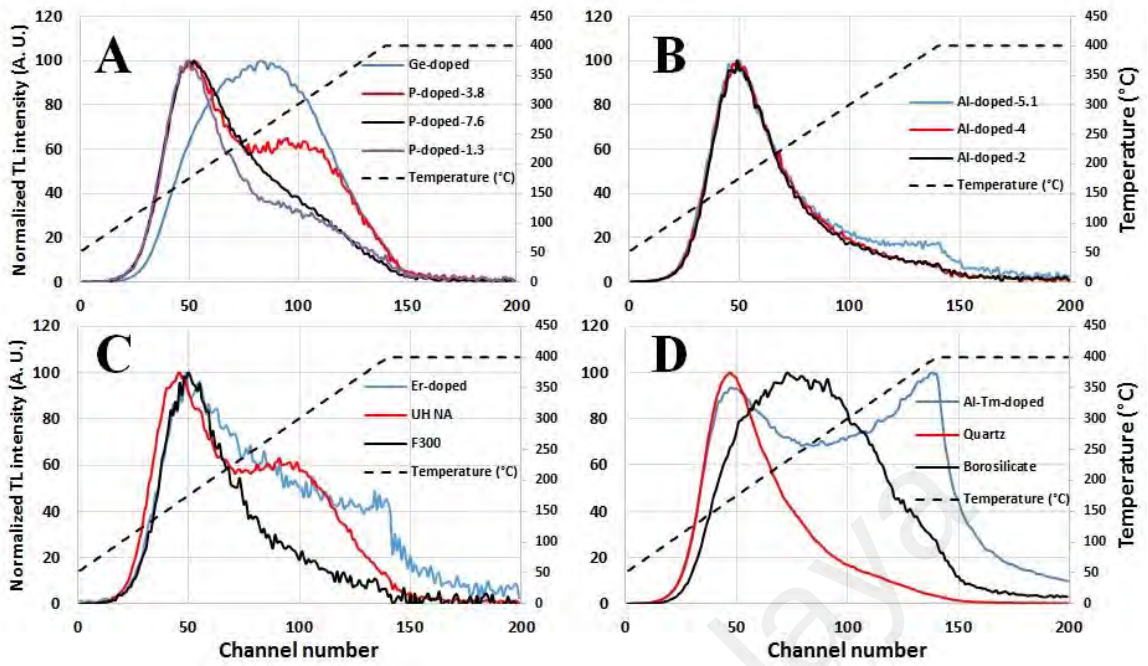

Figure 8.8: A to D show glow curves of all 13 samples examined in this study for 1 kGy gamma dose. TL intensities are normalized to the maximum of each glow curve to be comparable

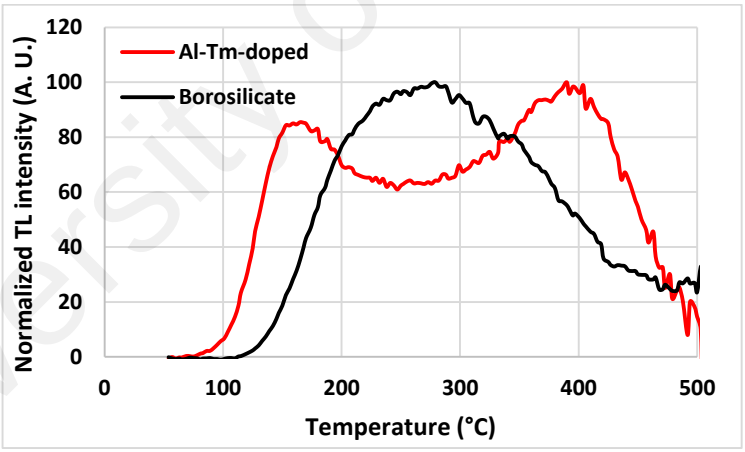

Figure 8.9: Glow curves of Al-Tm-doped and borosilicate fibres read with maximum temperature 500 °C

Figure 8.10 (A), (B) and (C) show the glow curve of three different fibre samples before and after saturation, while Figure 8.10 (D) demonstrates the changes in glow curve of borosilicate fibre which is still not saturated. Tracking the changes in the shape of the glow curve may assist in recognition of the saturation phenomenon at high dose levels. Ge-doped fibre glow curve does not show shifting in TL peak for doses from 1 to 20 kGy

(Figure 8.10 (C)), however it shows significant changes in T_{max} position in doses below 1 kGy (results in Chapter 3). This could indicate that the deep or so-called thermally disconnected traps are completely filled below 1 kGy dose and no longer contribute as re-trapping centres, therefore recombination events effectively prevail and T_{max} does not shift forward. Conversely, for borosilicate fibre in this dose range, deep traps actively act as re-trapping centres causing recombination events to be delayed to a more elevated temperature, resulting in T_{max} position shifting accordingly.

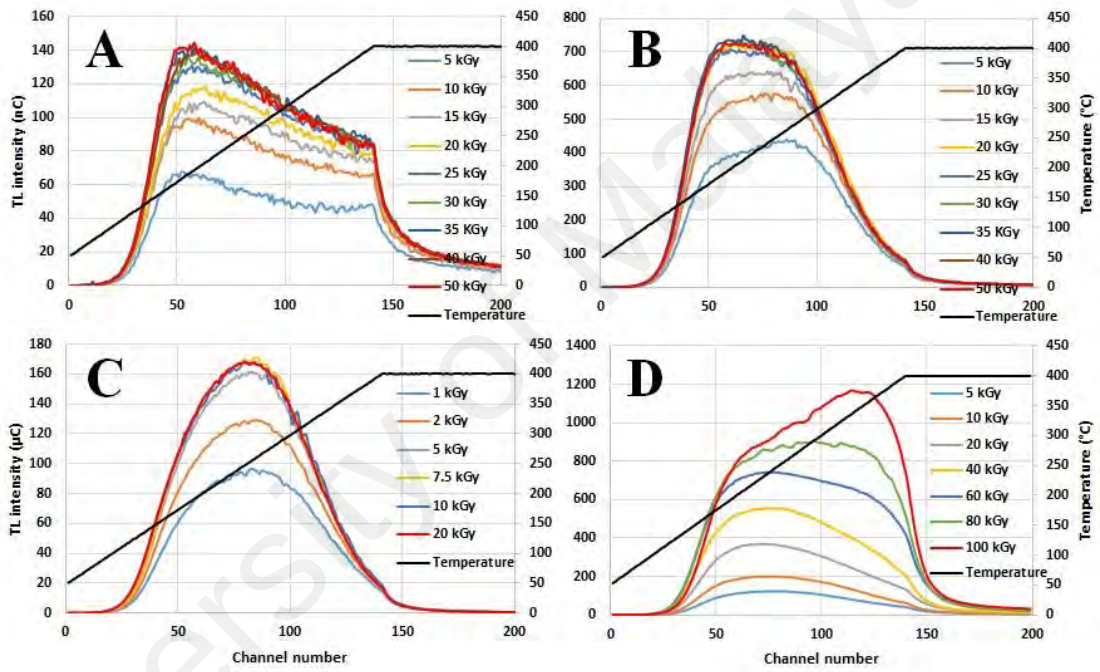

Figure 8.10: Changes in TL glow curves of A) Er-doped B) UH NA C) Ge-doped and D) borosilicate fibre samples at high electron doses, (borosilicate sample is still not saturated till 100 kGy)

8.3.5 FESEM/EDX analysis

Field emission scanning electron microscope (FESEM) attached to the energy dispersive X-ray analyzer (EDX) was used for further characterisation of the borosilicate fibre. Figure 8.11 (A) shows the magnified view of the fibre cross section. The presence of boron in the structure of silica fibre was confirmed with EDX result, also showing uniformity of the distribution for Silicon, Oxygen and boron in the fibre structure (Figure

8.11 (B-E)). The average value of EDX measured boron concentration from 9 scanned lines of 3 different samples (3 scanned line on each sample) is 4.4 %, which is expected with the concentration of B_2O_3 in the fabricated silica preform being 12.5 mol %.

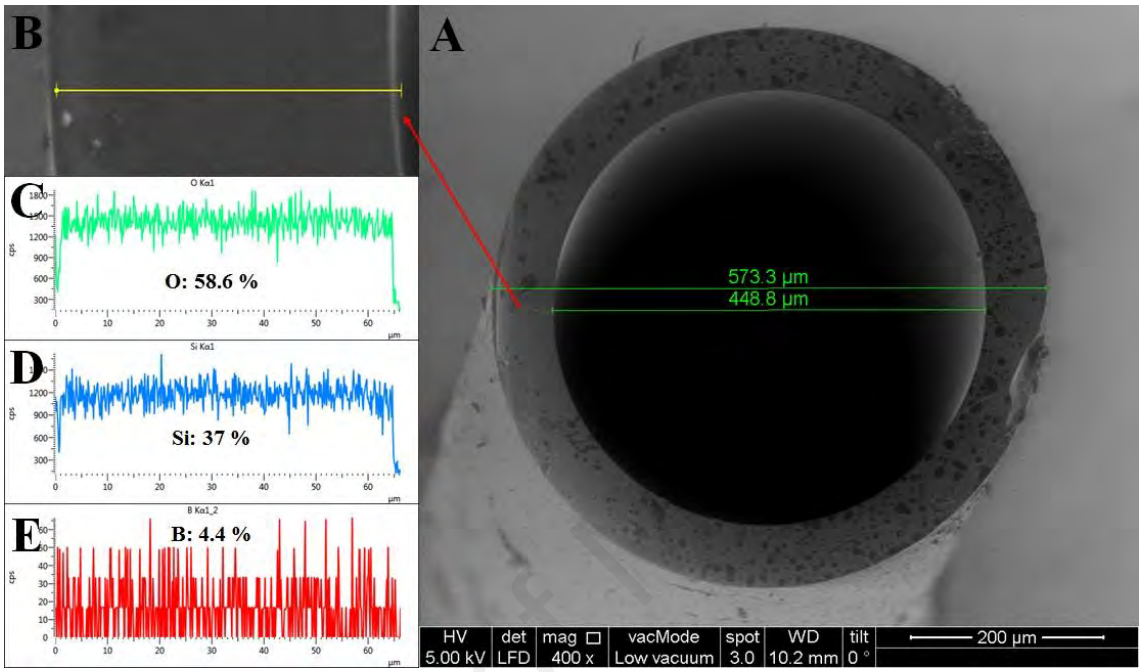

Figure 8.11: A) Cross-sectional view of a 570 µm borosilicate hollow fibre, as obtained in use of a FESEM facility; B) an example profile line used in the EDX analysis. The resulting quasi-uniform elemental distributions obtained along the profile are shown in sub panels C) to E), for oxygen, silicon and boron respectively. Note the relative difficulty typically experienced in use of such an X-ray fluorescence based technique in determining the elemental presence of a low atomic-number media such as boron (Z = 5), even if as in this case at 4.4 %.

8.3.6 Reproducibility test

Successive cycles of 1 kGy as well as 5 kGy doses from ^{60}Co source were applied to samples to check the reproducibility of the TL response in kGy dose range. It should be noted that the annealing temperature of 500 °C were applied after any irradiation and reading cycle. This temperature was selected based on the glow curve of borosilicate sample, and the findings of Chapter 3 regarding the choice of proper annealing temperature to be higher than the temperature completing glow curve of the material. Samples were cooled down to room temperature immediately after 1 hour in a pre-heated

furnace. Results for 10 cycles of reading are shown in Figure 8.12. It is observed that TL responses of fibres for 1 kGy sample dose, decreases by approximately 7 % after both first and second irradiation cycles but varies randomly from the third to tenth irradiation cycles without significant changes in sensitivity. However in case of 5 kGy sample dose, 36 % fall in fibres response happens after first irradiation cycle with then almost similar trend to that of the 1 kGy regime. The variation of fibre TL response from 2nd to 10th cycle is 15.6 % for test dose of 1 kGy and 11.8 for test dose of 5 kGy. The effect of applying a pre-conditioning stabilization dose prior to fibres use, similar to that applied in Chapter 3 for low doses open up an opportunity for investigation.

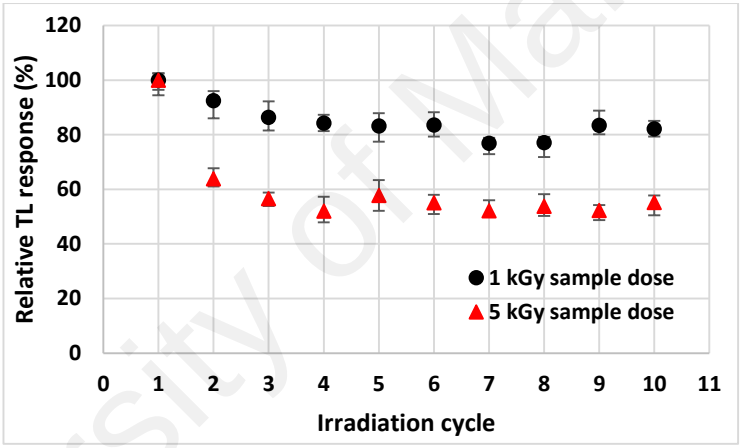

Figure 8.12: Borosilicate fibre TL response to successive irradiation cycles

8.3.7 Fading effect

Three batches of samples each included 6 number of groups were used for fading test. Each group included 5 pieces of borosilicate fibre (each 5 mm length). Batches were exposed to different doses of 0.1, 1 and 18 kGy to compare the fading effect for different dose levels. Again, the average reading of 5 samples in each group is considered and error bars show the variation among those samples. Average TL responses are normalized to the average mass of each group and the results are shown in Figure 8.13. For doses of 1 kGy and above, the extent of fading has been observed to be closely similar (at 4.4 % and

6.3 % after 1 day and 11.4 % and 12.4 % after 1 week, for the 1 and 18 kGy doses respectively), being greater however in the case of fibres exposed to doses of 0.1 kGy (15.3 % after 1 day and 18.7 % after 1 week).

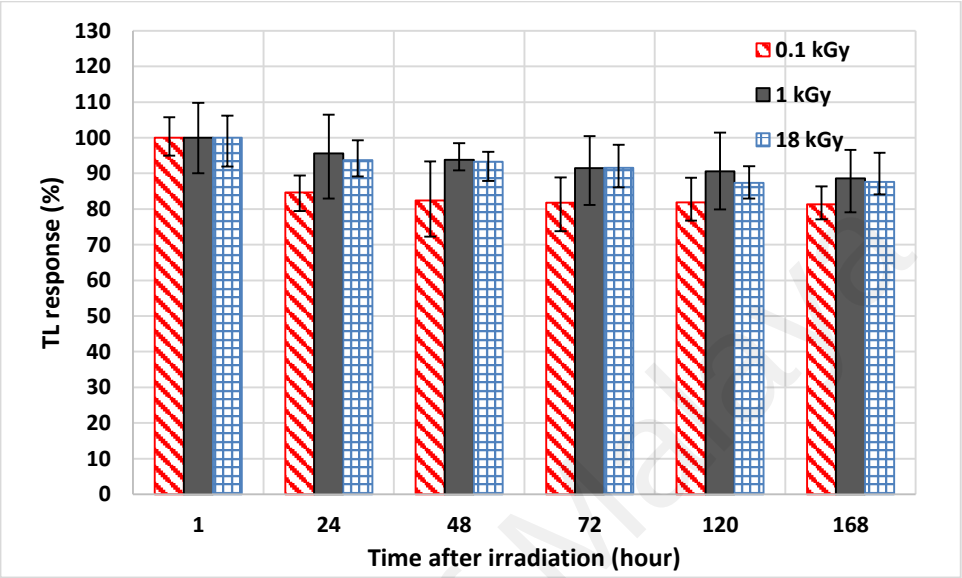

Figure 8.13: The mass-normalized mean TL yield of the borosilicate fibres readout over the period from 1 hour to 168 hours (7 days) subsequent to irradiation, expressed as a fraction of the TL yield measured one hour subsequent to irradiation, for doses of 0.1, 1 and 18 kGy doses

Figure 8.14 shows the associated glow curves for the borosilicate samples that were involved in the fading studies, showing the loss for the 0.1 kGy irradiated fibres, (Figure 8.14 A) to preferentially involve the less-deep traps, as reflected in the low temperature part of the glow curve for the various readout delays. At the more elevated doses of 1 kGy and 18 kGy (Figure 8.14 B, C), the preferential loss from superficial traps progressively reduces, an indicative of the greater involvement of more deeply occupied traps.

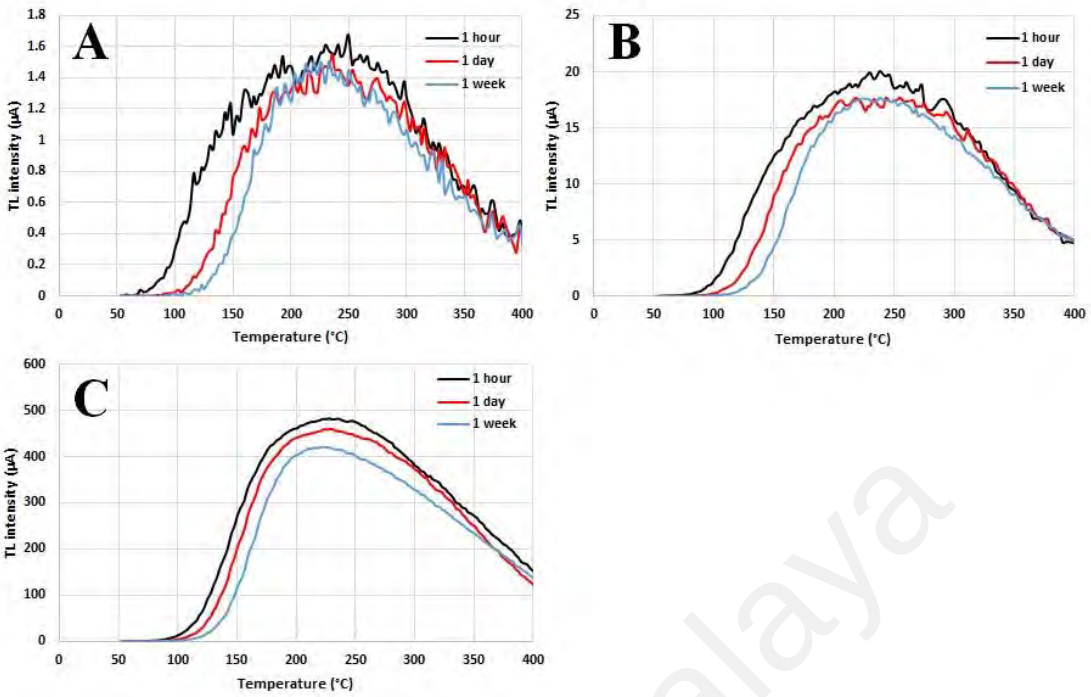

Figure 8.14: Glow curves showing fading following different test doses: A) 0.1 kGy; B) 1 kGy; C) 18 kGy

8.4 Conclusion

Thermoluminescence response of several types of silica fibres was studied in this chapter based on their dose-response behaviors at ultra-high doses from electron and photon sources. TL response at high dose for a high sensitive Ge-doped fibre was compared against a low sensitive fibre type. Results show that some silica fibres that do not show any sensitivity at low level doses possess the potential for high dose dosimetry applications. High doses from photon and electron sources were found to produce similar effects on fibre resulting in comparable TL responses. Different glassy fibres investigated in the chapter are useful and have high dose saturation levels. These include UH NA, Al-doped-4, Er-doped, F300, Al-Tm-doped and Al-doped-2 with respective saturation doses of 40, 60, 60, 60, 60 and 80 kGy respectively. The TL response of borosilicate fibre, however shows a very good linearity with dose range of up-to 100 kGy. Then more detailed TL characteristics of the borosilicate fibre were investigated accompanied by FESEM/EDX analysis. Fading effect for this fibre was found to be 5 to 6 % in the first

24 hours and 11 to 12 % in one week. Reproducibility test performed for 10 irradiation cycles showed that this TLD might be more reliable as a single use dosimeter, probably because of radiation damage phenomenon, however deeper investigation on this part is required. With the suitable properties reported in this chapter, combined with inherent characteristics of being very cost effective and resistant to humidity, temperature, magnetic and electrical fields, these silica based TL detectors are appropriate dosimeters for high dose application.

CHAPTER 9: CONCLUSIONS AND FUTURE WORK

Thermoluminescent sensors have been used as proper dosimeters in radiotherapy quality assurance, personal and environmental monitoring and other applications for several decades due to their inherent advantages such as sensitivity, reusability, small size, cost effectiveness and so on. However conventional TLDs also suffer from some intrinsic drawbacks including water permeability, limited dose response linearity range, saturation of response at very high doses, and insufficient spatial resolution (of the order of millimeters) for specific applications, that have resulted to appearance of some alternatives. Silica-based fibres are one of the more recently developed group of TL materials. They are water-resistant, cost effective and with spatial resolution down to about 100 μm, which provide for the possibility of precision measurement of dose. Among various type silica fibres, Ge-doped fibres (GDSFs) have been shown to be the most sensitive and also generally showing suitable performance. However, there is still a significant gap between the published works and practical use of GDSFs in routine dosimetry. As stated in the objective, the aim of this study was to characterize a high sensitive GDSF for different applications and develop a recipe that allows the use of the GDSF TLD in routine dosimetry. Thus, various TL properties and detailed dosimetric characteristics of this fibre including pre-dose effect, annealing and reproducibility, energy dependence, angular dependence and dose rate dependence were investigated in this work.

^{60}Co gamma rays, kVp X-rays, MeV X-rays and electrons from linear accelerator were used for irradiation of fibres. Glow curve of the fibre showed a broad and well defined high temperature peak around 275 °C with its position being dose dependent also being affected by pre-dose or dose history of fibre. Dose history effect was shown to affect the fibre response if annealing temperature was not high enough to empty deep traps in this

fibre. Regardless of the annealing temperature, it was proven that fibre with and without pre-dose do not show equal response, therefore a pre-dose of 100 Gy along with 500 °C annealing was suggested as the optimum regime to ensure reproducibility of dosimeter response. Observations made by comparison of two Ge-doped fibres showed that optimum annealing and pre-dose treatments to stabilize TL response and maintain its reproducibility might be different for other fibres and need to be optimized. The TL variation of the studied GDSF for repeatability over 10 irradiation cycles was ± 2.35 %.

Energy dependence of the GDSF in keV range relative to reference energy of ^{60}Co gammas were investigated theoretically using cavity theory in addition to experimental approach. It was shown that correction factor at each keV energy can be approximated well by simply using the ratio of mass attenuation coefficient of SiO_2:Ge to that of air. Theoretical predictions suggest that for fibre diameters of larger than approximately 125 μm, there is no significant effect of size on energy dependence and therefore, there is no need to consider weighting factor of the middle size dosimeters in cavity theory equation. The ratio of μ_{en}/ρ gives an acceptable approximation. It would be interesting to investigate and approve this through experiments since different size fibres with different combinations of core and cladding sizes can be fabricated. Energy dependence can also be included another term related to the dependence of TL response (in addition to absorbed dose) on size that requires clarification. With development of advanced and tailor made silica fibres, where the sensitivity can be improved to detect doses as low as environmental doses, designing filter and optimizing it to reduce energy dependence to an acceptable range suggested by authorities, would be a useful progress. Silica fibres as the most cost effective dosimeters can then be used for personal dosimetry of many radiation workers around the world.

Angular dependency was one of the significant findings of this study that was for the first time investigated in such detail in keV and MeV photon energies. Monte Carlo simulation results also confirmed experimental findings. In free-in-air irradiations, absorbed dose and TL responses in the fibre were significantly changed by angle of incidence, with inverse trends being observed from keV and MeV photons. In general, cross section of the dosimeter subject to radiation determines the absorbed dose and angular dependence. Results of this study suggest addition of another term in this general expression for response with consideration of the dosimeter size. Placing a small thickness dosimeter in a MeV photon field where sufficient build-up region cannot be provided for high energy photons, results in minimum dosimeter response which is not in agreement with expectation for normal size dosimeters. Effect of scattered radiation on angular dependence was also studied with on-phantom and in-phantom conditions. Angular dependence was significantly decreased when measured for a 6 MeV photon beam on the surface of a solid water phantom. For measurement inside phantom at depth of maximum dose, the angular dependence was reduced to 3 %, with the trend in agreement with prediction of general cross section rule. Studying the effect of fibre diameter and length on angular dependence and optimizing dimensions to decrease angular dependence of response is proposed as another issue to investigate.

After detailed characterisation of GDSF presented in Chapters 3 to 5, the feasibility of their use for dosimetry in three different applications were studied in Chapters 6 to 8. Gammacell 220 ^{60}Co irradiator was modeled using MCNP code and calculated dose distribution was compared to measured doses by GDSFs and literature data. Non-uniformity in dose rates on vertical and horizontal axes as well as bottom surface of the sample chamber of the machine was confirmed by agreement observed from simulation and experimental results, showing the usefulness of the fibres for dose mapping purpose.

Characterisation of GDSFs for *in vivo* dosimetry in IORT using the INTRABEAM system, a 50 kVp photon brachytherapy source, was presented in Chapter 7. Fibres response to doses ranged from 1 to 20 Gy from the bare X-ray source probe and also from spherical applicators with various diameters were obtained. Monte Carlo simulations were also used to obtain photon spectrums at different depths in water, on the surface of applicators and inside the fibre volume located on the surface of applicators as well as depth doses in water and delivered dose to water surface. Simulation results showed small variations of the mean energy of the photon spectrum with respect to applicator size. The differences are more pronounced in low energy part of the spectrums. The effect of such changes on TL response of GDSF when located on the surface of different size applicators was evaluated and correction factors for beam qualities were found to vary from 0.82 to 1. Dose rate effect on fibre response was also investigated using both kVp and MeV photon beams, with the results showing independence from dose rate in the studied range of 0.04 to 6 Gy/min. *In vivo* skin dose measurements using fibres located on skin at different positions were performed on three breast cancer patients undergoing IORT as part of their radiation treatment, where no overdosing of skin was observed. It was shown that associated uncertainty for *in vivo* dose measurements vary between 9.5 and 11.5 %.

In Chapter 8, in addition to GDSF that was saturated at 5 kGy dose, performance of 12 different fibre types were evaluated in high dose dosimetry of photon and electron sources. Various fibres showed different sensitivity and saturation levels. Borosilicate fibre demonstrated high potential for this application with a well linear response for doses up-to 100 kGy. More detailed dosimetric characterisation on this fibre showed radiation damage to affect its response with relatively high decrease in response from first to second cycle but smaller variations from 2^{nd} to 10^{th} cycles. Further study on the effect of high dose on trapping structure to find probable stabilization process and obtaining reproducible response is proposed.

REFERENCES

Abdul Rahman, A. T., Abu Bakar, N. K., Chandra Paul, M., & Bradley, D. A. (2014). Ultraviolet radiation (UVR) dosimetry system and the use of Ge-doped silica optical fibres. *Radiation Physics and Chemistry, 104*, 129-133.

Abdul Rahman, A. T., Bradley, D. A., Doran, S. J., Thierry, B., Bräuer-Krisch, E., & Bravin, A. (2010). The thermoluminescence response of Ge-doped silica fibres for synchrotron microbeam radiation therapy dosimetry. *Nuclear Instruments and Methods in Physics Research Section A: Accelerators, Spectrometers, Detectors and Associated Equipment, 619*(1-3), 167-170.

Abdul Rahman, A. T., Nisbet, A., & Bradley, D. A. (2011). Dose-rate and the reciprocity law: TL response of Ge-doped SiO2 optical fibers at therapeutic radiation doses. *Nuclear Instruments and Methods in Physics Research Section A: Accelerators, Spectrometers, Detectors and Associated Equipment, 652*(1), 891-895.

Abdul Sani, S. F., Grime, G. W., Palitsin, V., Mahdiraji, G. A., Abdul Rashid, H. A., Maah, M. J., & Bradley, D. A. (2014). Micro-PIXE analysis of doped SiO2fibres intended as TL dosimeters for radiation measurements. *X-Ray Spectrometry, 44*(2), 33-40.

Abdul Sani, S. F., Hammond, R., Jafari, S. M., Wahab, N., Mahdiraji, G. A., Siti Shafiqah, A. S. & Bradley, D. A. (2017). Measurement of a wide-range of X-ray doses using specialty doped silica fibre. *Radiation Physics and Chemistry, 137*, 49-55.

Abdulla, Y. A. (2003). *The use of Ge and Er-doped optical fibres as thermoluminescence dosimeter and their applications in radiotherapy.* (PhD), University of Malaya, Malaysia.

Abdulla, Y. A., Amin, Y. M., & Bradley, D. A. (2001). The thermoluminescence response of Ge-doped optical fibre subjected to photon irradiation. *Radiation Physics and Chemistry, 61*, 409–410.

Al-Senan, R. M., & Hatab, M. R. (2011). Characteristics of an OSLD in the diagnostic energy range. *Medical Physics, 38*(7), 4396-4405.

Alawiah, A., Alina, M. S., Bauk, S., Abdul-Rashid, H. A., Gieszczyk, W., Noramaliza, M. N. & Marashdeh, M. W. (2015). The thermoluminescence characteristics and the glow curves of Thulium doped silica fiber exposed to 10MV photon and 21MeV electron radiation. *Applied Radiation and Isotopes, 98*, 80-86.

Alawiah, A., Amin, Y. M., Abdul-Rashid, H. A., Abdullah, W. S. W., Maah, M. J., & Bradley, D. A. (2016). An ultra-high dose of electron radiation response of Germanium Flat Fiber and TLD-100. *Radiation Physics and Chemistry, 130*, 15-23.

Alawiah, A., Bauk, S., Abdul-Rashid, H. A., Gieszczyk, W., Hashim, S., Mahdiraji, G. A. & Bradley, D. A. (2015). Potential application of pure silica optical flat fibers for radiation therapy dosimetry. *Radiation Physics and Chemistry, 106*, 73-76.

Alawiah, A., Bauk, S., Marashdeh, M. W., Nazura, M. Z., Abdul-Rashid, H. A., Yusoff, Z. & Bradley, D. A. (2015). The thermoluminescence glow curve and the deconvoluted glow peak characteristics of erbium doped silica fiber exposed to 70-130 kVp x-rays. *Applied Radiation and Isotopes, 104*, 197-202.

Alawiah, A., Bauk, S., Marashdeh, M. W., Ng, K. S., Abdul-Rashid, H. A., Yusoff, Z., & Bradley, D. A. (2015). Thermoluminescence glow curves and deconvoluted glow peaks of Ge doped flat fibers at ultra-high doses of electron radiation. *Radiation Physics and Chemistry, 113*, 53-58.

Almond, P. R., & McCray, K. (1970). The energy response of LiF, CaF2, and Li2B4O7: Mn to high energy radiations. *Physics in Medicine and Biology, 15*(2), 335-342.

Antonio, P. L., Gronchi, C. C., Oliveira, R. A. P., Khoury, H. J., & Caldas, L. V. E. (2016). TL and OSL dosimetric properties of Opal gemstone for gamma radiation dosimetry. *Radiation Measurements, 90*, 219-223.

Armoogum, K. S., Parry, J. M., Souliman, S. K., Sutton, D. G., & Mackay, C. D. (2007). Functional intercomparison of intraoperative radiotherapy equipment - Photon Radiosurgery System. *Radiation Oncology, 2*(1), 11.

Bearden, J. A., & Burr, A. F. (1967). Reevaluation of X-ray atomic energy levels. *Reviews of Modern Physics, 39*(1), 125.

Beatty, J., Biggs, P. J., Gall, K., Okunieff, P., Pardo, F. S., Harte, K. J. & Sliski, A. P. (1996). A new miniature x-ray device for interstitial radiosurgery: dosimetry. *Medical Physics, 23*(1), 53-62.

Begum, M., Mizanur Rahman, A. K. M., Abdul-Rashid, H. A., Wan Abdullah, W. S., Noor, N. M., Zulkifli, M. I. & Bradley, D. A. (2013). *Thermoluminescence Response of Ge-doped Optical Fiber Dosimeters with Different Core Sizes*. IEEE 4th International Conference on Photonics (ICP), Malaysia.

Begum, M., Rahman, A. K., Abdul-Rashid, H. A., Yusoff, Z., Begum, M., Mat-Sharif, K. A. & Bradley, D. A. (2015). Thermoluminescence characteristics of Ge-doped optical fibers with different dimensions for radiation dosimetry. *Applied Radiation and Isotopes, 100*, 79-83.

Benabdesselam, M., Mady, F., Duchez, J. B., Mebrouk, Y., & Girard, S. (2014). *The Opposite Effects of the Heating Rate on the TSL Sensitivity of Ge doped Fiber and TLD500 Dosimeters*. IEEE Nuclear and Space Radiation Effects on Components NSREC, Paris, France.

Benabdesselam, M., Mady, F., & Girard, S. (2013a). Assessment of Ge-doped optical fibre as a TL-mode detector. *Journal of Non-Crystalline Solids, 360*, 9-12.

Benabdesselam, M., Mady, F., Girard, S., Mebrouk, Y., Duchez, J. B., Gaillardin, M., & Paillet, P. (2013b). Performance of Ge-Doped Optical Fiber as a Thermoluminescent Dosimeter. *IEEE Transactions on Nuclear Science, 60*(6), 4251-4256.

Berger, M. J., Coursey, J. S., Zucker, M. A., & Chang, J. (2017). Stopping-Power & Range Tables for Electrons, Protons, and Helium Ions. from National Institute of Standards and Technology (NIST), Physical Measurement Laboratory (PML).

Berger, M. J., Hubbell, J. H., Seltzer, S. M., Chang, J., Coursey, J. S., Sukumar, R. & Olsen, K. (2010). XCOM: Photon Cross Sections Database. US Department of Commerce

Bohm, M., & Scharmann, A. (1971). First order kinetics in thermoluminescence and thermally stimulated conductivity. *Physics Status Solidi A, 4*, 99-104.

Bouzid, D., Bert, J., Dupre, P. F., Benhalouche, S., Pradier, O., Boussion, N., & Visvikis, D. (2015). Monte-Carlo dosimetry for intraoperative radiotherapy using a low energy x-ray source. *Acta Oncologica, 54*, 1788-1795.

Bouzid, D., Boussion, N., Bert, J., Pradier, O., & Visvikis, D. (2014). A simulation based dosimetric study for a Kypho-IORT treatment using Intrabeam™. *Translational Cancer Research, 3*(1), 83-87.

Bradley, D. A., Hugtenburg, R. P., Nisbet, A., Abdul Rahman, A. T., Issa, F., Mohd Noor, N., & Alalawi, A. (2012). Review of doped silica glass optical fibre: their TL properties and potential applications in radiation therapy dosimetry. *Applied Radiation and Isotopes, 71*, 2-11.

Bradley, D. A., Mahdiraji, G. A., Ghomeishi, M., Dermosesian, E., Adikan, F. R., Rashid, H. A., & Maah, M. J. (2015). Enhancing the radiation dose detection sensitivity of optical fibres. *Applied Radiation and Isotopes, 100*, 43-49.

Brenner, D. J., Leu, C. S., Beatty, J. F., & Shefer, R. E. (1999). Clinical relative biological effectiveness of low-energy x-rays emitted by miniature x-ray devices. *Physica in. Medicine and Biolog., 44*, 323-333.

Buge, F., Chiavassa, S., Herve, C., Rigaud, J., Delpon, G., & Supiot, S. (2015). Preclinical Evaluation of Intraoperative Low-Energy Photon Radiotherapy Using Spherical Applicators in Locally Advanced Prostate Cancer. *Frontiers in Oncology, 5*, 204.

Burlin, T. E. (1966). A general theory of cavity ionisation. *British Journal of. Radiology, 39*, 727-734.

Burlin, T. E., & Chan, F. K. (1967). *Some applications of cavity theory to condensed-state radiation dosimetry*. IAEA Symposium of Solid State and Chemical Radiation Dosimetry in Medicine and Biology, Vienna: International Atomic Energy Agency.

Cardona, M., & Ley, L. (1978). *Photoemission in Solids I General Principles*. Berlin Heidelberg New York: Springer-Verlag.

Chappie, C. L., Faulkner, K., & Harrison, R. M. (1990). An investigation into the performance of an automated quality assurance and dosimetry system in diagnostic radiology. *British Journal of. Radiology, 63*, 635-639.

Chen, R. (1979). Saturation of sensitization of the 110 °C TL peak in quartz and its potential application in the pre-dose technique. *European Pact Journal., 3*, 325-335.

Chen, R., Gogel, G., & Kristianpoller, N. (1994). Theoretical account for the sensitization and de-sensitization in quartz. *Radiation Measurements., 23*(2/3), 277-279.

Chen, R., & Haber, G. A. (1968). Calculation of glow curves activation energies by numerical initial rise method. *Chemical Physics Letters, 2*(7), 483-485.

Chen, R., Kirsh, Y., & Pamplin, B. (1981). *The Analysis of Thermally Stimulated Processes*. Oxford: Pergamon Press.

Chen, R., Kirsh, Y., & Townsend, P. D. (1991). Models for the sensitization of thermoluminescence in silica fibres. *Nuclear Tracks and Radiation Measurements, 18*(2), 13-17.

Chen, R., & Leung, P. L. (1991). Modelling the pre-dose effect in thermoluminescence. *Radiation Protection Dosimetry, 84*, 43-46.

Chen, R., & Leung, P. L. (2000). A model for dose-rate dependence of thermoluminescence intensity. *Journal of Physics D: Applied Physics, 33*, 846-850.

Chen, R., & McKeever, S. W. (1997). *Theory of Thermoluminescence and Related Phenomena*. Singapore: World Scientific.

Clausen, S., Schneider, F., Jahnke, L., Fleckenstein, J., Hesser, J., Glatting, G., & Wenz, F. (2012). A Monte Carlo based source model for dose calculation of endovaginal TARGIT brachytherapy with INTRABEAM and a cylindrical applicator. *Zeitschrift für Medizinische Physik (German Journal of Medical Physics), 22*(3), 197-204.

Cooke, D. W., & Rhodes, J. F. (1981). Thermoluminescence studies of LiF (TLD100) in the temperature interval 10-300 K°, *Journal of Applied Physics, 52, 4244*.

Daniels, F., Boyd, C. A., & Saunders, D. F. (1953). Thermoluminescence as a Research Tool. *Science, 117*(3040).

Djouguela, A., Kollhoff, R., Rubach, A., D., H., & Poppe, B. (2005). The Schwarzschild effect of the dosimetry film Kodak EDR 2. *Physics in Medicine and Biology, 50*(21), N317–N321.

Dong, S. L., Chu, T. C., Lan, G. Y., Wu, T. H., Lin, Y. C., & Lee, J. S. (2002). Characterization of high-sensitivity metal oxide semiconductor field effect transistor dosimeters system and LiF:Mg,Cu,P thermoluminescence dosimeters for use in diagnostic radiology. *Applied Radiation and Isotopes, 57*, 883–891.

Dussel, G. A., & Bube, R. H. (1967). Theory of thermally stimulated conductvity in a previously photoexcited crystal. *Physical Review, 155, 764*.

Eaton, D. J. (2012). Quality assurance and independent dosimetry for an intraoperative x-ray device. *Medical Physics, 39*(11), 6908-6920.

Eaton, D. J., Best, B., Brew-Graves, C., Duck, S., Ghaus, T., Gonzalez, R. and Keshtgar, M. R. S., 2012, In vivo dosimetry for single fraction targeted intraoperative radiotherapy (TARGIT) for breast cancer, *International Journal of Radiation Oncology Biology Physics*, *82*, 819-824.

Ebert, M. A., & Carruthers, B. (2003). Dosimetric characteristics of a low-kV intra-operative x-ray source: implications for use in a clinical trial for treatment of low-risk breast cancer. *Medical Physics, 30*(9), 2424-2431.

Ehlermann, D. A. E. (2016a). The early history of food irradiation. *Radiation Physics and Chemistry, 129*, 10-12.

Ehlermann, D. A. E. (2016b). Particular applications of food irradiation: Meat, fish and others. *Radiation Physics and Chemistry, 129*, 53-57.

El-Kateb, A. H., & Abdul-Hamid, A. S. (1991). Photon Attenuation Coefficient Study of some Materials Containing Hydrogen, Carbon and Oxygen. *Applied Radiation and Isotopes, 42*(3), 303-307.

Ellis, A. D., Moskowitz, P. D., Townsend, J. E., & Townsend, P. D. (1989). An optical fibre rereadable radiation dosimeter for use at high doses and at elevated temperature. *Journal of Physics D: Applied Physics, 22*, 1758-1762.

Entezam, A., Khandaker, M. U., Amin, Y. M., Ung, N. M., Bradley, D. A., Maah, J. & Moradi, F. (2016). Thermoluminescence Response of Ge-Doped Cylindrical-, Flat- and Photonic Crystal Silica-Fibres to Electron and Photon Radiation. *PLoS One, 11*(5), e0153913.

Espinosa, G., Golzarri, J. I., Bogard, J., & Garcia-Macedo, J. (2006). Commercial optical fibre as TLD material. *Radiation Protection Dosimetry, 119*, 197-200.

Fairhild, R. G., Mattern, P. L., Lengweiler, K., & Levy, P. W. (1978). Thermoluminescence of LiF TLD-100: Glow curve kinetics. *Journal of Applied Physics, 49, 4523*.

Fitting, H. J., Ziems, T., von Czarnowski, A., & Schmidt, B. (2004). Luminescence center transformation in wet and dry SiO_2. *Radiation Measurements, 38*, 649-653.

Fleming, S. J., & Thompson, J. (1970). Quarts as a heat resistant dosimeter. *Health Physics, 18*, 567-578.

Fogg, P., Das, K. R., Kron, T., Fox, C., Chua, B., & Hagekyriakou, J. (2010). Thermoluminescence dosimetry for skin dose assessment during intraoperative radiotherapy for early breast cancer. *Australasian Physical and Engineering Science in Medicine, 33*(2), 211-214.

Friebele, E. J. (1979). Optical fiber waveguides in radiation environments. *Optical Engineering, 18*(6), 186552.

Furetta, C. (2010). *Handbook of Thermoluminescence* (3rd edition.): World Scientific Publishing Co. Pte. Ltd, Singapore.

Furetta, C., Prokic, M., Salamon, R., Prokic, V., & Kitis, G. (2001). Dosimetric characteristics of tissue equivalent thermoluminescent solid TL detectors based on lithium borate. *Nuclear Instruments and Methods in Physics Research A, 456*, 411-417.

Garlick, G. F. J., and Gibson, A. F., (1948). The Electron Trap Mechanism of Luminescence in Sulphide and Silicate Phosphors. *Proceedings of the Physical Society, 60*(574).

Geleijns, J., & Wondergem, J. (2005). X-ray imaging and the skin: radiation biology, patient dosimetry and observed effects. *Radiation Protection Dosimetry, 114*(1-3), 121-125.

Gilbert, R. M. (1982). Photobleaching of Radiation-Induced Color Centers in a Germania-Doped Glass Fiber. *IEEE Transactions on Nuclear Science, 29*(6), 1-5.

Girard, S., Baggio, J., & Bisutti, J. (2006). 14-MeV Neutron, γ-Ray, and Pulsed X-Ray Radiation-Induced Effects on Multimode Silica-Based Optical Fibers. *IEEE Transactions on Nuclear Science, 53*(6), 3750-3757.

Griscom, D. L. (1985). *Nature Of Defects And Defect Generation In Optical Glasses.* Proceeding of the Society of Photo-Optical Instrumentation Engineers (SPIE) 0541, Radiation Effects on Optical Materials.

Guimarães, C. C., Moralles, M., & Okuno, E. (2007). GEANT4 simulation of the angular dependence of TLD-based monitor response. *Nuclear Instruments and Methods in Physics Research Section A: Accelerators, Spectrometers, Detectors and Associated Equipment, 580*(1), 514-517.

Hashim, S., Al-Ahbabi, S., Bradley, D. A., Webb, M., Jeynes, C., Ramli, A. T., & Wagiran, H. (2009). The thermoluminescence response of doped SiO2 optical fibres subjected to photon and electron irradiations. *Applied Radiation and Isotopes, 67*(3), 423-427.

Hashim, S., Bradley, D. A., Peng, N., Ramli, A. T., & Wagiran, H. (2010). The thermoluminescence response of oxygen-doped optical fibres subjected to photon and electron irradiations. *Nuclear Instruments and Methods in Physics Research Section A: Accelerators, Spectrometers, Detectors and Associated Equipment, 619*(1-3), 291-294.

Hashim, S., Ibrahim, S. A., Che Omar, S. S., Alajerami, Y. S., Saripan, M. I., Noor, N. M. & Alzimami, K. (2014). Photon irradiation response of photonic crystal fibres and flat fibres at radiation therapy doses. *Applied Radiation and Isotopes, 90*, 258-260.

Hashim, S., Omar, S. S. C., Ibrahim, S. A., Hassan, W. M. S. W., Ung, N. M., Mahdiraji, G. A. & Alzimami, K. (2015). Thermoluminescence response of flat optical fiber subjected to 9MeV electron irradiations. *Radiation Physics and Chemistry, 106*, 46-49.

Hashim, S., Saripan, M. I., Abdul Rahman, A. T., Yaakob, N. H., Bradley, D. A., & Alzimami, K. (2013). Effective Atomic Number of Ge-Doped and Al-Doped Optical Fibers for Radiation Dosimetry Purposes. *IEEE Transactions on Nuclear Science, 60*(2), 555-559.

Hefne, J. (2000). The Dose Distribution Inside the Irradiation Chamber of the Gamma Cell 220 at KACST Using MCNP4B. *Journal of Nuclear Science and Technology, 37*, 402-405.

Henschel, H., Köhn, O., & Schmidt, H. U. (1992). Optical fibres as radiation dosimeters. *Nuclear Instruments and Methods in Physics Research B, 69*, 307-314.

Herman, R. C., & Meyer, C. F. (1946). The Thermoluminescence and Conductivity of Phosphors. *Journal of Applied Physics, 17*(743).

Hernandez, A. M., & Boone, J. M. (2014). Tungsten anode spectral model using interpolating cubic splines: unfiltered x-ray spectra from 20 kV to 640 kV. *Medical Physics, 41*(4), 042101.

Horowitz, Y. S., Moscovitc, M., & Dubi, A. (1983). Modified general cavity theory applied to the calculation of gamma dose in '^{60}Co thermoluminescence dosimetry. *Physics in Medicine and Biology, 28*(7), 829.

Hubbell, J. H. (1969). Photon Cross Sections, Attenuation Coefficients, and Energy Absorption Coefficients from 10 keV to 100 GeV, *NSRDS-NBS 29*.

IAEA HUMAN HEALTH SERIES No. 24. (2013). *Dosimetry in Diagnostic Radiology for Paediatric Patients*. Vienna, Austria: International atomic energy agency (IAEA).

ICRP. (1992). Publication 59: The Biological Basis for Dose Limitation in the Skin (ICRP Skin Task Group Report, Annals of the ICRP).

Instruction manual Gammacell 220 Cobalt 60 irradiation unit. (1968). Atomic Energy of Canada Limited, Edition 6.

International Electrotechnical Commission, (2005). Medical Diagnostic X-Ray Equipment *Radiation Conditions for use in the Determination of Characteristics* (Vol. IEC 61267). Geneva.

Issa, F., Abdul Rahman, A. T., Hugtenburg, R. P., Bradley, D. A., & Nisbet, A. (2012). Establishment of Ge-doped optical fibres as thermoluminescence dosimeters for brachytherapy. *Applied Radiation and Isotopes, 70*(7), 1158-1161.

Issa, F., Latip, N. A. A., Bradley, D. A., & Nisbet, A. (2011). Ge-doped optical fibres as thermoluminescence dosimeters for kilovoltage X-ray therapy irradiations. *Nuclear Instruments and Methods in Physics Research Section A: Accelerators, Spectrometers, Detectors and Associated Equipment, 652*(1), 834-837.

Jackson, D. F., & Hawkes, D. J. (1981). X-Ray attenuation coefficients of elements and mixtures. *Phisics Reports (Review Section of Physics Letters), 70*(3), 169-233.

Jafari, S. M., Alalawi, A. I., Hussein, M., Alsaleh, W., Najem, M. A., Hugtenburg, R. P. & Nisbet, A. (2014). Glass beads and Ge-doped optical fibres as thermoluminescence dosimeters for small field photon dosimetry. *Physics in Medicine and Biology, 59*(22), 6875-6889.

Janovsky, I., & Ross, C. K. (1993). *The IRS thermoluminescent dosimetry system*. (PIRS-0369). Ottawa, Ontario, Canada: National Research Council Publications.

Jin, H., Duftschmid, K. E., & Strachotinsky, C. (1992). Investigation of a New LiF TLD Individual Dosimeter for Measuring Personal Dose Equivalent Hp(d) on Different Phantoms. Austria: Institute for Radiation Protection , Austrian Research Centre Seibersdorf, Austria.

Jursinic, P. A. (2007). Characterization of optically stimulated luminescent dosimeters, OSLDs, for clinical dosimetric measurements. *Medical Physics, 34*(12), 4594-4604.

Kerns, J. R., Kry, S. F., Sahoo, N., Followill, D. S., & Ibbott, G. S. (2011). Angular dependence of the nanoDot OSL dosimeter. *Medical Physics, 38*(7), 3955-3962.

Khan, F. M. (2003). *The Physics of Radiation Therapy* (3 ed.). Philadelphia, PA 19106 USA: Lippincott Williams & Wilkins.

Kraus-Tiefenbacher, U., Steil, V., Bauer, L., Melchert, F., & Wenz, F. (2003). A novel mobile device for intraoperative radiotherapy (IORT). *ONKOLOGIE, 26*, 596-598.

Kuntz, F., & Strasser, A. (2016). The specifics of dosimetry for food irradiation applications. *Radiation Physics and Chemistry, 129*, 46-49.

Kvasnicka, J. (1983). TL response dependence on the dose rate and its consequences. *International Journal of Applied Radiation and. Isotopes, 34*(4), 713-715.

Lyons, P. B. (1986). *Radiation Effects*. Proceeding of the Society of Photo-Optical Instrumentation Engineers (SPIE0648), Los Angeles, CA, USA, 128-133.

Lyytikäinen, K., Huntington, S. T., Carter, A. L. G., McNamara, P., Fleming, S., Abramczyk, J. & Schötz, G. (2004). Dopant diffusion during optical fibre drawing. *Optics Express, 12*(6).

Mady, F., Benabdesselam, M., Duchez, J. B., Mebrouk, Y., & Girard, S. (2013). *Global view on dose rate effects in silica-based fibers and devices damaged by radiation-induced carrier trapping*. IEEE Nuclear and Space Radiation Effects Conference (NSREC), San Francisco, United States.

Mady, F., Bindi, R., Iacconi, P., & Wrobel, F. (2006). Influence of absorbed dose and deep traps on thermoluminescence response: a numerical simulation. *Radiation Protection Dosimetry, 119*, 37-40.

Mahdiraji, G. A., Adikan, F. R. M., & Bradley, D. A. (2015c). Collapsed optical fiber: A novel method for improving thermoluminescence response of optical fiber. *Journal of Luminescence, 161*, 442-447.

Mahdiraji, G. A., Dermosesian, E., Safari, M. J., Adikan, F. R. M., & Bradley, D. A. (2015a). Collapsed-Hole Ge-Doped Photonic Crystal Fiber as a Diagnostic Radiation Dosimeter. *Journal of Lightwave Technology, 33*(16), 3439-3445.

Mahdiraji, G. A., Ghomeishi, M., Adikan, F. R. M., & Bradley, D. A. (2017). Influence of optical fiber diameter on thermoluminescence response. *Radiation Physics and Chemistry*, *140*, 2-10.

Mahdiraji, G. A., Ghomeishi, M., Dermosesian, E., Hashim, S., Ung, N. M., Adikan, F. R. M., & Bradley, D. A. (2015b). Optical fiber based dosimeter sensor: Beyond TLD-100 limits. *Sensors and Actuators A: Physical, 222*, 48-57.

Marrone, M. J. (1983). Optical fiber radiation detector and real-time dosimeter: US Patent number: US4413184A.

Marrone, M. J., & Attix, F. H. (1964). Damage effects in CaF_2:Mn and LiF thermoluminescent dosimeters. *Health Physics, 10*, 431-436.

McKeever, S. W. (1983). *Thermoluminescence of Solids*. U.K.: Cambridge University Press.

MCNPX user's manual, version 2.6.0. (2007). In D. B. Pelowitz (Ed.): Los Alamos National Laboratory.

Medlin, W. L. (1968). *In thermoluminescence of geological materials*: Academic Press London.

Miljanic, S., & Ranogajec-Komor, M. (1997). Application of cavity theory to the response of various TLDs to 60Co gammas degraded in water. *Physics in Medicine and Biology, 42*, 1335–1349.

Miljanic, S., & Razem, D. (1996). The effects of size and shape of the irradiation vessel on the response of some chemical dosimetry systems to photon irradiation. *Radiation Physics and Chemistry, 47*, 653–662.

Mobit, P. N., Mayles, P., & Nahum, A. E. (1996). The quality dependence of LiF TLD in megavoltage photon beams: Monte Carlo simulation and experiments. *Physics in Medicine and Biology, 41*, 387–398.

Negron-Mendoza, A., Uribe, R. M., Ramos-Bernal, S., Camargo-Raya, C., Gomez-Vidales, V., & Kobayashi, K. (2015). Calcium carbonate as a possible dosimeter for high irradiation doses. *Applied Radiation and Isotopes, 100*, 55-59.

Nicholas, K. H., & Woods, J. (1964). The evaluation of electron trapping parameters from conductivity glow curves in cadmium sulphide. *British Journal of Applied Physics, 15*, 783-795.

Noor, N. M., Hussein, M., Bradley, D. A., & Nisbet, A. (2010). The potential of Ge-doped optical fibre TL dosimetry for 3D verification of high energy IMRT photon beams. *Nuclear Instruments and Methods in Physics Research Section A: Accelerators, Spectrometers, Detectors and Associated Equipment, 619*(1-3), 157-162.

Noor, N. M., Hussein, M., Kadni, T., Bradley, D. A., & Nisbet, A. (2014). Characterization of Ge-doped optical fibres for MV radiotherapy dosimetry. *Radiation Physics and Chemistry, 98*, 33-41.

Noor, N. M., Shukor, N. A., Hussein, M., Nisbet, A., & Bradley, D. A. (2012). Comparison of the TL fading characteristics of Ge-doped optical fibres and LiF dosimeters. *Applied Radiation and Isotopes, 70*(7), 1384-1387.

Nwankwo, O., Clausen, S., Schneider, F., & Wenz, F. (2013). A virtual source model of a kilo-voltage radiotherapy device. *Physics in Medicine and Biology, 58*(7), 2363-2375.

O'Keeffe, S., Fitzpatrick, C., Lewis, E., & Al-Shamma'a, A. I. (2008). A review of optical fibre radiation dosimeters. *Sensor Review, 28*(2), 136-142.

Obryk, B., Glaser, M., Mandić, I., Bilski, P., Olko, P., & Sas-Bieniarz, A. (2011). Response of various types of lithium fluoride MCP detectors to high and ultra-high thermal neutron doses. *Radiation Measurements, 46*(12), 1882-1885.

Oliveira, C., & Salgado, J. (2001). Isodose distributions and dose uniformity in the Portuguese gamma irradiation facility calculated using the MCNP code. *Radiation Physics and Chemistry, 61*, 791–793.

Ong, C. L., Kandaiya, S., Kho, H. T., & Chong, M. T. (2009). Segments of a commercial Ge-doped optical fiber as a thermoluminescent dosimeter in radiotherapy. *Radiation Measurements, 44*(2), 158-162.

Pacchioni, G., Skuja, L. and Griscom, D. (Eds.), (2000). proceedings of the NATO Advanced Study Institute on Defects in SiO_2 and Related Dielectrics: Science and Technolgy, Erice, Italy.

Pagonis, V., & Kitis, G. (2012). Prevalence of first-order kinetics in thermoluminescence materials: an explanation based on multiple competition processes. *Physica Status Solidi B*, *249*(8), 1590-1601.

Palmer, A. L., Di Pietro, P., Alobaidli, S., Issa, F., Doran, S., & Bradley, D. A. (2013). Comparison of methods for the measurement of radiation dose distributions in high dose rate (HDR) brachytherapy: Ge-doped optical fiber, EBT3 Gafchromic film, and PRESAGER radiochromic plastic. *Medical Physics, 40*(6), 0617071.

Perumallu, A., Nageswara Rao, A. S., & Krishna Rao, G. (1984). Photon interaction measurements of certain compounds in the energy range 30-660 keV. *Canadian Journal of Physics, 62*(5), 454-459.

Poludniowski, G., Landry, G., DeBlois, F., Evans, P. M., & Verhaegen, F. (2009). SpekCalc: a program to calculate photon spectra from tungsten anode x-ray tubes. *Physics in Medicine and Biology, 54*, 433–438.

Powers, Stopping, Ranges for Electrons (ESTAR). (2015). The National Institute of Standards and Technology (NIST) (last update 30/12), Physical Measurement laboratory, U.S. Department of Commerce.

Raisali, G. R., & Sohrabpour, M. (1993). Application of EGS4 computer code for determination of gamma ray spectrum and dose rate distribution in Gamacell 220. *Radiation. Physics and Chemistry, 42*, 799-805.

Ramli, A. T., Bradley, D. A., Hashim, S. & Wagiran, H. (2009). The thermoluminescence response of doped SiO2 optical fibres subjected to alpha-particle irradiation. *Applied Radiation and Isotopes, 67*(3), 428-432.

Sahare, P. D., Ranjan, R., Salah, N., & Lochab, S. P. (2007). K3Na(SO4)2 : Eu nanoparticles for high dose of ionizing radiation. *Journal of Physics D: Applied Physics, 40*(3), 759-764.

Sahini, M. H., Hossain, I., Wagiran, H., Saeed, M. A., & Ali, H. (2014). Thermoluminescence responses of the Yb- and Yb-Tb-doped SiO2 optical fibers to 6-MV photons. *Applied Radiation and Isotopes, 92*, 18-21.

Salh, R. (2011). Defect Related Luminescence in Silicon Dioxide Network: A Review. Prof. Sukumar Basu (Ed.), *Crystalline Silicon - Properties and Uses*: InTech.

Schneider, F., Clausen, S., Thölking, J., Wenz, F., & Abo-Madyan, Y. (2014). A novel approach for superficial intraoperative radiotherapy (IORT) using a 50 kV X-ray source: a technical and case report. *Journal of Applied Clinical Medical Physics, 15*(1)*,* 167-176.

Schneider, F., Greineck, F., Clausen, S., Mai, S., Obertacke, U., Reis, T., & Wenz, F. (2011). Development of a novel method for intraoperative radiotherapy during Kyphoplasty for spinal metastases (KYPHO-IORT). *International Journal of Radiation Oncology Biology Physics, 81*(4), 1114–1119.

Seddighi, A., Akbari, M. E., Seddighi, A. S., Rakhsha, A., Vaezi, M., & Zohrevand, A. H. (2015). First Experience of Intraoperative Radiation Therapy in Cerebral High Grade Glioma in Iran: A Report of Three Cases and Literature Review. *Iranian Journal of Cancer Prevenstion, 8*(5), e3795.

Seitz, F., & Turnbull, D. (1958). *Solid state physics: advances in research and application* (Vol. 7). New York: Academic Press Inc.

Sheikh-Bagheri, D., & Rogers, D. W. (2002). Monte Carlo calculation of nine megavoltage photon beam spectra using the BEAM code. *Medical Physics, 29*(3), 391-402.

Shiragai, A. (1984). A comment on a modification of Burlin's general cavity theory. *Physics in Medicine and Biology, 29*, 427-432.

Soares, C., Drupieski, C., Wingert, B., Pritchett, G., Pagonis, V., O'Brien, M. & Olko, P. (2006). Absorbed dose measurements of a handheld 50 kVP X-ray source in water with thermoluminescence dosemeters. *Radiation Protection Dosimetry, 120*(1-4), 78-82.

Soares, O. D. D. (1994). *Trends in Optical Fibre Metrology and Standards.* NATO Advanced Study Series E conference, Applied Science, Viana do Castelo, Portugal.

Sohrabpoura, M., Hassanzadehb, M., Shahriarib, M., & Sharifzadeh, M. (2002). Gamma irradiator dose mapping simulation using the MCNP code and benchmarking with dosimetry. *Applied Radiation and Isotopes, 57*, 537–542.

Soliman, Y. S., & Abdel-Fattah, A. A. (2013). Leuco crystal violet/poly(vinyl butyral) thin film as a high-dose dosimeter. *Radiation Measurements, 49*, 1-6.

Sporea, D., Sporea, A., O'Keeffe, S., McCarth, D., & Lewis, E. (2012). Optical Fibers and Optical Fiber Sensors Used in Radiation Monitoring. Yasin, M., Harun, S. W. & Arof, H., (Eds.), Selected topics on optical fibre technology.

Standardization, I. O. f. (2013). ISO11137-2:2013 *Sterilization of health care products; Radiation; Part 2: Establishing the sterilization dose* (pp. 68). Geneva, Switzerland.

Keshtgar, M., Pigott, K. & Wenz, F., (2014). *Targeted Intraoperative Radiotherapy in Oncology*.

Thompson, A. C., & Vaughan, D. (2001). *X-Ray Data Booklet* (2 ed.). Berkeley, CA: Lawrence Berkeley National Laboratory.

Trukhin, A. N., Goldberg, M., Jansons, J., Fitting, H. J., & Tale, I. A. (1998). Silicon dioxide thin film luminescence in comparison with bulk silica *Journal of Non-Crystalline Solids, 223*, 114-122.

Tsoulfanidis, N. (1995). *Measurement and Detection of Radiation* (2 ed.). Washington, DC: Taylor & Francis.

Vaidya, J. S. (2014). Targeted intraoperative radiotherapy boost vs. standard external beam radiotherapy boost, TARGIT B Protocol Version 4 01.

Vohra, K. G., Bhatt, R. C., Chandra, B., Pradhan, A. S., Lakshmanan, A. R., & Shastry, S. S. (1980). A personnel dosimeter TLD badge based on CaS0,:Dy teflon TLD discs. *Health Physics, 38*, 193-197.

White, S. A., Reniers, B., de Jong, E. E., Rusch, T., & Verhaegen, F. (2016). A comparison of the relative biological effectiveness of low energy electronic brachytherapy sources in breast tissue: a Monte Carlo study. *Physics in Medicine and Biology, 61*(1), 383-399.

Wrobel, F., Benabdesselam, M., Iacconi, P., & Mady, F. (2006). Kerma rate effects on thermoluminescent response of CVD Diamond. *Radiation Protection Dosimetry, 119*(1-4), 115–118.

Yanch, J. C., & Harte, K. J. (1996). Monte Carlo simulation of a miniature, radiosurgery x-ray tube using the ITS 3.0 coupled electron-photon transport code. *Medical Physics, 23*(9), 1551-1558.

Yusoff, A. L., Hugtenburg, R. P., & Bradley, D. A. (2005). Review of development of a silica-based thermoluminescence dosimeter. *Radiation Physics and Chemistry, 74*(6), 459-481.

Zaragoza, E. C., Gaste´lum, S., Mele´ndrez, R., Chernov, V., & Barboza-Flores, M. (2010). Dose rate effects on the performance of MWCVD diamond films as TL gamma radiation dosimeter. *Physica Status Solidi A, 207*(8), 1944–1948.

Zimmerman, J. (1971). The radiation induced increase of the 100 °C TL sensitivity of fired quartz. *Journal of Physics C: Solod State Physics, 4*, 3265-3276.

LIST OF PUBLICATIONS AND PAPERS PRESENTED

Journal Papers

Moradi, F., Mahdiraji, G. A., Dermosesian, E., Khandaker, M. U., Ung, N. M., Adikan, F. R. M. & Amin, Y. M. (2017). Influence of dose history on thermoluminescence response of Ge-doped silica optical fibre dosimeters. *Radiation Physics and Chemistry 134*, 62-70.

Moradi, F., Khandaker, M. U., Mahdiraji, G. A., Ung, N. M. & Bradley, D.A. (2017). Dose mapping inside a gamma irradiator measured with doped silica fibre dosimetry and Monte Carlo simulation. *Radiation Physics and Chemistry 140*, 107-111.

Moradi, F., Ung, N. M., Mahdiraji, G. A., Khandaker, M. U., Entezam, A., See, M. H., Taib, N. A., Amin, & Y. M., Bradley, D. A. (2017). Angular dependence of optical fibre thermoluminescent dosimeters irradiated using kilo- and megavoltage X-rays. *Radiation Physics and Chemistry 135,* 4-10.

Moradi, F., Ung, N. M., Khandaker, M. U., Mahdiraji, G. A., Saad, M., Abdul Malik, R., Bustam, A. Z., Zaili, Z., & Bradley, D. A. (2017). Monte Carlo skin dose simulation in intraoperative radiotherapy of breast cancer using spherical applicators. *Physics in Medicine and Biology, 62*(16), 6550-6566.

Moradi, F., Mahdiraji, G. A., Khandaker, M. U., Ung, N. M., Adikan, F. R. M., Khellaf, I., Bradley, D. A. (2018). A Silica fibre thermoluminescent sensor for ultrahigh dose radiation dosimetry. *Sensors and Actuators A: Physical, 273,* 197-205.

Moradi, F., Ung, N. M., Mahdiraji, G. A., Khandaker, M. U., See, M. H., Taib, N. A. & Bradley, D. A. In vivo intraoperative radiotherapy TL dosimetry using Ge-doped silica fibres, Under review with the journal "*Physica Medica"*.

International Conferences

Moradi, F., Ung, M. N., Mahdiraji, G. A., Khandaker, M. U., Entezam, A. & Bradley, D. A., Angular dependence of the response of optical fibre Thermoluminescence dosimeters, *2nd International Conference on Dosimetry and its Applications*, University of Surrey, Guildford, U.K. 3rd – 8th July 2016. (Poster presentation) (Abstract-Reviewed)

Moradi, F., Dermosesian, E., Mahdiraji, G. A., Khandaker, M. U. & Ung, N. M., Influence of dose history on thermoluminescence response of silica optical fibre dosimeters, *2nd International Conference on Dosimetry and its Applications*, University of Surrey, Guildford, U.K. 3rd – 8th July 2016. (Oral presentation) (Abstract-Reviewed)

Moradi, F., Ung, N. M., Khandaker, M. U. & Mahdiraji, G. A., Optical fibre thermoluminescence sensor: A novel option for IORT dosimetry, *10th Carl Zeiss Inrabeam system user meeting* 29th June – 1st July 2016, Mannheim, Germany. (Oral presentation) (Abstract-Reviewed)

Moradi, F., Ung, N. M., Khandaker, M. U. & Zaili, Z., Breast skin dose in intraoperative radiotherapy using spherical applicators: A Monte Carlo study, *12th international breast cancer congress*, 22nd-24th Feb. 2017, Shahid Beheshti University of Medical Sciences, Tehran, Iran. (Poster presentation) (Abstract-Reviewed)